DOT/FAA/AR-07/9

Air Traffic Organization
Operations Planning
Office of Aviation Research
and Development
Washington, D.C. 20591

Teardown Evaluation of Two T-34A Wing Sets

July 2007

Final Report

This document is available to the U.S. public through the National Technical Information Service (NTIS), Springfield, Virginia 22161.

U.S. Department of Transportation
Federal Aviation Administration

NOTICE

This document is disseminated under the sponsorship of the U.S. Department of Transportation in the interest of information exchange. The United States Government assumes no liability for the contents or use thereof. The United States Government does not endorse products or manufacturers. Trade or manufacturer's names appear herein solely because they are considered essential to the objective of this report. This document does not constitute FAA certification policy. Consult your local FAA aircraft certification office as to its use.

This report is available at the Federal Aviation Administration William J. Hughes Technical Center's Full-Text Technical Reports page: actlibrary.tc.faa.gov in Adobe Acrobat portable document format (PDF).

Technical Report Documentation Page

1. Report No.	2. Government Accession No.	3. Recipient's Catalog No.
DOT/FAA/AR-07/9		

4. Title and Subtitle	5. Report Date
TEARDOWN EVALUATION OF TWO T-34A WING SETS	July 2007
	6. Performing Organization Code

7. Author(s)	8. Performing Organization Report No.
Melinda Laubach[1], Dale Cope[1], Michael Shiao[2], and Marvin Nuss[2]	

9. Performing Organization Name and Address	10. Work Unit No. (TRAIS)
[1]National Institute for Aviation Research Wichita State University 1845 Fairmount Wichita, Kansas 67260 [2]Federal Aviation Administration William J. Hughes Technical Center Atlantic City International Airport, NJ 08245	
	11. Contract or Grant No. 01-C-AW-WISU

12. Sponsoring Agency Name and Address	13. Type of Report and Period Covered
U.S. Department of Transportation Federal Aviation Administration Air Traffic Organization Operations Planning Office of Aviation Research and Development Washington, DC 20591	Final Report
	14. Sponsoring Agency Code ACE-110

15. Supplementary Notes

16. Abstract

To aid with the assessment of aging acrobatic aircraft, the Federal Aviation Administration (FAA) teamed with the National Institute for Aviation Research of Wichita State University to teardown and inspect two sets of high-time Beech T-34A wings. Due to the recent history of fatigue cracking and failure, a destructive evaluation of the T-34A would be useful to the FAA to specifically address the T-34A concerns, and in a general sense, to assess the condition of a high-time acrobatic category aircraft. The teardown evaluation involved performing inspections prescribed in Airworthiness Directive 2001-13-18; disassembly to gain access to the underlying primary structure; paint removal and etching of the wing primary structure to enhance damage detection; post-disassembly nondestructive inspections, and a detailed microscopic examination of all primary structure. Selected cracks were also analyzed to determine failure modes.

17. Key Words	18. Distribution Statement
Aging aircraft, Teardown evaluation, Structural integrity, Airworthiness, Cracks, Corrosion	This document is available to the U.S. public through the National Technical Information Service (NTIS), Springfield, Virginia 22161.

19. Security Classif. (of this report)	20. Security Classif. (of this page)	21. No. of Pages	22. Price
Unclassified	Unclassified	140	

Form DOT F 1700.7 (8-72) Reproduction of completed page authorized

TABLE OF CONTENTS

	Page
EXECUTIVE SUMMARY	xv
1. INTRODUCTION	1
2. FIRST WING SET	2
2.1 The SB 57-3329 Inspections	3
2.2 Disassembly Phase	5
2.3 Post-Disassembly NDIs	6
2.3.1 Left Wing	6
2.3.2 Right Wing	20
2.4 Microscopic Examination	27
2.4.1 Left Wing	27
2.4.2 Right Wing	35
2.5 Fractographic Examination	40
2.5.1 Macroscopic Analysis	40
2.5.2 The SEM Observation	44
2.5.3 Optical Microstructural Analysis and Hardness Measurement	48
2.5.4 Conclusion	51
2.5.5 Suggestions	51
2.6 Summary of First WS Findings	52
3. SECOND WING SET	54
3.1 The SB 57-3329 Inspections	55
3.2 Disassembly Phase	57
3.3 Post-Disassembly NDIs	57
3.3.1 Left Wing	57
3.3.2 Right Wing	78
3.4 Microscopic Examination	89

3.4.1 Left Wing 89
3.4.2 Right Wing 105

3.5 Summary of Second WS Findings 118

4. SUMMARY 123

LIST OF FIGURES

Figure		Page
1	Typical T-34A Aircraft	2
2	First Set of T-34A Wings as Received	4
3	Locations of Eddy-Current Inspections	5
4	Front Spar Structural Stackup	7
5	Front Spar Forward and Aft Cap Structural Stackup	7
6	Left Wing Front Spar Forward Upper Cap	8
7	Corrosion on the Left Wing Front Spar Forward Upper Cap WS 37.5-39	8
8	Corrosion on the Left Wing Front Spar Forward Upper Cap WS 49-57.5	9
9	Left Wing Front Spar Aft Upper Cap	9
10	Corrosion on the Left Wing Front Spar Aft Upper Cap WS 38-40	10
11	Corrosion on the Left Wing Front Spar Aft Upper Cap WS 48.75-54.5	10
12	Rear Spar Structural Stackup	11
13	Left Wing Rear Spar Web	11
14	Crack in the Left Wing Rear Spar Web WS 168.75	12
15	Left Wing Rear Spar Lower Doubler	12
16	Cracks in the Left Wing Rear Spar Lower Doubler WS 66	13
17	Left Wing Rear Spar Lower Cap	13
18	Crack in the Left Wing Rear Spar Lower Cap WS 66	14
19	Left Wing Front Spar Inboard Landing Gear Attachment Fitting	15
20	Corrosion on the Left Wing Front Spar Inboard Landing Gear Attachment Fitting at WS 46	15
21	Left Wing Rear Spar Inboard Landing Gear Attachment Fitting	16
22	Corrosion on the Left Wing Rear Spar Inboard Landing Gear Attachment at WS 46	16

23	Left Wing Front Spar Upper Bathtub Fitting	17
24	Corrosion on the Left Wing Front Spar Upper Bathtub Fitting WS 23.5-25.75	18
25	Left Wing Front Spar Lower Bathtub Fitting	18
26	Corrosion on the Left Wing Front Spar Lower Bathtub Fitting WS 23-27.5	19
27	Left Wing Rear Spar Lower Bathtub Fitting	19
28	Corrosion on the Left Wing Rear Spar Lower Bathtub Fitting WS 24.75-26	20
29	Right Wing Front Spar Inboard Landing Gear Attachment Fitting	21
30	Corrosion on the Right Wing Front Spar Inboard Landing Gear Attachment Fitting WS 46	22
31	Right Wing Rear Spar Inboard Landing Gear Attachment Fitting	22
32	Corrosion on the Right Wing Rear Spar Inboard Landing Gear Attachment Fitting WS 46	23
33	Right Wing Front Spar Lower Bathtub Fitting	24
34	Corrosion on the Right Wing Front Spar Lower Bathtub Fitting WS 23-27.75	24
35	Right Wing Front Spar Upper Bathtub Fitting	25
36	Corrosion on the Right Wing Front Spar Upper Bathtub Fitting WS 23.5-28	25
37	Right Wing Rear Spar Upper Bathtub Fitting	26
38	Corrosion on the Right Wing Rear Spar Upper Bathtub Fitting WS 23.5-27	26
39	Corrosion on the Left Wing Front Spar Forward Upper Cap WS 40, 50, and 52	28
40	Corrosion on the Left Wing Front Spar Aft Upper Cap WS 38-40	28
41	Corrosion on the Left Wing Front Spar Aft Upper Cap WS 48.75-54.5	29
42	Corrosion on the Left Wing Rear Spar Web WS 123-191	30
43	Crack in the Left Wing Rear Spar Lower Cap WS 66	30
44	Fractograph of the Left Wing Rear Spar Lower Cap Crack Face WS 66	31
45	Cracks in the Left Wing Rear Spar Lower Doubler WS 66	31

46 Corrosion on the Left Wing Front Spar Inboard Landing Gear Attachment Fitting WS 46 32

47 Corrosion on the Left Wing Rear Spar Inboard Landing Gear Attachment Fitting WS 46 33

48 Corrosion on the Left Wing Front Spar Upper Bathtub Fitting WS 24-28 34

49 Corrosion on the Left Wing Front Spar Lower Bathtub Fitting WS 23-27.5 34

50 Corrosion on the Left Wing Rear Spar Lower Bathtub Fitting WS 25 35

51 Corrosion on the Right Wing Front Spar Inboard Landing Gear Attachment Fitting WS 46 36

52 Corrosion on the Right Wing Rear Spar Inboard Landing Gear Attachment Fitting WS 46 37

53 Corrosion on the Right Wing Front Spar Lower Bathtub Fitting WS 23-27 38

54 Corrosion on the Right Wing Front Spar Upper Bathtub Fitting WS 24-28 38

55 Corrosion on the Right Wing Front Spar Upper Bathtub Fitting WS 24-28 39

56 Corrosion on the Right Wing Rear Spar Upper Bathtub Fitting WS 24-26 39

57 Schematic of the Formed Angle, Dimension, and Location of the Crack 41

58 Schematic of the Features Observed on the Fracture Surface and Macroscopic Stereomicrograph Taken at 7X 42

59 Stereomicrograph Showing Beach Marks, Crack Origin, and Direction of the Crack Propagation 43

60 Stereomicrograph of the Part From the Side Shows Strain on Fastener Hole During Crack Propagation 44

61 The SEM Micrograph of the Fracture Surface Shows the Primary Crack Nucleation Site (a) at Low-magnification and (b) at Higher Magnification of the Rectangular Inset (a) 45

62 (a) Low-Magnification Micrograph Shows Machining Defect in the Form Rough Surface and (b) High-Magnification Micrograph of the Region From Inset (a) 45

63 The SEM Micrograph of the Fracture Striations Observed on the Fracture Surface 46

64 The SEM Micrographs of Fracture Surface From the Lower Part of the Hole 47

65 The 3-D Optical Microstructure View of the Specimen 48

66 Optical Micrograph of (a) the Clad Layer of about 70 µm Thickness Observed on Both Sides of the Section and (b) Subsurface Deformation and Roughening Due to Shot-Peening 49

67 Composite Optical Micrograph Showing Subsurface Crack Running Parallel to the Surface on the Clad Layer 50

68 Optical Micrograph of the Cross Section of the Angle Showing Grain Coarsening Near Bent Surface 51

69 Second Set of T-34A Wings as Received 55

70 Crack in the Right Wing Stiffener Panel in Wheel Well Common to the Upper Skin WS 29 56

71 Crack in the Right Wing Leading-Edge Aft Lower Spar Cap WS 64 57

72 Front Spar Structural Stackup 58

73 Front Spar Forward and Aft Cap Structural Stackup 59

74 Rear Spar Structural Stackup 59

75 Left Wing Front Spar Web 60

76 Corrosion on the Left Wing Front Spar Web WS 37-42 61

77 Left Wing Front Spar Upper Cap 61

78 Damage on the Left Wing Front Spar Upper Cap WS 39.5 62

79 Exfoliation Corrosion on the Left Wing Front Spar Upper Cap WS 118-122.5 63

80 Exfoliation Corrosion on the Left Wing Front Spar Upper Cap WS 136-142.75 63

81 Intergranular Corrosion on the Left Wing Front Spar Upper Cap WS 139 64

82 Exfoliation Corrosion on the Left Wing Front Spar Upper Cap WS 156.25-157.25 65

83 Damage on the Left Wing Front Spar Upper Cap WS 156.75 65

84 Intergranular Corrosion on the Left Wing Front Spar Upper Cap WS 157.25 Bottom View 66

85 Intergranular Corrosion on the Left Wing Front Spar Upper Cap WS 157.25 Top View 67

86 Intergranular Corrosion on the Left Wing Front Spar Upper Cap WS 163.75 67

87	Exfoliation Corrosion on the Left Wing Front Spar Upper Cap WS 164	68
88	Damage on the Left Wing Front Spar Upper Cap WS 164	68
89	Exfoliation Corrosion on the Left Wing Front Spar Upper Cap WS 166.5	69
90	Intergranular Corrosion on the Left Wing Front Spar Upper Cap WS 166.75	70
91	Exfoliation and Intergranular Corrosion on the Left Wing Front Spar Upper Cap WS 170.25	70
92	Exfoliation and Intergranular Corrosion on the Left Wing Front Spar Upper Cap WS 171.25 and 171.5	71
93	Pitting Corrosion on the Left Wing Front Spar Upper Cap WS 174 and 174.25	72
94	Left Wing Leading-Edge Aft Lower Spar Cap	72
95	Crack in the Left Wing Leading-Edge Aft Lower Spar Cap WS 64	73
96	Pitting Corrosion on the Left Wing Leading-Edge Aft Lower Spar Cap WS 57-69	73
97	Left Wing Leading-Edge Forward Upper Spar Cap	74
98	Pitting Corrosion on the Left Wing Leading-Edge Forward Upper Spar Cap WS 100.5-102.5	74
99	Left Wing Rear Spar Lower Doubler	74
100	Crack in the Left Wing Rear Spar Lower Doubler WS 64	75
101	Left Wing Rear Spar Forward Lower Spar Cap	75
102	Crack in the Left Wing Rear Spar Forward Lower Cap WS 64	76
103	Left Wing Rear Spar Upper Bathtub Fitting	77
104	Intergranular Corrosion on the Left Wing Rear Spar Upper Bathtub Fitting WS 27	77
105	Right Wing Front Spar Web	78
106	Pitting Corrosion on the Right Wing Front Spar Web WS 36-48	79
107	Right Wing Front Spar Upper Cap	79
108	Intergranular Corrosion on the Right Wing Front Spar Upper Cap WS 89.5-90	80
109	Intergranular Corrosion on the Right Wing Front Spar Upper Cap WS 109.5	80

110	Exfoliation Corrosion on the Right Wing Front Spar Upper Cap WS 183.5	81
111	Intergranular Corrosion on the Right Wing Front Spar Upper Cap WS 184	82
112	Intergranular Corrosion on the Right Wing Front Spar Upper Cap WS 185.25	82
113	Intergranular Corrosion on the Right Wing Front Spar Upper Cap WS 187 Bottom View	83
114	Intergranular Corrosion on the Right Wing Front Spar Upper Cap WS 187 Top View	83
115	Right Wing Leading-Edge Forward Lower Cap	84
116	Crack in the Right Wing Leading-Edge Forward Lower Spar Cap WS 47.5	84
117	Crack in the Right Wing Leading-Edge Aft Lower Spar Cap WS 64	85
118	Crack in the Right Wing Leading-Edge Forward Lower Spar Cap WS 65.25	85
119	Crack in the Right Wing Leading-Edge Forward Lower Spar Cap WS 65.5	86
120	Crack in the Right Wing Leading-Edge Forward Lower Spar Cap WS 68.25	86
121	Right Wing Rear Spar Upper Bathtub Fitting	87
122	Pitting Corrosion on the Right Wing Rear Spar Upper Bathtub Fitting WS 25	88
123	Pitting Corrosion on the Right Wing Rear Spar Upper Bathtub Fitting WS 27	88
124	Pitting Corrosion on the Left Wing Front Spar Web WS 23-56	90
125	Pitting Corrosion on the Left Wing Front Spar Web WS 30.5	90
126	Exfoliation Corrosion on the Left Wing Front Spar Upper Cap WS 120 Outboard View	91
127	Exfoliation Corrosion on the Left Wing Front Spar Upper Cap WS 120 Inboard View	92
128	Intergranular Corrosion on the Left Wing Front Spar Upper Cap WS 136-142.75	92
129	Exfoliation Corrosion on the Left Wing Front Spar Upper Cap WS 136-142.75 Inboard View	93
130	Exfoliation Corrosion on the Left Wing Front Spar Upper Cap WS 136-142.75 Outboard View	93
131	Exfoliation Corrosion on the Left Wing Front Spar Upper Cap WS 156.5-157.25	94

132	Intergranular Corrosion on the Left Wing Front Spar Upper Cap WS 158.25	95
133	Exfoliation Corrosion on the Left Wing Front Spar Upper Cap WS 164	95
134	Intergranular Corrosion on the Left Wing Front Spar Upper Cap WS 170.25	96
135	Intergranular Corrosion on the Left Wing Front Spar Upper Cap WS 170.5	97
136	Pitting Corrosion on the Left Wing Front Spar Upper Cap WS 174.5	97
137	Crack in the Left Wing Leading-Edge Aft Lower Spar Cap WS 64.5 Bottom View	98
138	Crack in the Left Wing Leading-Edge Aft Lower Spar Cap WS 64.5	99
139	Crack Face of Crack in the Left Wing Leading-Edge Aft Lower Spar Cap WS 64.5	99
140	Pitting Corrosion on the Left Wing Leading-Edge Aft Lower Spar Cap WS 59-64	100
141	Pitting Corrosion on the Left Wing Leading-Edge Aft Upper Spar Cap WS 100.5-101	100
142	Crack in the Left Wing Rear Spar Lower Doubler WS 64	101
143	Crack in the Left Wing Rear Spar Forward Lower Spar Cap WS 64	102
144	Crack Face of Crack in the Left Wing Rear Spar Lower Doubler WS 64	102
145	Crack Face of Crack in the Left Wing Rear Spar Forward Lower Spar Cap WS 64	103
146	Pitting Corrosion on the Left Wing Rear Spar Upper Bathtub Fitting WS 27	104
147	Left Wing Front Spar Lower Bathtub Fitting WS 23-35	104
148	Pitting Corrosion on the Left Wing Front Spar Lower Bathtub Fitting WS 24	105
149	Scattered Pitting Corrosion on the Right Wing Front Spar Web WS 33-56	106
150	Intergranular Corrosion on the Right Wing Front Spar Upper Cap WS 89.5-90 Bottom View	106
151	Intergranular Corrosion on the Right Wing Front Spar Upper Cap WS 89.5-90 Top View	107
152	Intergranular Corrosion on the Right Wing Front Spar Upper Cap WS 110 Bottom View	107
153	Intergranular Corrosion on the Right Wing Front Spar Upper Cap WS 110 Top View	108

154 Corrosion on the Right Wing Front Spar Upper Cap WS 122-126 109

155 Intergranular Corrosion on the Right Wing Front Spar Upper Cap WS 184 109

156 Intergranular Corrosion on the Right Wing Front Spar Upper Cap WS 185.5 110

157 Intergranular Corrosion on the Right Wing Front Spar Upper Cap WS 187 Bottom View 110

158 Intergranular Corrosion on the Right Wing Front Spar Upper Cap WS 187 Top View 111

159 Crack in the Right Wing Leading-Edge Forward Lower Spar Cap WS 47.5 112

160 Crack Face of the Crack in the Right Wing Leading-Edge Forward Lower Spar Cap WS 47.5 112

161 Crack in the Right Wing Leading-Edge Aft Lower Spar Cap WS 64.5 Top View 113

162 Crack in the Right Wing Leading-Edge Aft Lower Spar Cap WS 64.5 113

163 Crack Face of the Crack in the Right Wing Leading-Edge Aft Lower Spar Cap WS 64.5 114

164 Cracks in the Right Wing Leading-Edge Forward Lower Spar Cap WS 65.25 and 65.5 114

165 Crack Face of the Crack in the Right Wing Leading-Edge Forward Lower Spar Cap WS 65.25 115

166 Crack Face of the Crack in the Right Wing Leading-Edge Forward Lower Spar Cap WS 65.5 115

167 Crack in the Right Wing Leading-Edge Forward Lower Spar Cap WS 68.25 116

168 Crack Face of the Crack in the Right Wing Leading-Edge Forward Lower Spar Cap WS 68.25 116

169 Pitting Corrosion on the Right Wing Rear Spar Upper Bathtub Fitting WS 27 117

170 Pitting Corrosion on the Right Wing Rear Spar Upper Bathtub Fitting WS 25 118

LIST OF TABLES

Table		Page
1	Summary of Findings for T-34A WS 1	52
2	Summary of Findings for T-34A WS 2	118

LIST OF ACRONYMS

3-D	Three-dimensional
AD	Airworthiness Directive
DN	Down
FAA	Federal Aviation Administration
FWD	Forward
HB	Brinell Hardness number
I/B	Inboard
NDI	Nondestructive Inspection
NIAR	National Institute for Aviation Research
NTSB	National Transportation Safety Board
O/B	Outboard
SB	Service Bulletin
SEM	Scanning Electron Microscope
WS	Wing station

EXECUTIVE SUMMARY

To aid with the assessment of aging acrobatic aircraft, the Federal Aviation Administration (FAA) teamed with the National Institute for Aviation Research (NIAR) of Wichita State University to teardown and inspect two sets of high-time Beech T-34A wings. Due to the recent history of fatigue cracking and failure, a destructive evaluation of the T-34A would be useful to the FAA to specifically address the T-34A concerns and, in a general sense, to assess the condition of a high-time acrobatic category aircraft. The teardown evaluation involved performing the inspections prescribed in Airworthiness Directive (AD) 2001-13-18; disassembly to gain access to the underlying primary structure; paint removal and etching of the wing primary structure to enhance damage detection; post-disassembly nondestructive inspections; and a detailed, microscopic examination of all primary structure. Selected cracks were also analyzed to determine failure modes.

In May 2004, wings were acquired from a high-time T-34A acrobatic category airplane with approximately 15,000 flight hours. These wings had been removed from service due to a crack in the left wing rear spar lower cap at Wing Station (WS) 66. In June 2004, another set of wings from a high-time T-34A became available for teardown examination. Instead of repairing the wings, which had known cracks on the rear spars, the maintenance facility elected to replace the wings, providing the damaged wings to the FAA and NIAR to conduct a teardown evaluation.

A total of four cracks were found on the first set of T-34A wings: one occurring on the left wing rear spar web at WS 168.75, another occurring on the left wing rear spar lower cap at WS 66, and two more cracks occurring at the corresponding location on the left wing rear spar lower doubler. The cracks on the left wing rear spar cap and doubler were determined to be caused by fatigue. At least one area of severe corrosion was found on the left wing front spar forward and aft upper caps and the left wing rear spar web. Light corrosion was found on the front and rear spar inboard landing gear attachment fittings on both the left and right wings. Corrosion was also observed on the following bathtub fittings: left wing front spar upper and lower, left wing rear spar lower, right wing front spar upper and lower, and right wing rear spar upper. An assessment of the severity of the corrosion in the bathtub fittings was not possible since the location of the corrosion prevented accurate measurements of pit depth. In general, the upper bathtub fittings exhibited more corrosion than the lower ones. Pitting was the only type of corrosion observed on this first set of T-34A wings.

Three cracks were found on the left wing of the second set located on the leading-edge aft lower cap, rear spar lower doubler, and the rear spar lower cap. On the right wing, four cracks were found on the leading-edge forward lower spar cap, and one crack was found on the right wing leading-edge aft lower spar cap. Nine areas of pitting corrosion were observed on the left wing, while five areas of pitting corrosion were found on the right wing. Pitting corrosion was also found on the left and right wing front spar webs, left and right wing front spar upper caps, left wing leading-edge aft upper and lower spar caps, and the left and right wing rear spar upper bathtub fittings. Three areas of mechanical damage were also noted on the left wing front spar upper cap. Seven areas of exfoliation corrosion occurred on the left wing front spar upper cap. Nine areas of intergranular corrosion were detected on the left wing front spar upper cap, while six areas were found on the right wing front spar upper cap. One area of intergranular corrosion was found on the left wing rear spar upper bathtub fitting.

1. INTRODUCTION.

The Beech Model T-34A was built in the 1950s and 1960s for the U.S. Navy and Air Force as military trainers. Although the military used the designation T-34A, the airplanes are designated as Model A45 on the Federal Aviation Administration (FAA) Type Certificate. The more common designation of T-34A is used in this report. A typical T-34A aircraft is shown in figure 1.

On April 19, 1999, a Beech T-34A (tail number N140SW) collided with the ground following the in-flight separation of the right wing near Rydal, Georgia. The aircraft entered a spiral and impacted the ground resulting in two fatalities. The examination of the airplane disclosed fatigue cracking in the spar material. The National Transportation Safety Board (NTSB) determined that the probable cause of this accident (investigation number ATL99FA072) was as follows: "Fracture of the wing spar as a result of fatigue cracking that occurred over an unknown number of flights and flight hours with a wing loading spectrum not anticipated during the design of the airplane." The failures were located on the front spar lower cap at Wing Station (WS) 34 and on the rear spar lower cap at WS 66. These failures were caused by metal fatigue.

Following this accident, the FAA issued an Airworthiness Directive (AD) AD 99-12-02, which limited the maximum speed to 175 miles per hour and the flight envelope from +6/-3 to +2.5/-0 g's in an effort to prevent future overload failures in the vicinity of pre-existing fatigue cracks. AD 2001-13-18 was also issued to inspect critical areas for fatigue cracks on the front and rear spars per Raytheon Service Bulletin (SB) 57-3329. This AD required the bolthole eddy-current inspection of nine fasteners on the front spar at WS 34, one fastener site on the front spar at WS 64, and two fastener locations on the rear spar at WS 66. This AD also required the eddy-current inspection of the rear spar lower bathtub fittings.

On November 19, 2003, another in-flight breakup occurred involving a T-34A near Montgomery, Texas. While maneuvering in a simulated air-to-air combat scenario with another aircraft, the accident aircraft (registration number N44KK) was in a climbing right turn when the right wing separated from the aircraft. Subsequently, the aircraft spun uncontrolled to the ground, resulting in two fatalities. Examination of the separated wing revealed extensive fatigue cracking in both the front and rear spars. The NTSB determined that the probable causes of this accident (investigation number FTW04FA025) were as follows: "The non-compliance with applicable Airworthiness Directive, which required wing spar inspections, and the continued operation of the aircraft beyond the compliance time extension granted and per the approved Alternate Means of Compliance. Also causal was the operation of the aircraft outside of its flight "G" load limitations."

On December 7, 2004, a T-34A single-engine airplane (tail number N141SW) was destroyed when it impacted terrain following an in-flight separation of the left wing and subsequent loss of control near Montgomery, Texas. The airline transport pilot and pilot-rated passenger were both fatally injured. A review of maintenance records showed that the accident airplane was in compliance with AD 2001-13-18 R1, which the FAA issued as a result of an accident near Montgomery, Texas, in November 2003. Examination of the wreckage revealed the left wing forward spar carry-through structure failed about 6 inches inboard of the forward wing attachment point, and the aft spar failed about 4 inches outboard of the aft wing attachment point.

In addition, the investigation of the accident (investigation number DEN05FA032) revealed visual evidence of fatigue in locations not previously addressed by AD 2001-13-18 R1.

On December 10, 2004, the FAA issued an Emergency Airworthiness Directive, AD 2004-25-51, to address the preliminary findings of the investigation. According to this AD, the owners/operators had 10 hours time-in-service, and no later than 30 days after receipt of the emergency AD to return/position the airplane to a home base, hangar, maintenance facility, etc., until further action was determined by the FAA.

To aid with the assessment of aging acrobatic aircraft, the FAA contracted with the Aging Aircraft Research Laboratory at the National Institute for Aviation Research (NIAR) to teardown and inspect two sets of wings from a high-time T-34A aircraft. Due to the recent history of fatigue cracking and failure, a destructive evaluation of the T-34A would be useful to the FAA for specifically addressing T-34A concerns and, in a general sense, for assessing the condition of a high-time acrobatic category aircraft. The teardown evaluation involved performing the inspections prescribed in AD 2001-13-18; disassembly to gain access to the underlying primary structure; paint removal and etching of the wing primary structure to enhance damage detection; post-disassembly nondestructive inspections (NDI), and a detailed, microscopic examination of all primary structure. Cracks were analyzed to determine failure modes.

Figure 1. Typical T-34A Aircraft

2. FIRST WING SET.

In May 2004, wings were acquired from a high-time T-34A acrobatic category airplane with approximately 15,000 flight hours. These wings had been removed from service due to a crack in the left wing rear spar lower cap at WS 66. Prior to the delivery of the wings to NIAR's facility, both wings were already partially disassembled. Since some disassembly was

accomplished prior to the SB inspections, areas called out for inspection in the SB were inspected using an eddy-current surface scanning technique as opposed to bolthole eddy-current. No indications were found during the eddy-current inspection other than the known crack on the left wing rear spar lower cap at WS 66.

A total of four cracks were found on the T-34A wings: one occurring on the left wing rear spar web at WS 168.75, another occurring on the left wing rear spar lower cap at WS 66, and two more occurring at the corresponding location on the left wing rear spar lower doubler. The cracks on the left wing rear spar cap and doubler were determined to be caused by fatigue. At least one area of severe corrosion was found on the left wing front spar forward and aft upper caps and the left wing rear spar web. Light corrosion was found on the front and rear spar inboard landing gear attachment fittings on both the left and right wings. Corrosion was also observed on the following bathtub fittings: left wing front spar upper and lower, left wing rear spar lower, right wing front spar upper and lower, and right wing rear spar upper. An assessment of the severity of the corrosion was not possible because the location of the corrosion in the attachment fittings prevented accurate measurements of pit depth. In general, the upper bathtub fittings exhibited more corrosion than the lower ones. Pitting was the only type of corrosion observed on the first set of T-34A wings.

2.1 THE SB 57-3329 INSPECTIONS.

Figure 2 shows the first set of T-34A wings as received, and figure 3 shows the areas of the T-34A wings that were inspected per Raytheon SB 57-3329. Since the left and right wings were partially disassembled, all areas were inspected with an eddy-current surface probe. The aft reinforcement and the leading-edge were removed prior to delivery to NIAR, so these areas were not inspected. The only indication found with the pencil probe was the known crack at WS 66. As shown in figure 3, Raytheon SB 57-3329 prescribes bolthole eddy-current inspections at the following locations:

- Five fasteners on the aft lower reinforcement of the front spar inboard of WS 34
- Four fasteners on the lower side of the front spar at WS 34
- Two fasteners on the lower leading-edge hinge angle outboard of WS 63
- Forward trunnion fastener location
- Two aft trunnion fasteners

The following locations required eddy-current surface scan:

- Front spar lower cap outside of each fastener row from the attachment fittings to the wing tips
- Step tang in the lower aft bathtub fittings
- Aft reinforcement on the front spar

- Aft flange of the leading-edge access panel at WS 63
- Aft flange of the leading-edge fuel cell access panel

Figure 2. First Set of T-34A Wings as Received

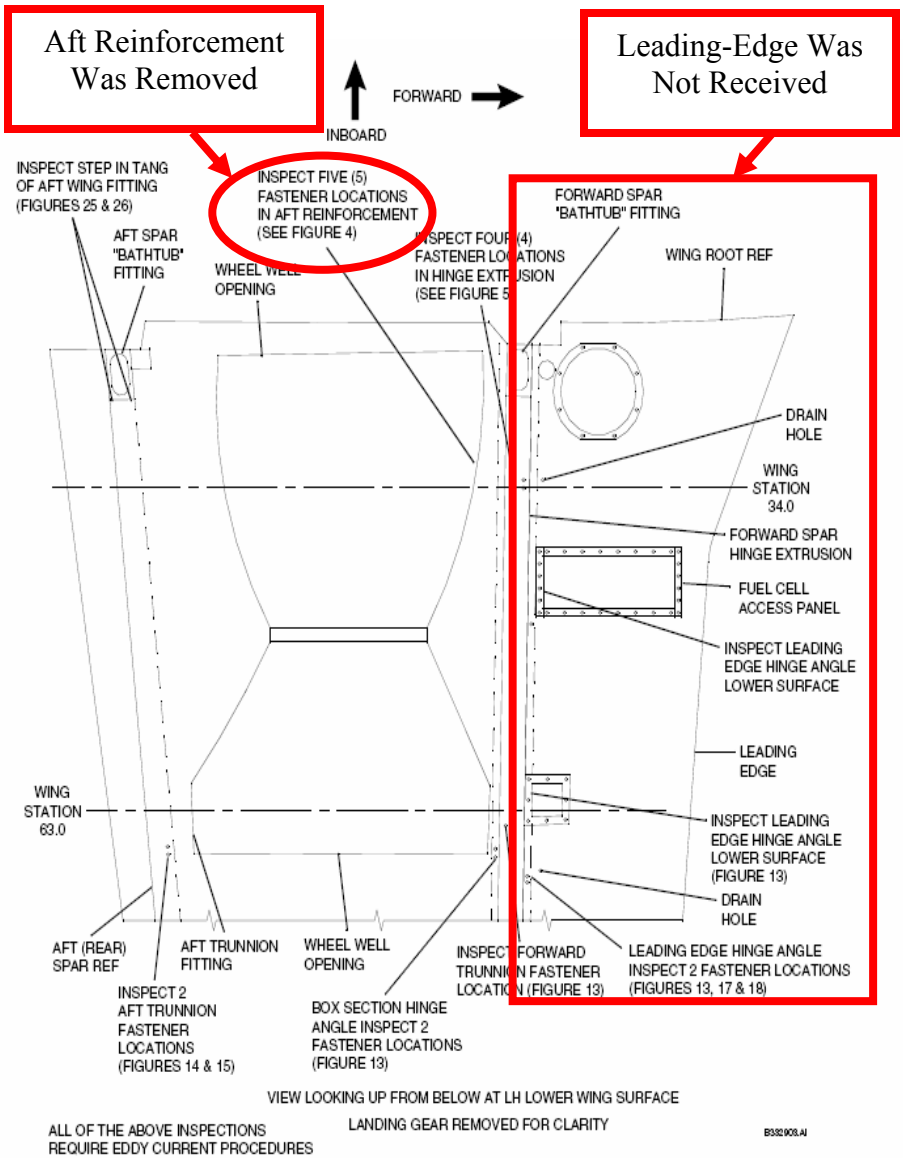

Figure 3. Locations of Eddy-Current Inspections

2.2 DISASSEMBLY PHASE.

The wings were disassembled to better evaluate damage to the critical structure. All details were fully disassembled, paint stripped, and etched to enhance damage detection. Disassembly methods were selected to minimize potential damage to the underlying structure. Following the disassembly, all structural details were paint stripped using plastic media blasting and etched with a sodium hydroxide base to enhance damage detection during the post-disassembly NDI and microscopic examination.

2.3 POST-DISASSEMBLY NDIs.

Following the disassembly of the first set of T-34A wings, a comprehensive NDI using fluorescent liquid penetrant was performed on all primary structure including the components of the spars and all attachment fittings. This inspection was performed to aid in the identification of all defects present in the structure. At least one defect was found during the post-disassembly NDI on each of the following wing components: left wing front spar, left wing rear spar, left and right wing landing gear attachment fittings, and left and right wing bathtub fittings.

2.3.1 Left Wing.

Four cracks were identified on the left wing during the post-disassembly NDI: one on the left-wing rear spar web, one on the rear spar lower cap, and two on the rear spar lower doubler. Nine areas of corrosion were found on the left wing during these inspections on the front spar forward and aft upper caps, front and rear spar inboard landing gear attachment fittings, front spar upper and lower bathtub fittings, and the rear spar lower bathtub fitting.

2.3.1.1 Left Wing Front Spar.

The structural stackup of the left wing front spar is shown in figures 4 and 5. Two areas of corrosion were found on the left wing front spar forward upper cap, shown in figure 6. These areas of corrosion, located from WS 37.5 to 39 and from WS 49 to 57.5, are shown in figures 7 and 8, respectively. Combined, these two areas of corrosion covered a surface area of 1.84 square inches. Two areas of corrosion were also found on the left wing front spar aft upper cap, shown in figure 9. Located from WS 38 to 40 and WS 48.75 to 54.5, these two areas of corrosion covered a total surface area of 1.24 square inches. The area of corrosion located from WS 38 to 40 is shown in figure 10, and figure 11 shows the area of corrosion from WS 48.75 to 54.5.

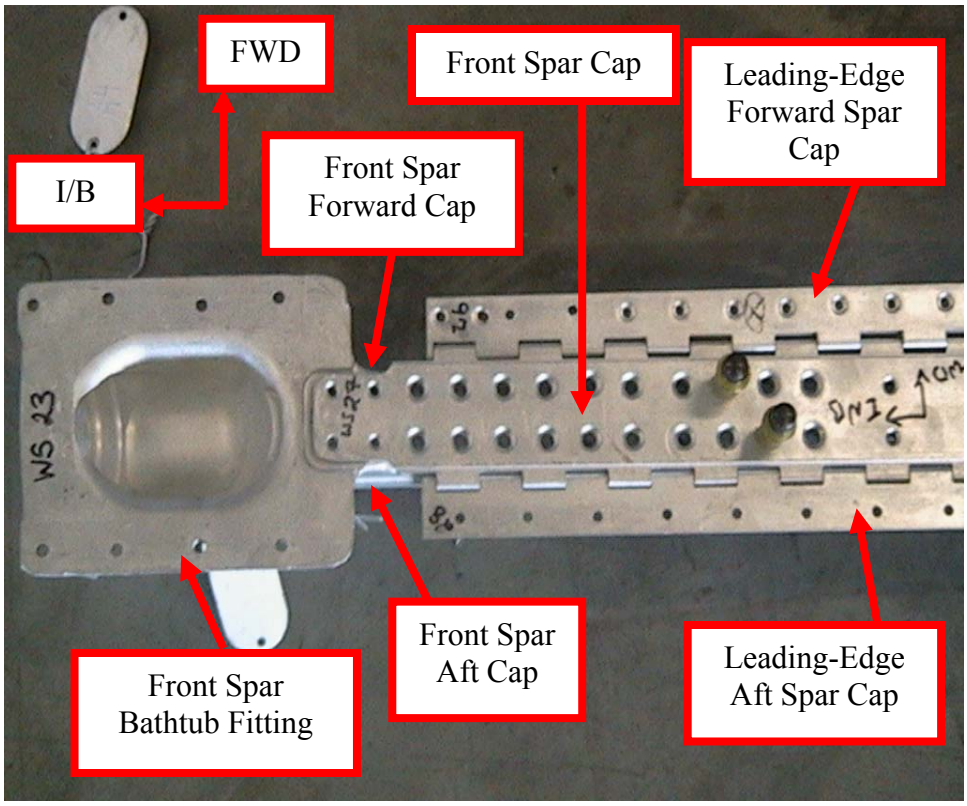

Figure 4. Front Spar Structural Stackup

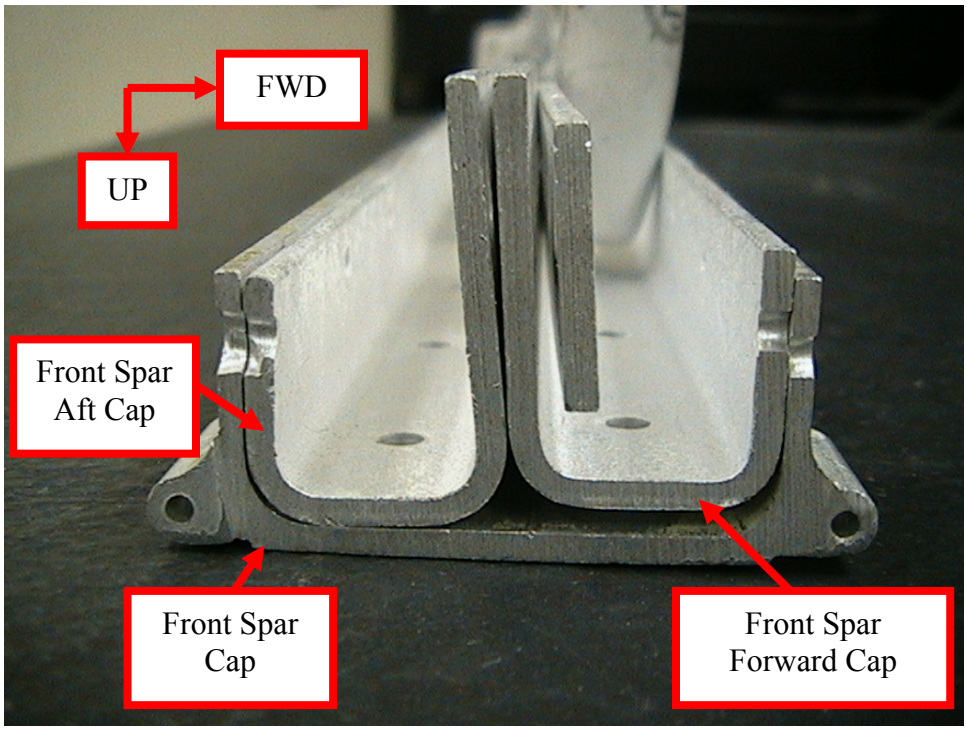

Figure 5. Front Spar Forward and Aft Cap Structural Stackup

Figure 6. Left Wing Front Spar Forward Upper Cap

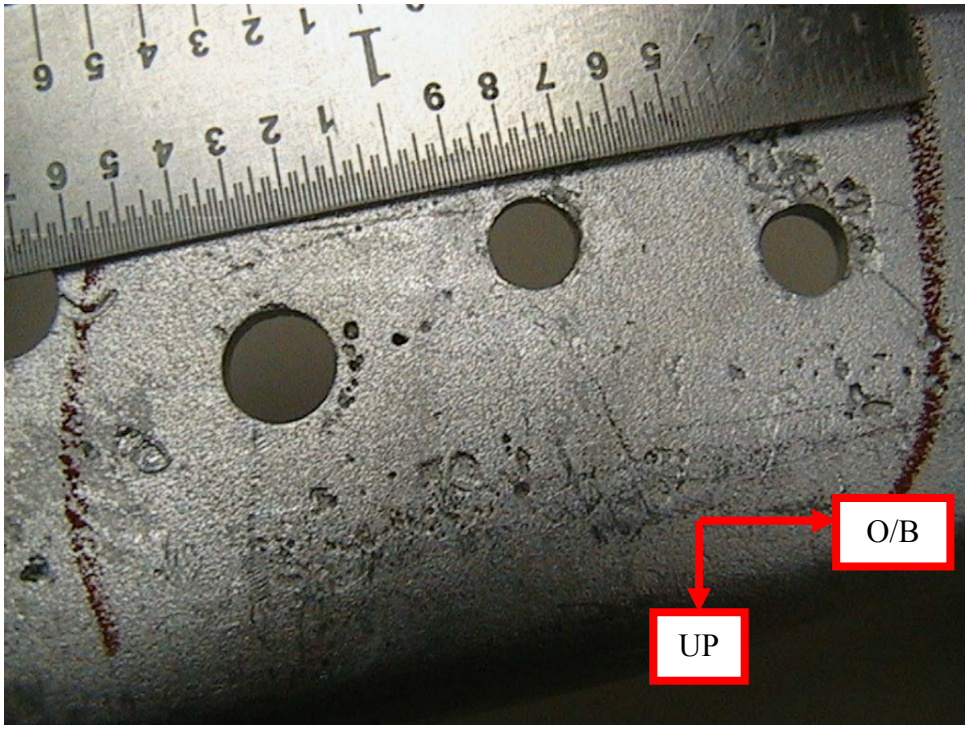

Figure 7. Corrosion on the Left Wing Front Spar Forward Upper Cap
WS 37.5-39

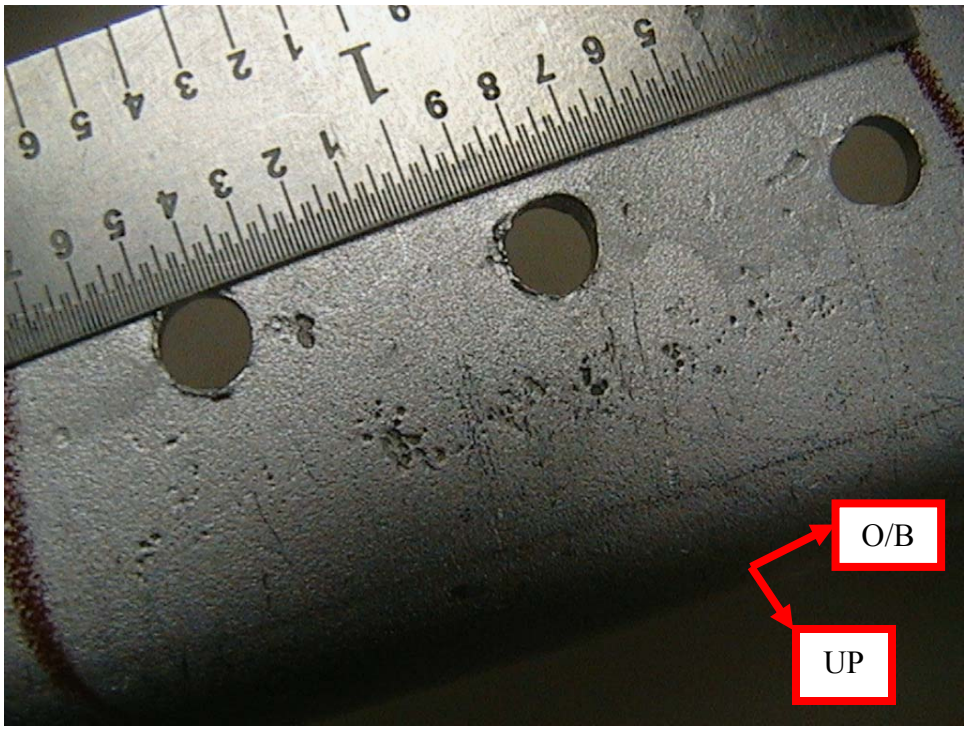

Figure 8. Corrosion on the Left Wing Front Spar Forward Upper Cap
WS 49-57.5

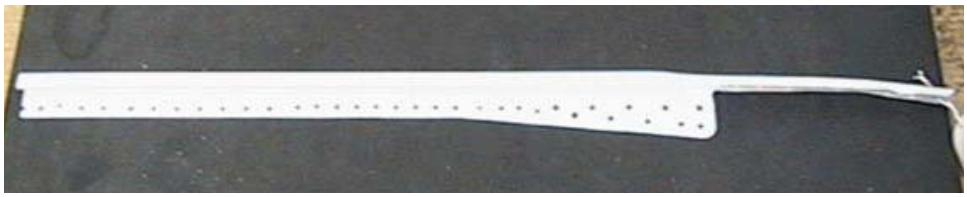

Figure 9. Left Wing Front Spar Aft Upper Cap

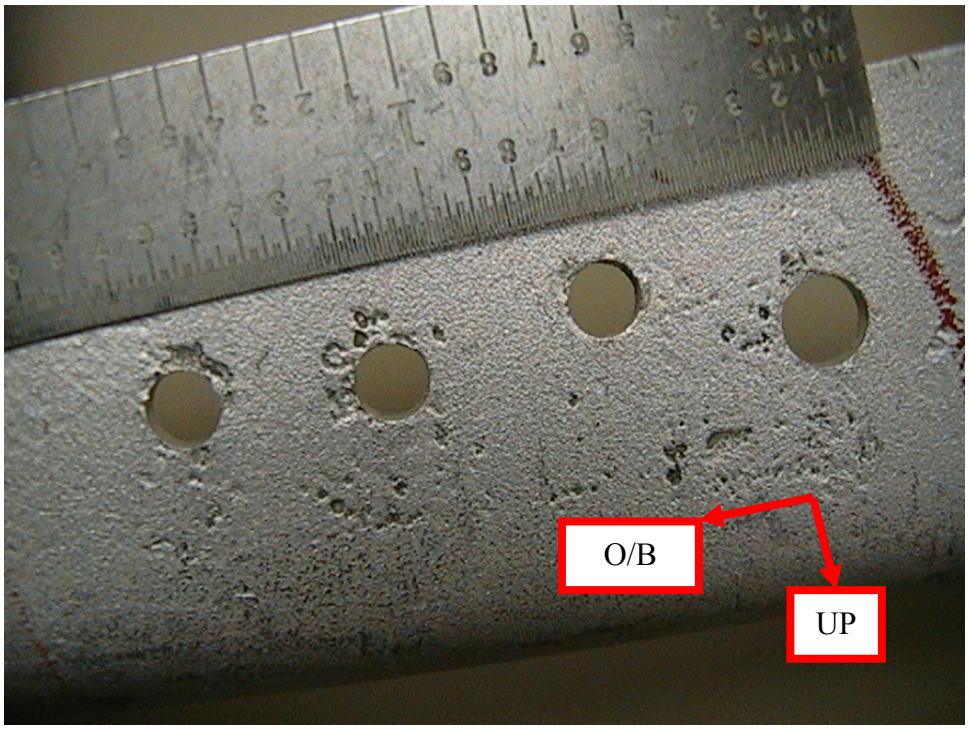

Figure 10. Corrosion on the Left Wing Front Spar Aft Upper Cap
WS 38-40

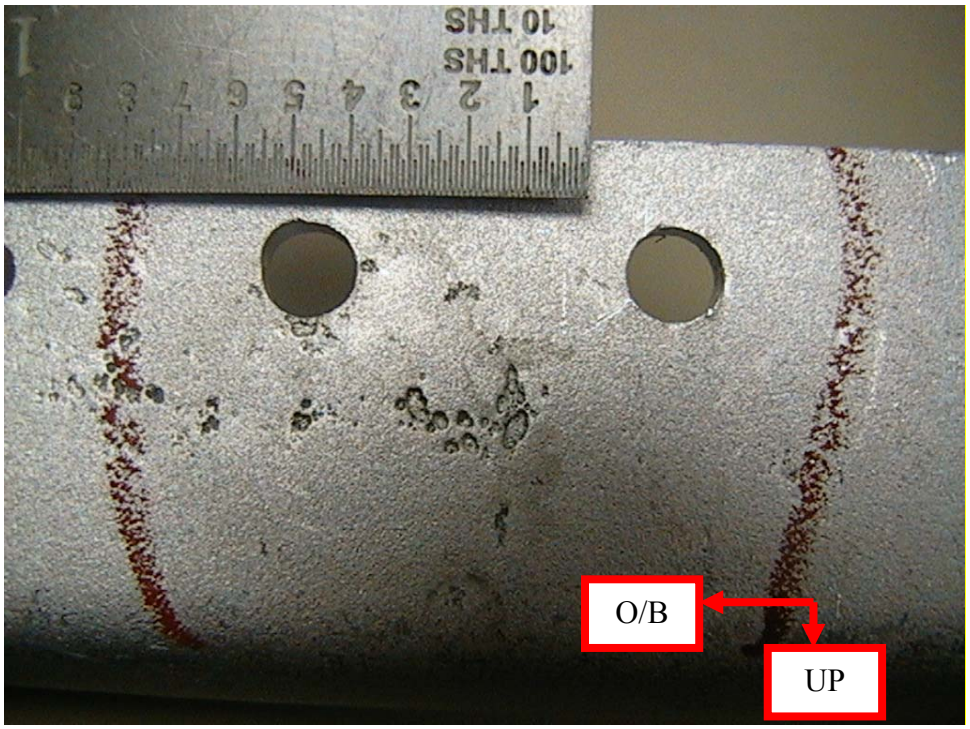

Figure 11. Corrosion on the Left Wing Front Spar Aft Upper Cap
WS 48.75-54.5

2.3.1.2 Left Wing Rear Spar.

Four cracks were found on the left wing rear spar, whose structural stackup is shown in figure 12. The web, shown in figure 13, had a 0.1-inch crack, which is pictured in figure 14 during the fluorescent liquid penetrant process, at WS 168.75. The left wing rear spar lower doubler, shown in figure 15, had two cracks, measuring 0.12 and 0.07 inch in length, at WS 66. A picture of these cracks under ultraviolet light is provided in figure 16. Another crack was found on the left wing rear spar lower cap, shown in figure 17, at WS 66. This crack measured 0.17 inch, and it is shown in figure 18.

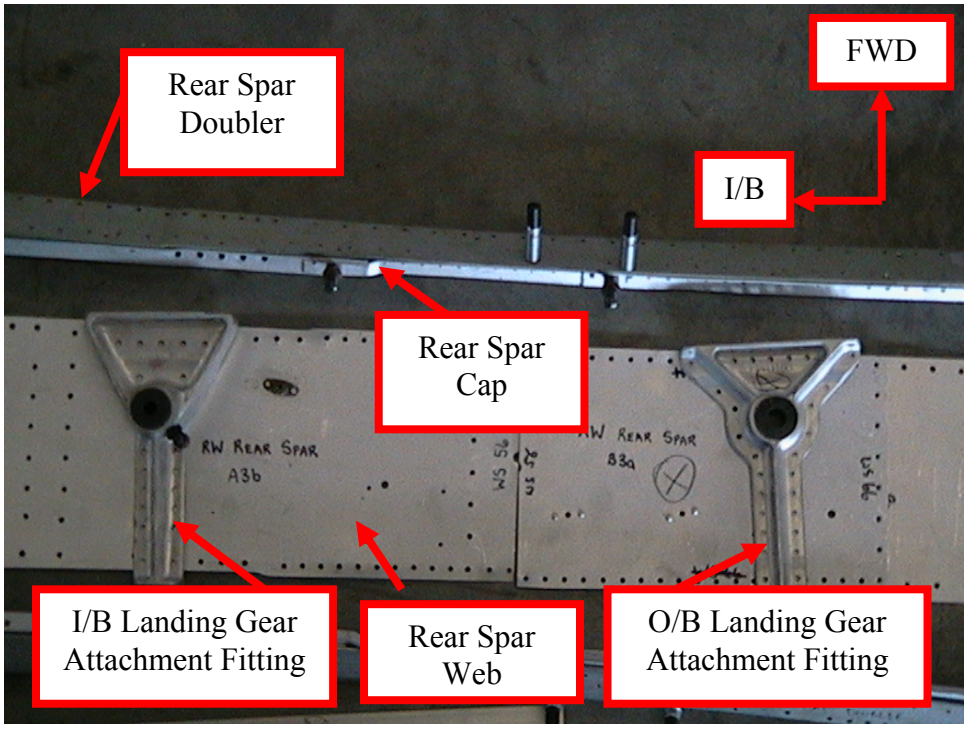

Figure 12. Rear Spar Structural Stackup

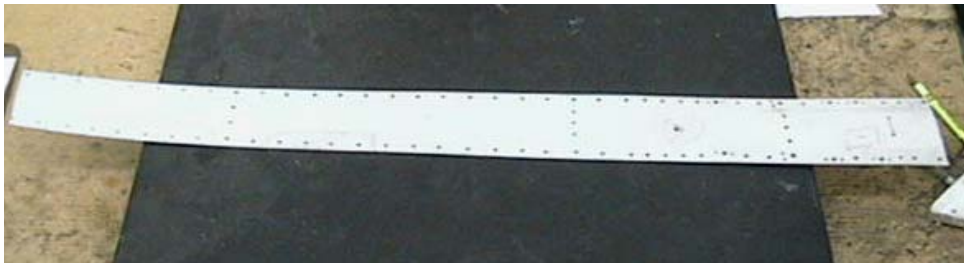

Figure 13. Left Wing Rear Spar Web

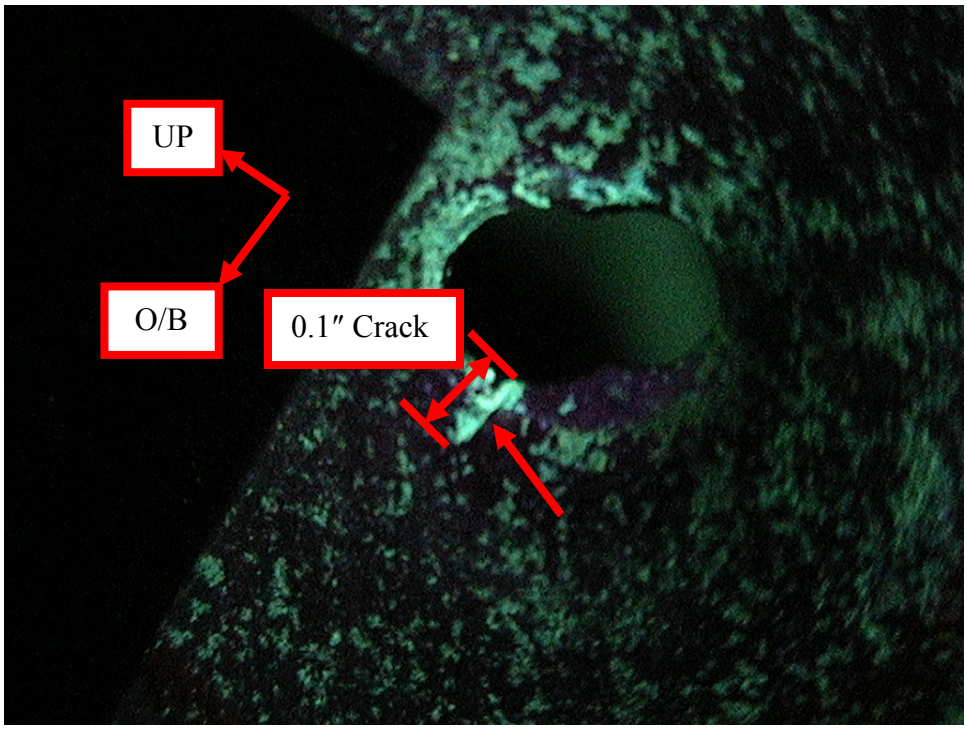

Figure 14. Crack in the Left Wing Rear Spar Web WS 168.75

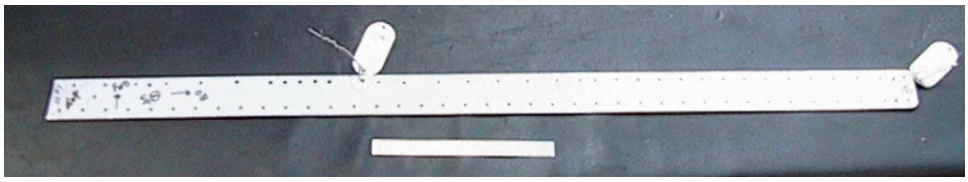

Figure 15. Left Wing Rear Spar Lower Doubler

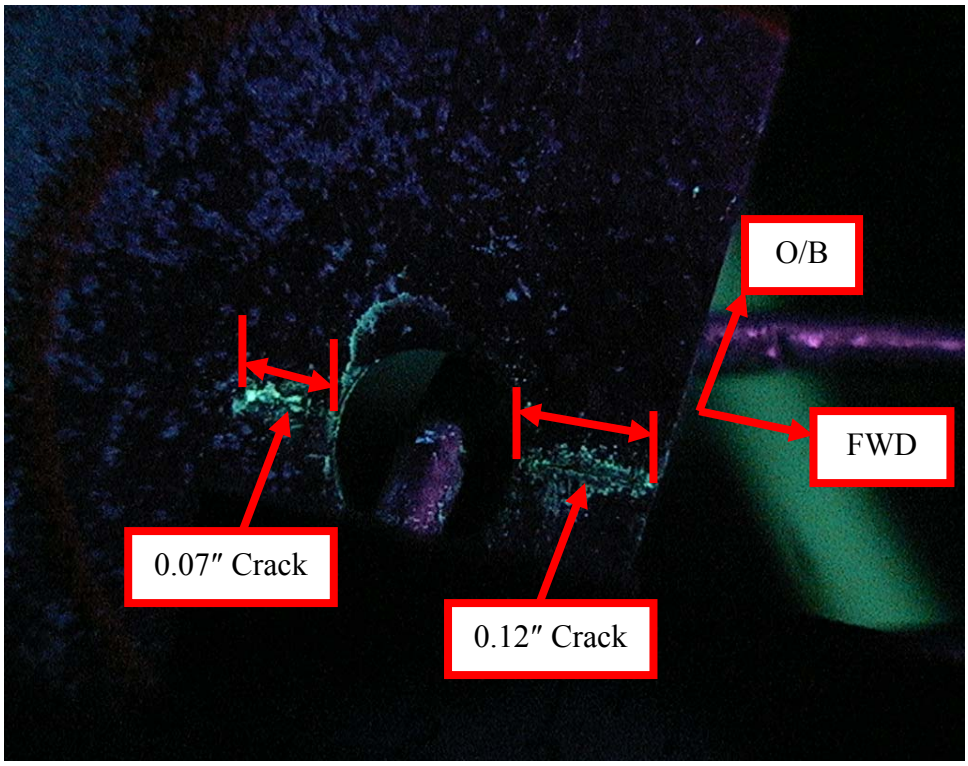

Figure 16. Cracks in the Left Wing Rear Spar Lower Doubler WS 66

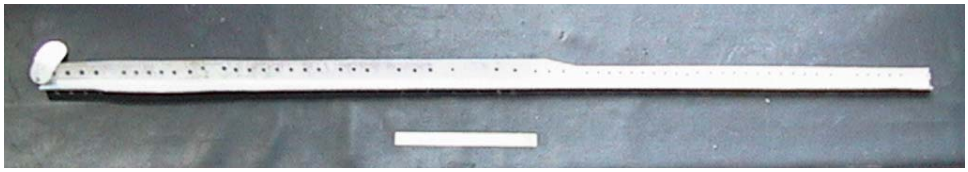

Figure 17. Left Wing Rear Spar Lower Cap

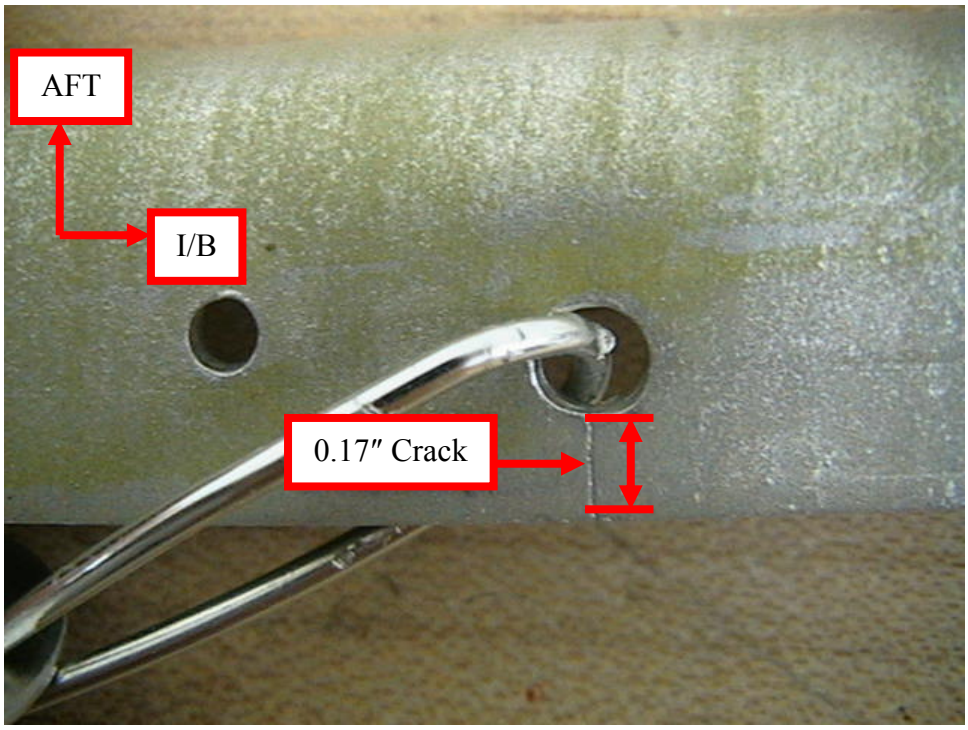

Figure 18. Crack in the Left Wing Rear Spar Lower Cap WS 66

2.3.1.3 Left Wing Attachment Fittings.

Three areas of corrosion were found on the left wing attachment or bathtub fittings, ranging in surface area from 1.56 to 6 square inches. The corrosion occurred on the left wing front spar upper and lower bathtub fittings and the rear spar lower bathtub fitting. Two areas of corrosion were also noted on the left wing front and rear spar inboard landing gear attachment fittings.

2.3.1.3.1 Left Wing Landing Gear Attachment Fittings.

One area of corrosion, measuring 0.38 square inch, was noted on the left wing front spar inboard landing gear attachment fitting, shown in figure 19. This area of corrosion is shown in figure 20. Another area of corrosion was found on the left wing rear spar inboard landing gear attachment fitting, shown in figure 21. This area of corrosion, shown in figure 22, encompassed an area of 2.57 square inches. Both areas of corrosion were located on the landing gear attachment fittings at WS 46.

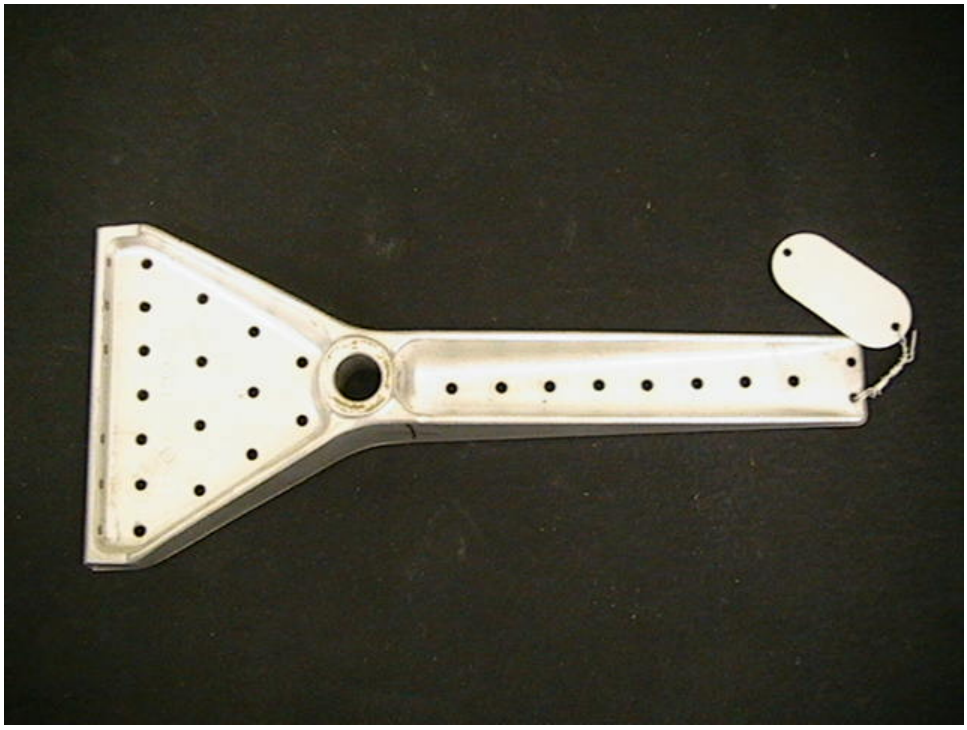

Figure 19. Left Wing Front Spar Inboard Landing Gear Attachment Fitting

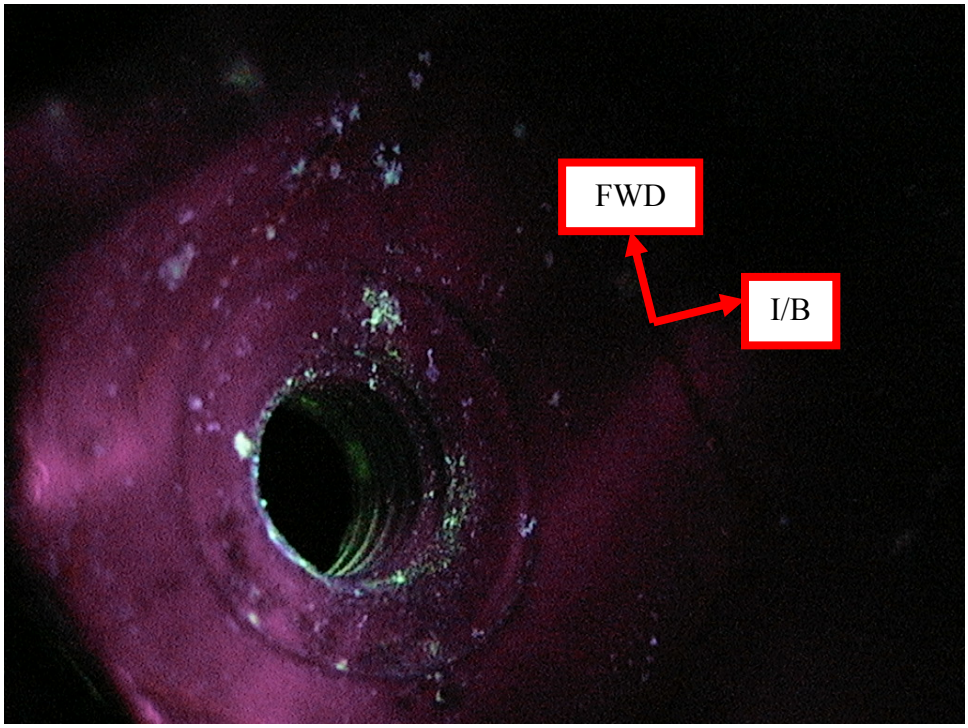

Figure 20. Corrosion on the Left Wing Front Spar Inboard Landing Gear Attachment Fitting at WS 46

Figure 21. Left Wing Rear Spar Inboard Landing Gear Attachment Fitting

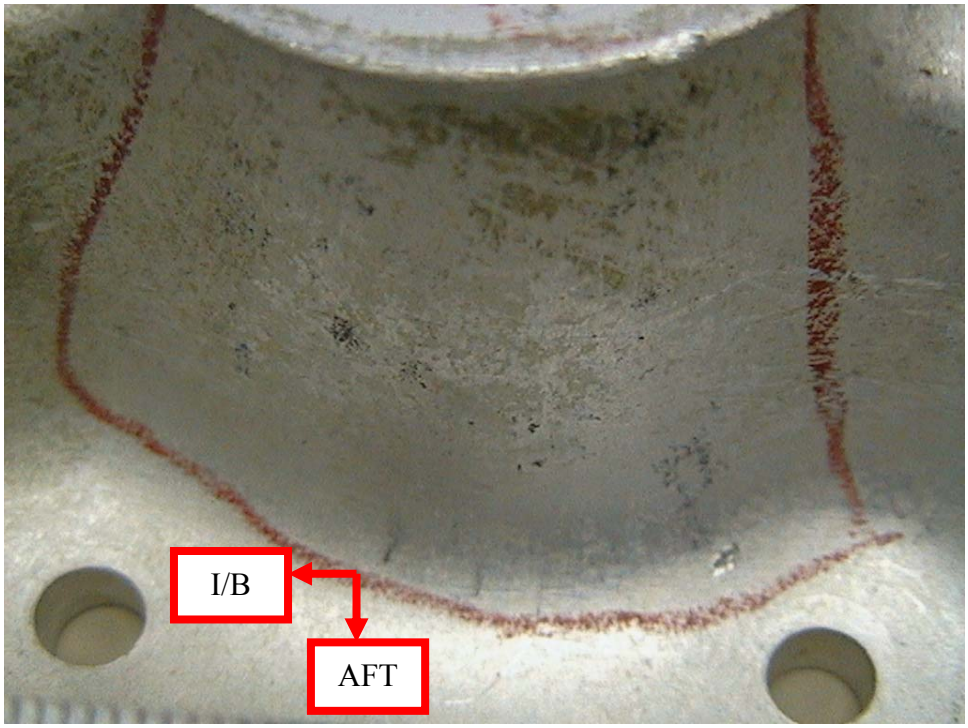

Figure 22. Corrosion on the Left Wing Rear Spar Inboard Landing Gear Attachment at WS 46

2.3.1.3.2 Left Wing Bathtub Fittings.

Three areas of corrosion were found on the left wing bathtub fittings. Figure 23 shows the front spar upper bathtub fitting, and figure 24 shows a 4.48-square-inch area of corrosion located from WS 23.5 to 25.75. Figure 25 shows the left wing front spar lower bathtub fitting, and figure 26 shows a 6-square-inch area of corrosion located on the bathtub fitting from WS 23 to 27.5. The rear spar lower bathtub fitting, shown in figure 27, had an area of corrosion located from WS 24.75 to 26. This 1.56-square-inch area of corrosion is shown in figure 28.

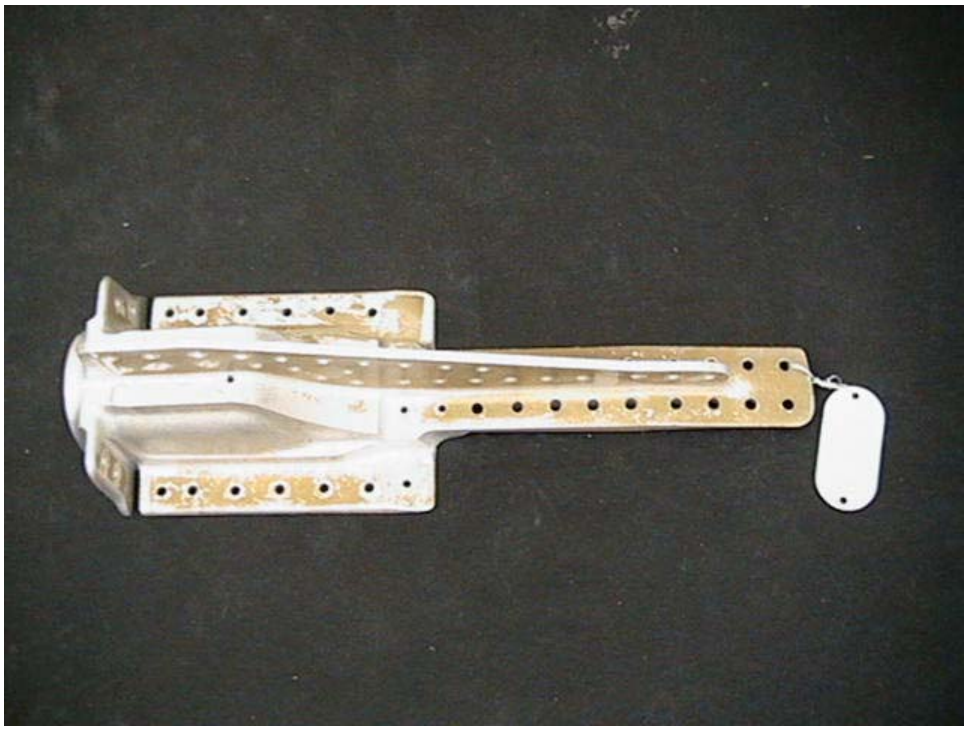

Figure 23. Left Wing Front Spar Upper Bathtub Fitting

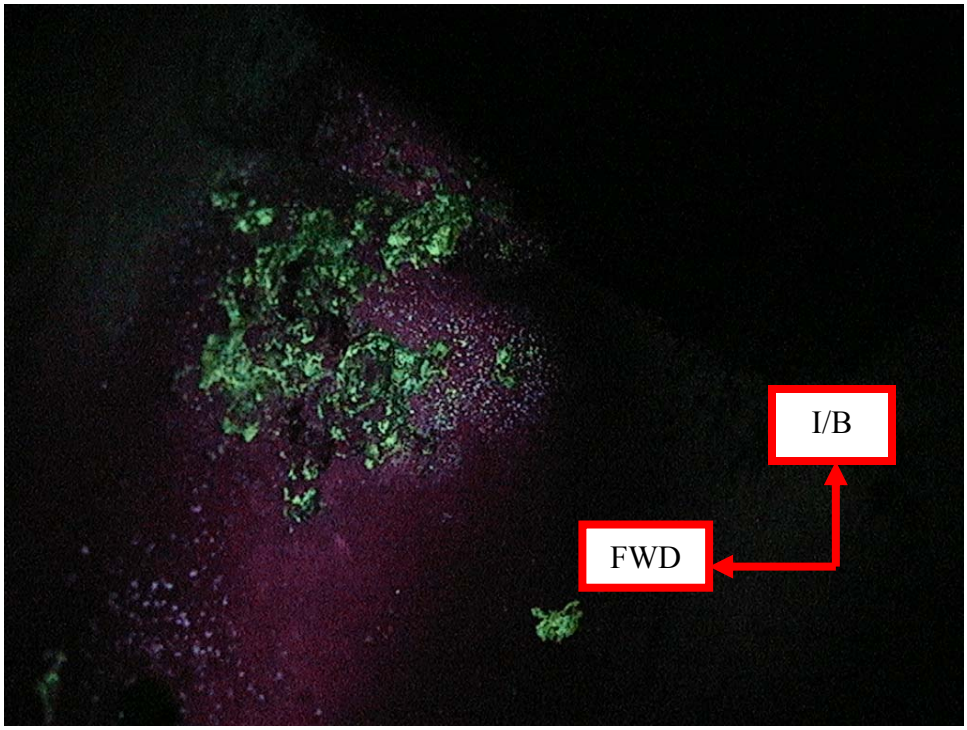

Figure 24. Corrosion on the Left Wing Front Spar Upper Bathtub Fitting
WS 23.5-25.75

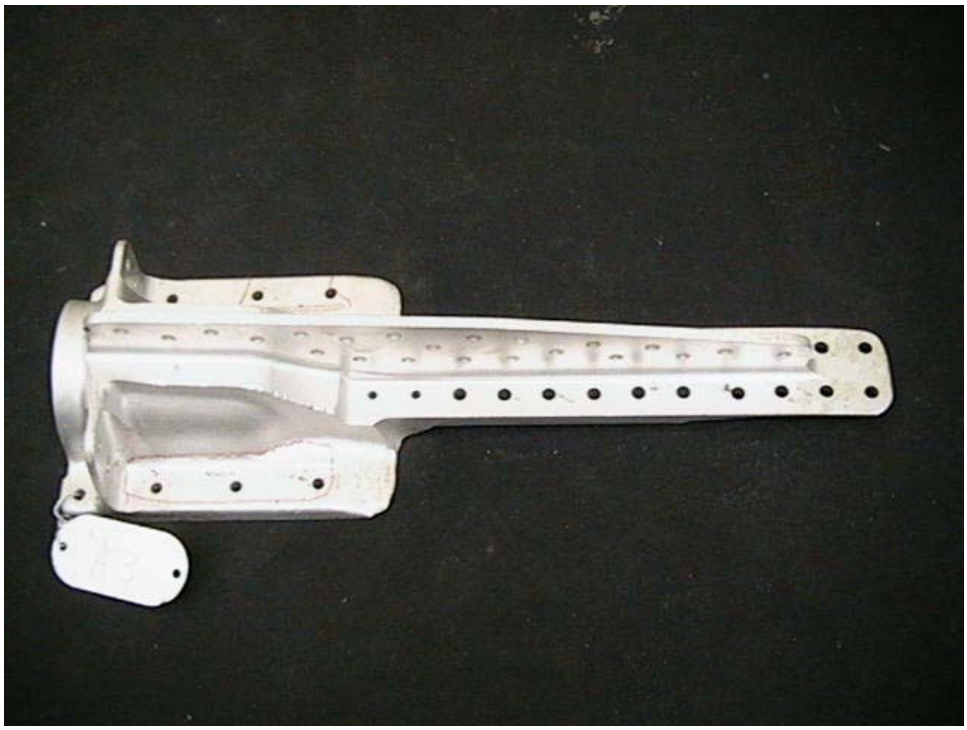

Figure 25. Left Wing Front Spar Lower Bathtub Fitting

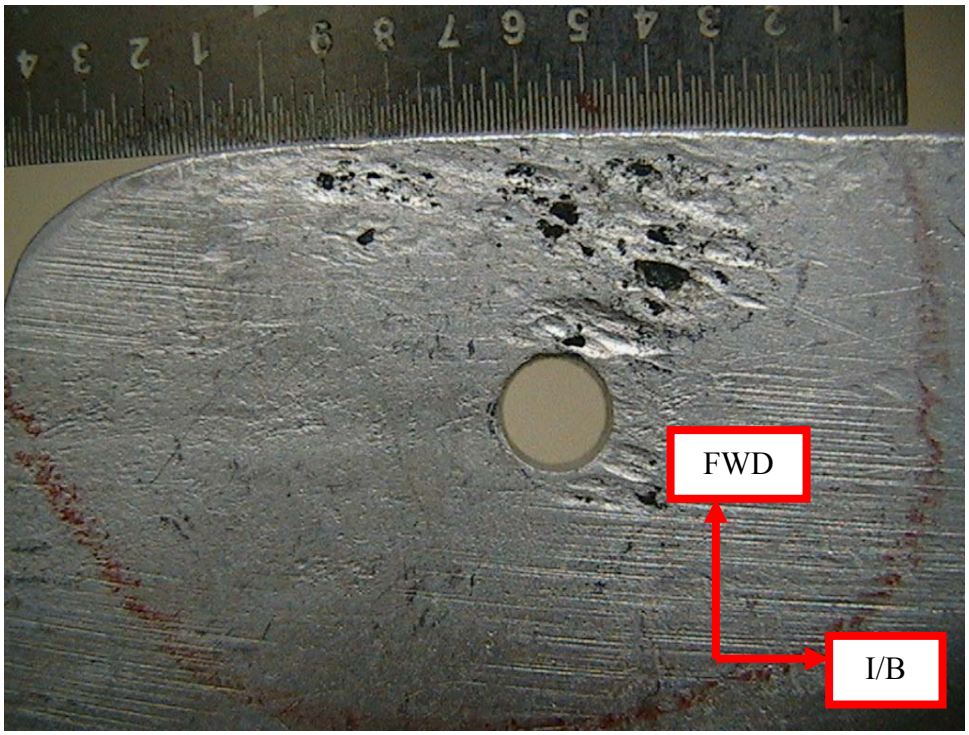

Figure 26. Corrosion on the Left Wing Front Spar Lower Bathtub Fitting WS 23-27.5

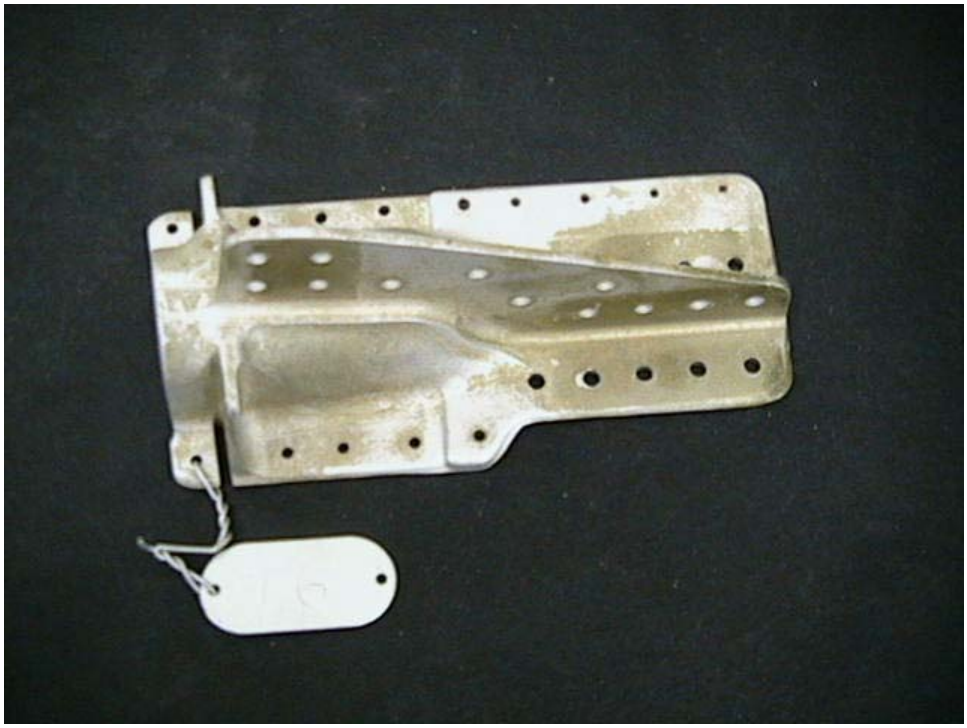

Figure 27. Left Wing Rear Spar Lower Bathtub Fitting

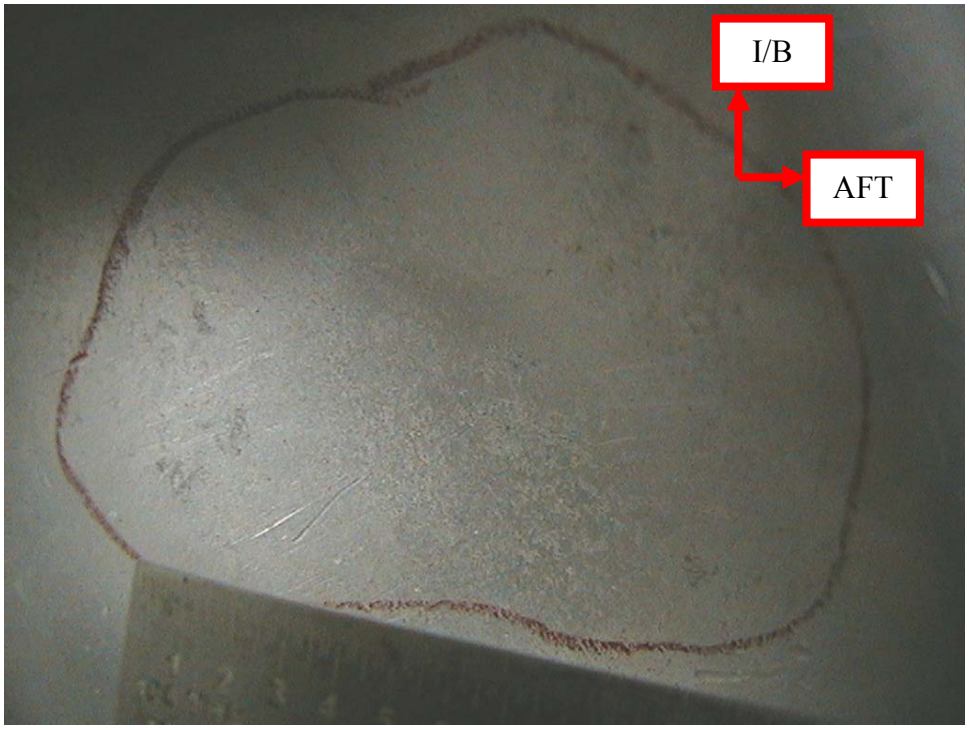

Figure 28. Corrosion on the Left Wing Rear Spar Lower Bathtub Fitting WS 24.75-26

2.3.2 Right Wing.

Two areas of corrosion were identified on the right wing landing gear attachment fittings, and three areas of corrosion were found on the right wing bathtub fittings, ranging in surface area from 3.05 to 5.12 square inches.

2.3.2.1 Right Wing Front Spar.

No defects were found on the right wing front spar during post-disassembly NDI.

2.3.2.2 Right Wing Rear Spar.

No defects were found on the right wing rear spar during post-disassembly NDI.

2.3.2.3 Right Wing Attachment Fittings.

A total of five areas of corrosion were found on the right wing landing gear attachment fittings and the bathtub fittings, ranging in surface area from 0.88 to 5.12 square inches. These areas of corrosion were located on the front and rear spar inboard landing gear attachment fittings, front spar upper and lower bathtub fittings, and the rear spar upper bathtub fitting.

2.3.2.3.1 Right Wing Landing Gear Attachment Fittings.

The right wing front spar inboard landing gear attachment fitting, shown in figure 29, had one area of corrosion, shown in figure 30, which covered a surface area of 0.99 square inch.

Figure 31 shows the right wing rear spar inboard landing gear attachment fitting with a 0.88-square-inch area of corrosion, shown in figure 32. Both defects were located at WS 46 of their respective fittings.

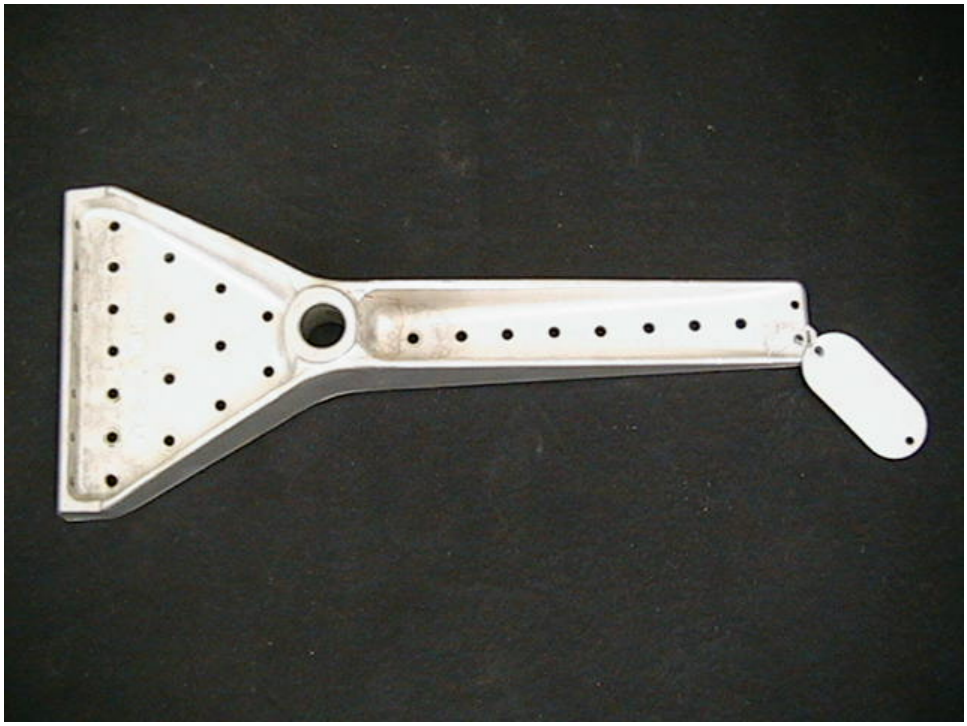

Figure 29. Right Wing Front Spar Inboard Landing Gear Attachment Fitting

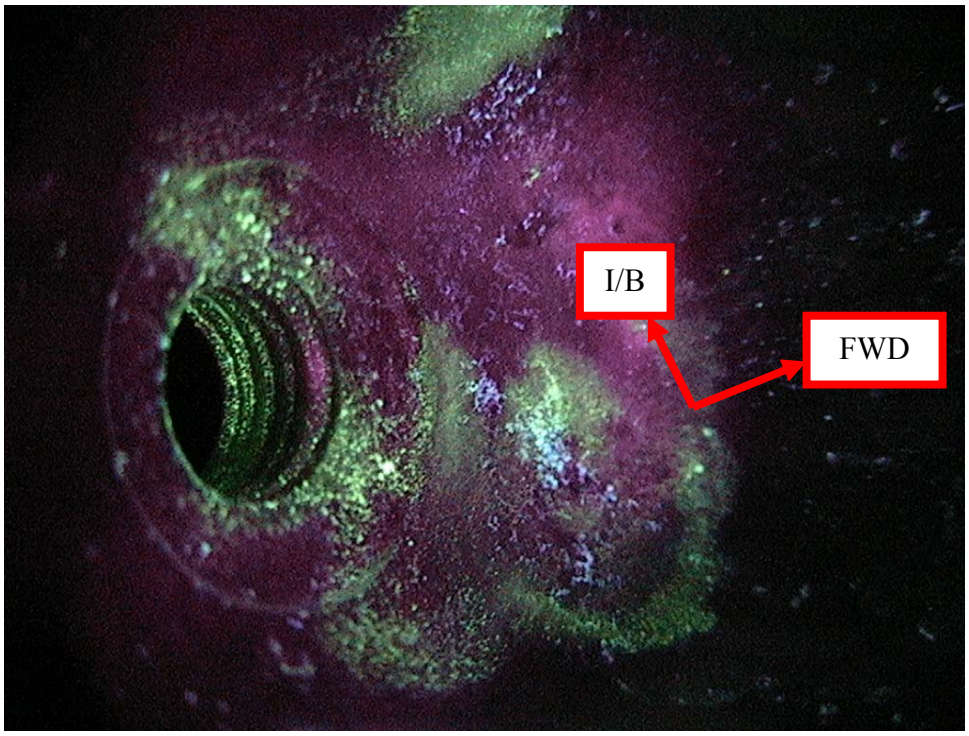

Figure 30. Corrosion on the Right Wing Front Spar Inboard Landing Gear Attachment Fitting WS 46

Figure 31. Right Wing Rear Spar Inboard Landing Gear Attachment Fitting

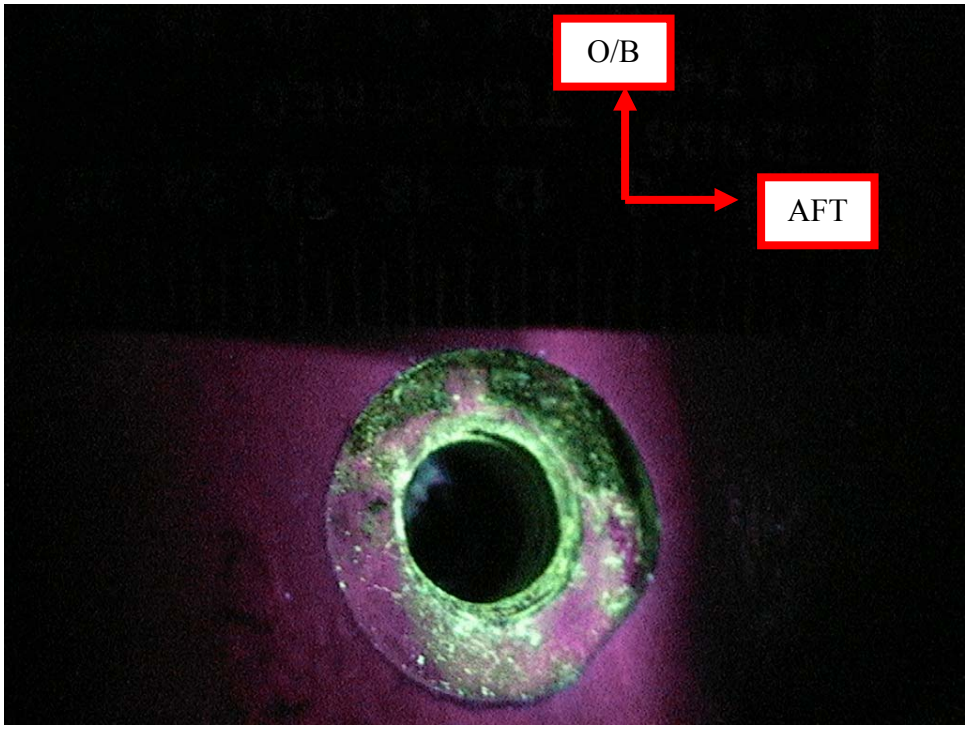

Figure 32. Corrosion on the Right Wing Rear Spar Inboard Landing Gear Attachment Fitting WS 46

2.3.2.3.2 Right Wing Bathtub Fittings.

Three areas of corrosion were found on the right wing bathtub fittings during the post-disassembly NDIs. A 4.71-square-inch area of corrosion was found on the right wing front spar lower bathtub fitting, shown in figure 33, from WS 23 to 27.25, as shown in figure 34. The right wing front spar upper bathtub fitting, pictured in figure 35, had a 3.05-square-inch area of corrosion, shown in figure 36, from WS 23.5 to 28. A 5.12-square-inch area of corrosion was found on the right wing rear spar upper bathtub fitting, pictured in figure 37, from WS 23.5 to 27. This area of corrosion is shown in figure 38.

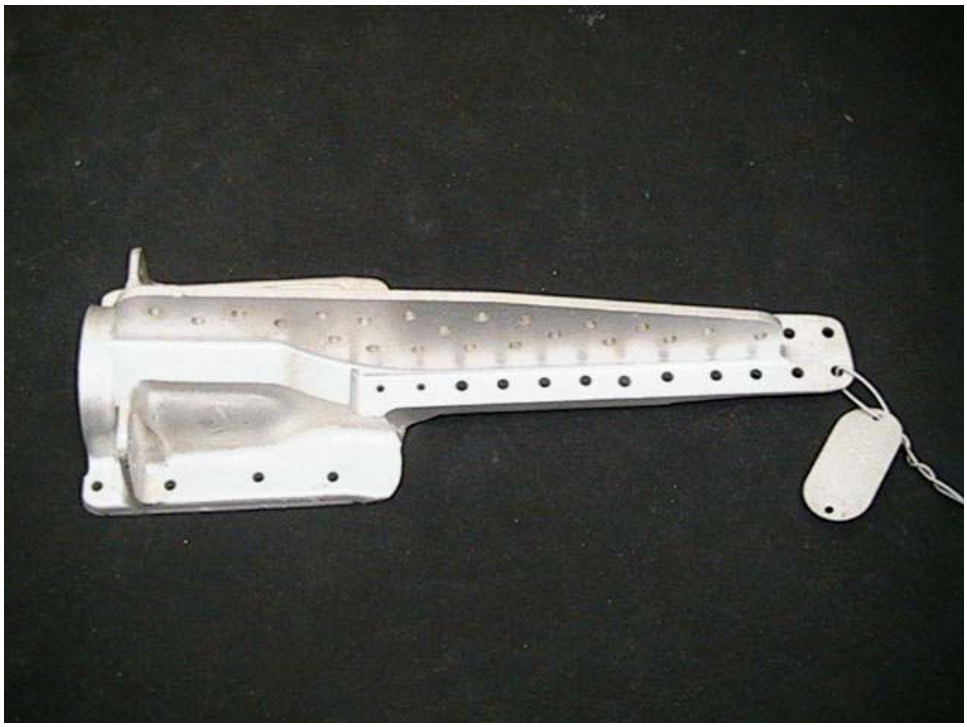

Figure 33. Right Wing Front Spar Lower Bathtub Fitting

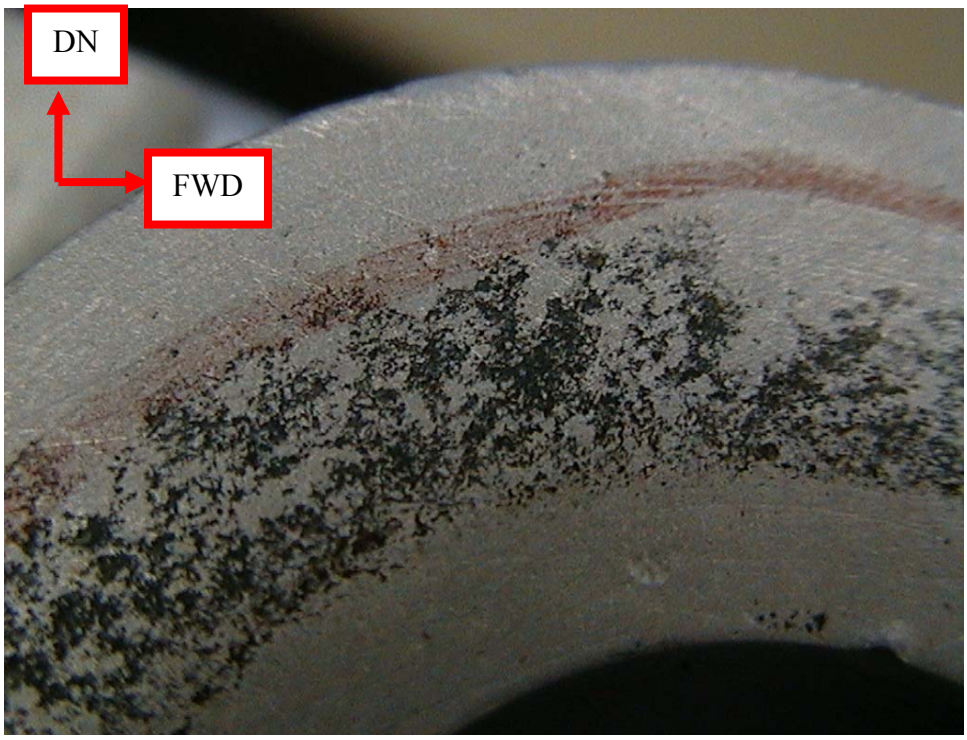

Figure 34. Corrosion on the Right Wing Front Spar Lower Bathtub Fitting WS 23-27.75

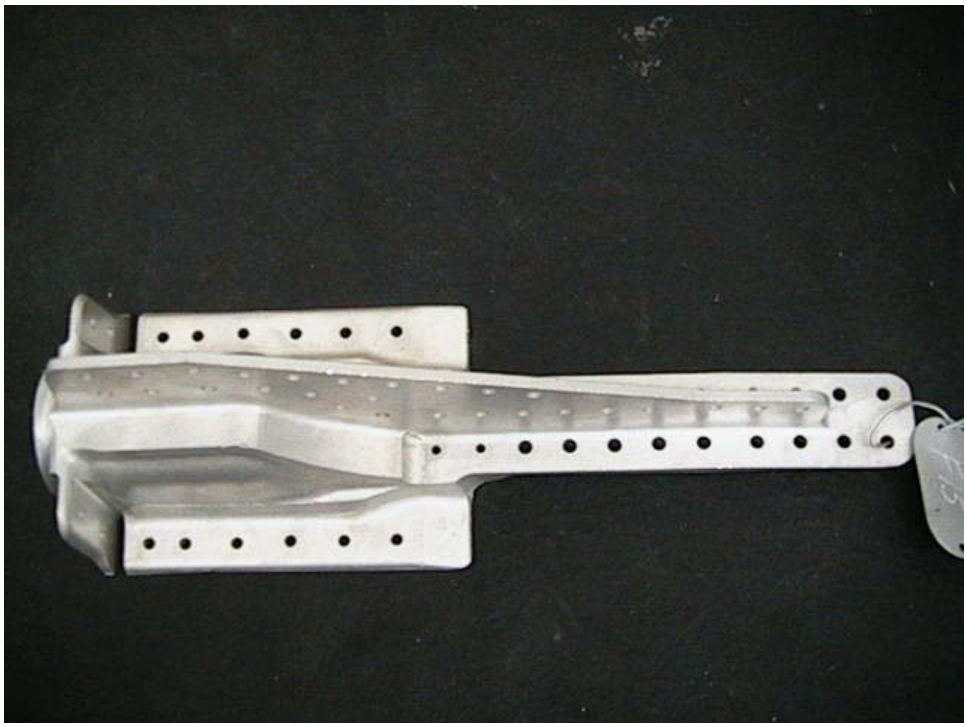

Figure 35. Right Wing Front Spar Upper Bathtub Fitting

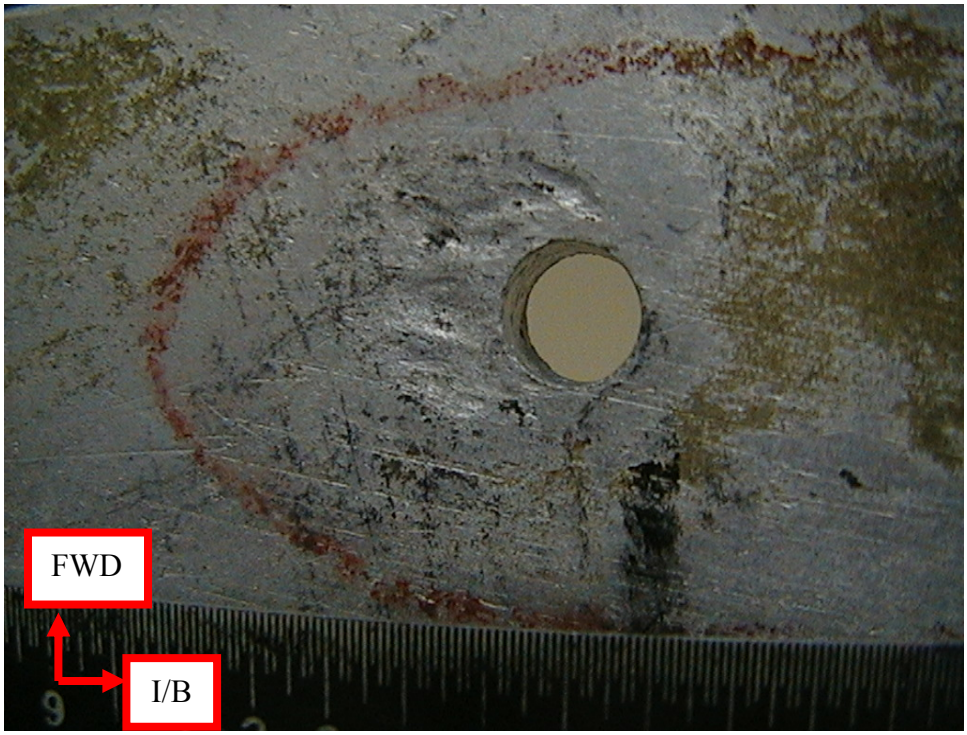

Figure 36. Corrosion on the Right Wing Front Spar Upper Bathtub Fitting WS 23.5-28

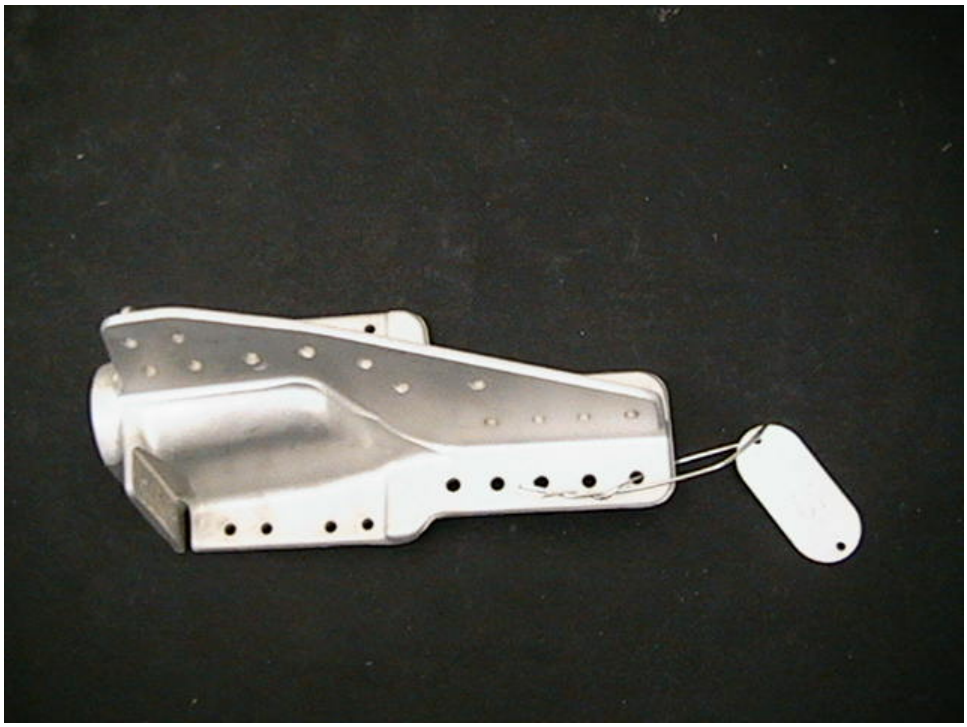

Figure 37. Right Wing Rear Spar Upper Bathtub Fitting

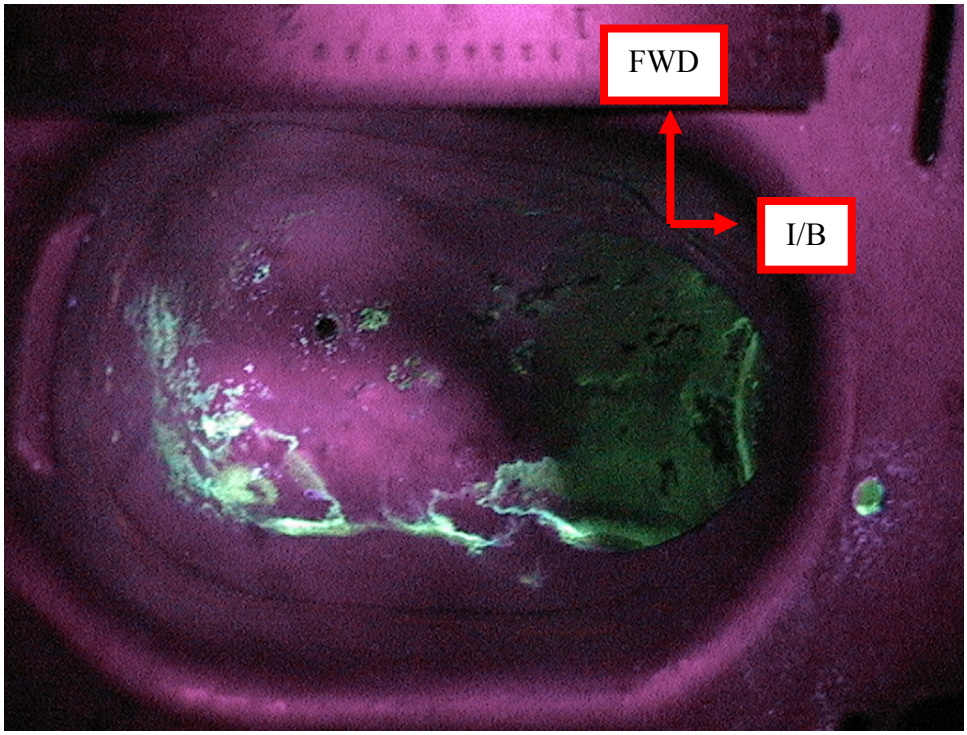

Figure 38. Corrosion on the Right Wing Rear Spar Upper Bathtub Fitting WS 23.5-27

2.4 MICROSCOPIC EXAMINATION.

All primary structure was examined with the aid of a 7-45 power optical microscope following the post-disassembly NDI. The lengths of all cracks were noted, as well as the surface area and depth of each area of corrosion. The severity of the corrosion was classified by the percentage of the thickness loss as follows:

- Light = 0%-2% thickness loss
- Light-Moderate = 2%-5% thickness loss
- Moderate = 5%-7% thickness loss
- Moderate-Severe = 7%-10% thickness loss
- Severe =>10% thickness loss

Corrosion effects were classified by percentage of thickness loss since it seemed most representative of the actual damage done by corrosion. Typically, corrosion is classified by pit depth; however, for the purposes of this study, pit depth would not be representative of the severity of damage caused. The different classification levels used in this program are unique to this research and are not representative of other studies. NIAR recommends that these classification levels be used for future studies. It is important to note that corrosion is not assumed as uniform throughout the entire area, but that it represents the maximum depth of corrosion in that area.

2.4.1 Left Wing.

Three cracks and eleven areas of corrosion were identified during the microscopic examination of the left wing. These cracks, located in the left wing rear spar lower cap and the left wing rear spar lower doubler, varied in length from 0.078 to 0.172 inch. Corrosion was found on the left wing front spar forward and aft caps, rear spar web, front and rear spar inboard landing gear attachment fittings, front spar upper and lower bathtub fittings, and the rear spar lower bathtub fitting. These areas of corrosion ranged in severity from light corrosion to severe corrosion with localized thickness losses of up to 23.5%. Accurate pit depths could not be determined on the bathtub fittings due to the location of the corrosion in the fittings. Refer to figures 4 and 5 for the structural stackup of the front spar and figure 12 for the stackup of the rear spar.

2.4.1.1 Left Wing Front Spar.

Five areas of corrosion were found on the left wing front spar. Figure 39 shows an example of the corrosion observed on the left wing front spar forward upper cap at WS 40, 50, and 52. This corrosion encompassed a total surface area of 8.71 square inches and resulted in a maximum localized thickness loss of 23.5%, which is classified as severe corrosion. Two areas of corrosion, pictured in figures 40 and 41, were located on the front spar aft upper cap. Figure 40 shows the area of corrosion located from WS 38 to 40, and figure 41 shows the area of corrosion located from WS 48.75 to 54.5. These two areas of corrosion covered a total surface area of 21.66 square inches and resulted in a local thickness loss of 19.4%, which is classified as severe corrosion.

Figure 39. Corrosion on the Left Wing Front Spar Forward Upper Cap WS 40, 50, and 52

Figure 40. Corrosion on the Left Wing Front Spar Aft Upper Cap WS 38-40

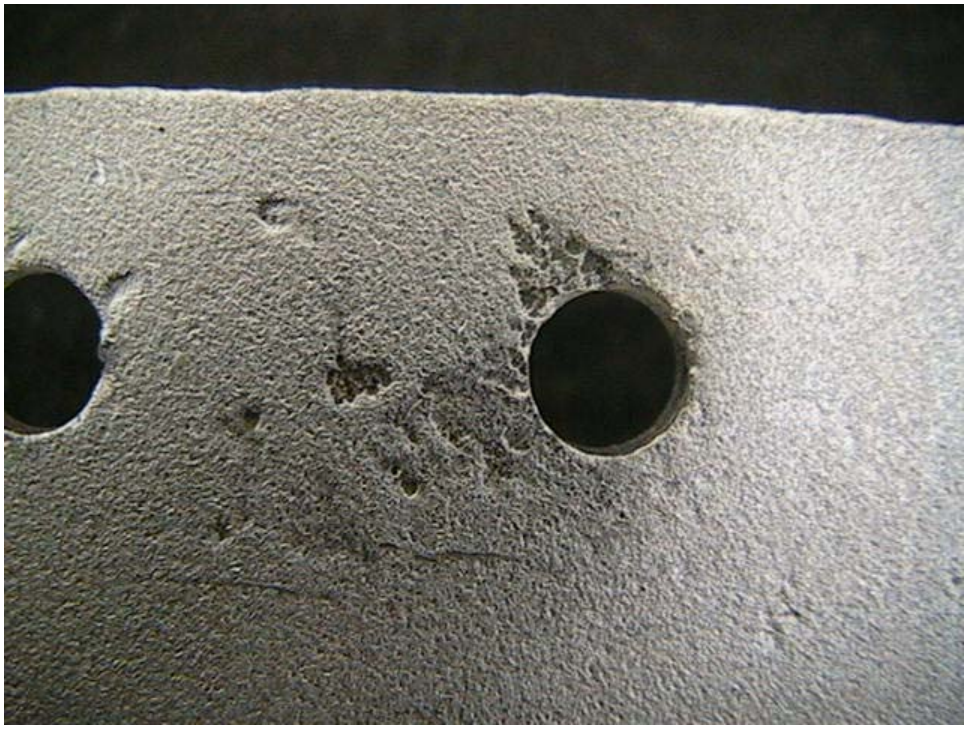

Figure 41. Corrosion on the Left Wing Front Spar Aft Upper Cap WS 48.75-54.5

2.4.1.2 Left Wing Rear Spar.

One area of corrosion and three cracks were found during the microscopic examination of the left wing rear spar. A 14.23-square-inch area of severe corrosion was observed from WS 123 to 191 on the rear spar web. This corrosion is shown in figure 42 and resulted in a maximum localized thickness loss of 15%. A 0.172-inch crack, shown in figure 43, was observed on the rear spar lower cap at WS 66. The fractograph, or high-magnification picture, of the fracture face is provided in figure 44. Prominent fatigue striations, or crack face characteristics indicative of fatigue, as well as the direction of crack growth, are shown in figure 44. Figure 45 shows two cracks found on the left wing rear spar lower doubler at WS 66, measuring 0.128 and 0.078 inch. The locations of these two cracks correspond exactly with the 0.172-inch crack on the lower spar cap. All three of these cracks emanated from a fastener hole and were determined to be caused by fatigue.

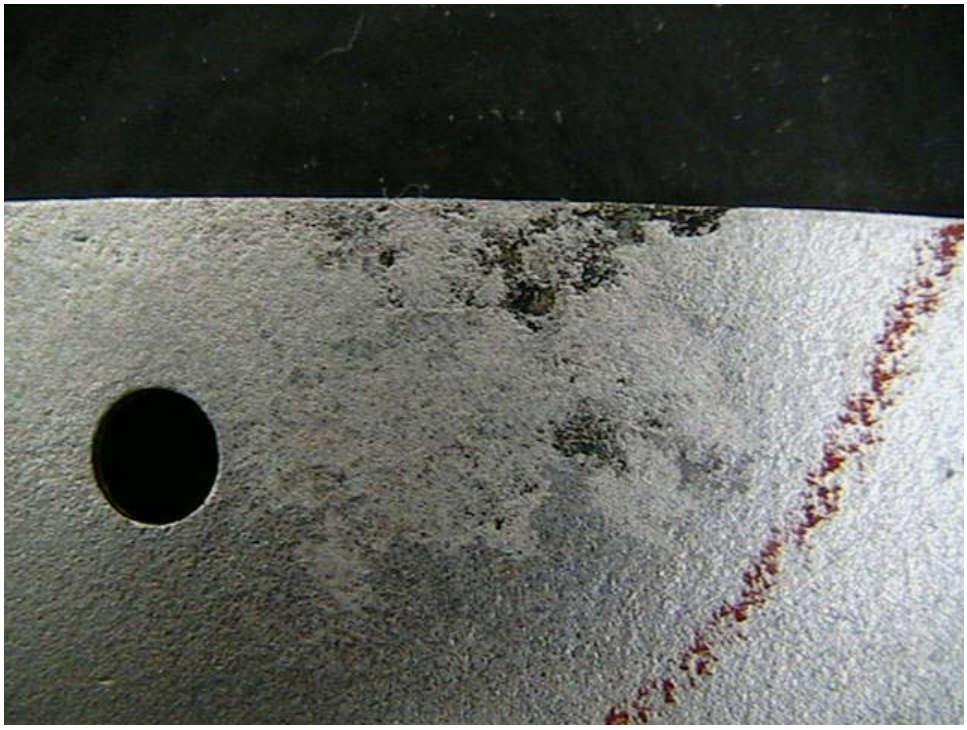

Figure 42. Corrosion on the Left Wing Rear Spar Web WS 123-191

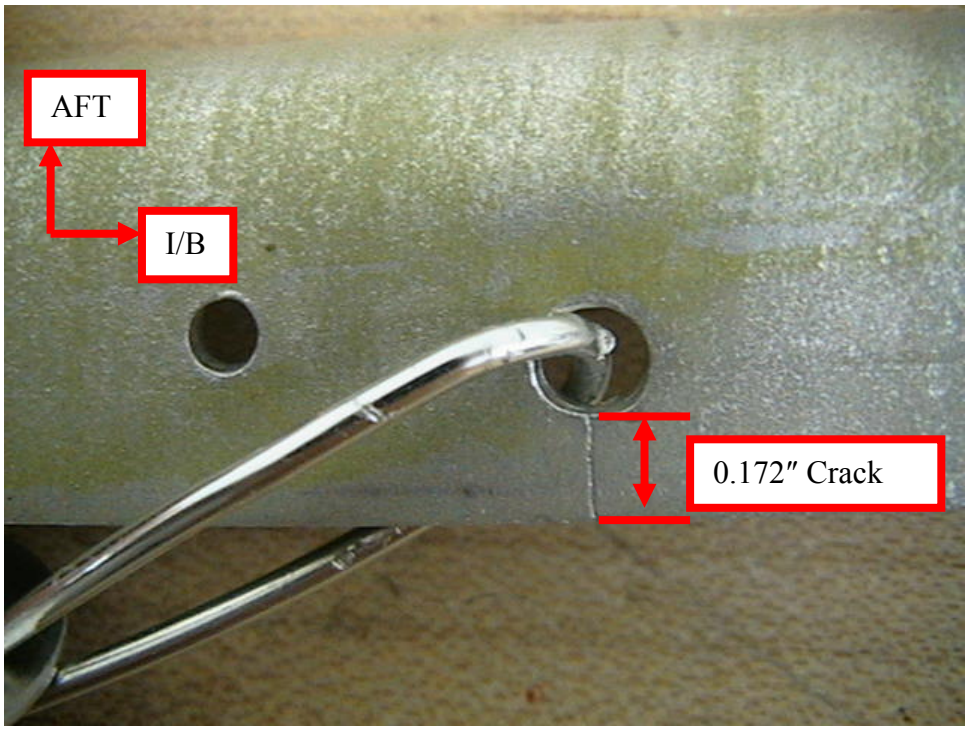

Figure 43. Crack in the Left Wing Rear Spar Lower Cap WS 66

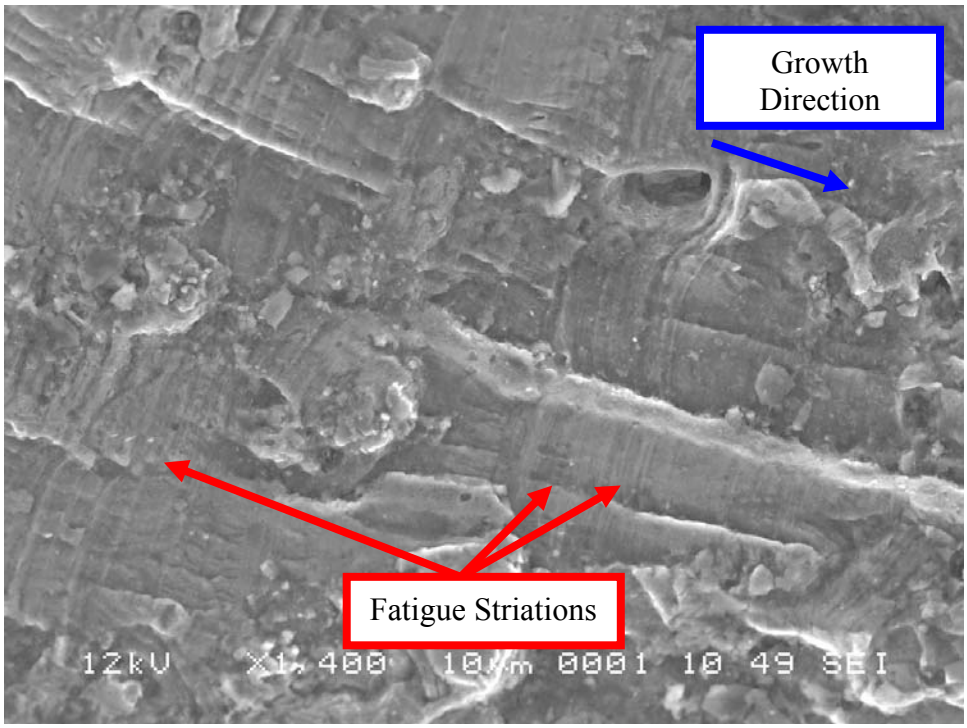

Figure 44. Fractograph of the Left Wing Rear Spar Lower Cap Crack Face WS 66

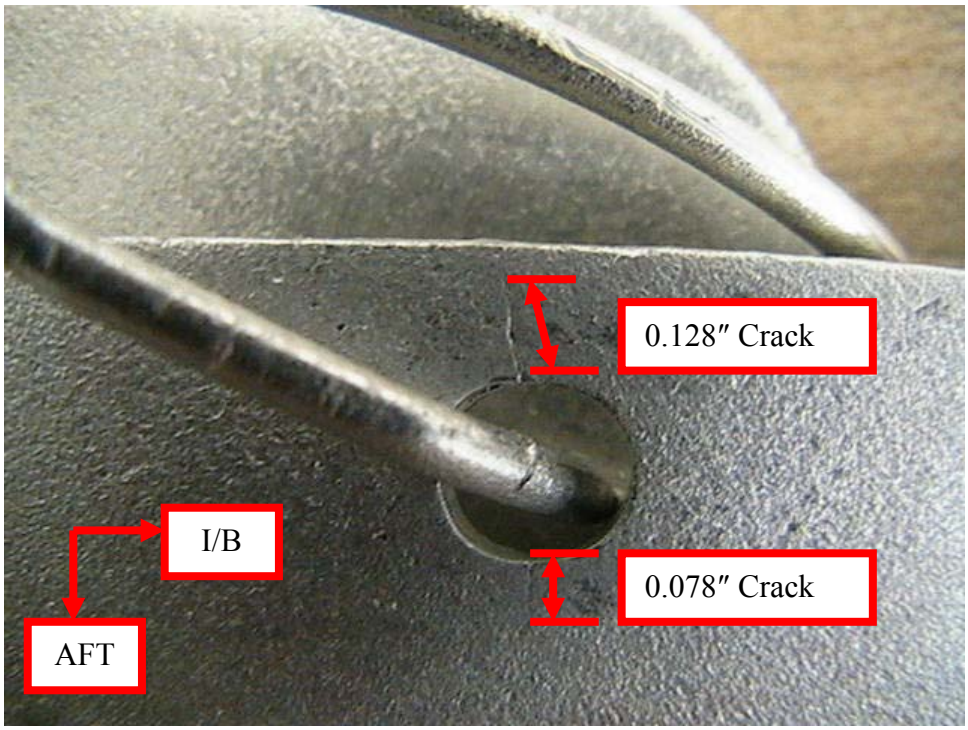

Figure 45. Cracks in the Left Wing Rear Spar Lower Doubler WS 66

2.4.1.3 Left Wing Attachment Fittings.

Two areas of light corrosion were identified on the landing gear attachment fittings, and three areas of corrosion were found on the left wing bathtub fittings. The severity of the corrosion in the bathtub fittings was not able to be determined because the corrosion was located in an area of the fittings that prevented an accurate pit depth measurement. The five areas of corrosion on the wing attachment fittings were located on the front and rear inboard landing gear attachment fittings, front spar upper and lower bathtub fittings, and the rear spar lower bathtub fitting.

2.4.1.3.1 Left Wing Landing Gear Attachment Fittings.

Two areas of light corrosion were found on the left wing landing gear attachment fittings. Figure 46 shows the corrosion found at WS 46 on the front spar inboard landing gear attachment fitting. This area of corrosion covers 0.20 square inch and resulted in a thickness loss of 1.1%. Figure 47 shows a 2.32-square-inch area of corrosion found on the left wing rear spar inboard landing gear attachment fitting at WS 46. This area of corrosion caused a 0.5% local thickness loss.

Figure 46. Corrosion on the Left Wing Front Spar Inboard Landing Gear Attachment Fitting WS 46

Figure 47. Corrosion on the Left Wing Rear Spar Inboard Landing Gear Attachment Fitting WS 46

2.4.1.3.2 Left Wing Bathtub Fittings.

Three areas of corrosion were found on the left wing bathtub fittings. Corrosion was found on the front spar upper and lower bathtub fittings as well as the rear spar lower bathtub fitting. Due to the location of corrosion on the fitting, accurate pit depth measurements were not possible. Figure 48 shows a 1.82-square-inch area of corrosion on the left wing front spar upper bathtub fitting from WS 24 to 28. A 4-square-inch area of corrosion, pictured in figure 49, was identified on the front spar lower bathtub fitting from WS 23 to 27.5. Figure 50 shows a 1.54-square-inch area of corrosion on the left wing rear spar lower bathtub fitting at WS 25.

Figure 48. Corrosion on the Left Wing Front Spar Upper Bathtub Fitting WS 24-28

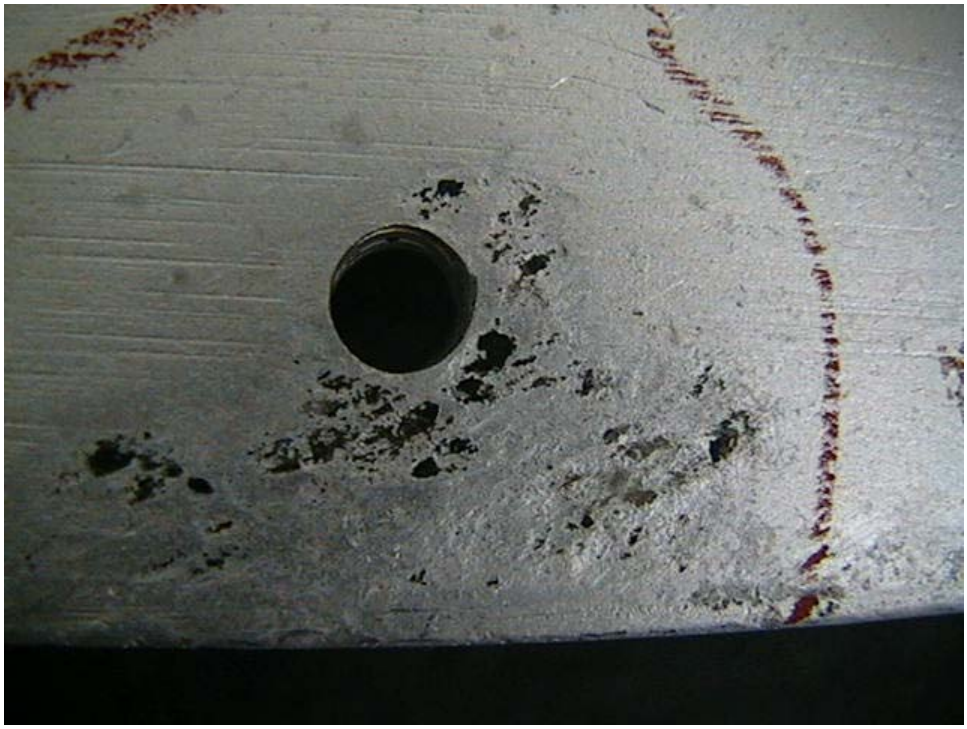

Figure 49. Corrosion on the Left Wing Front Spar Lower Bathtub Fitting WS 23-27.5

Figure 50. Corrosion on the Left Wing Rear Spar Lower Bathtub Fitting WS 25

2.4.2 Right Wing.

Five areas of corrosion were found on the right wing. This corrosion was located on the front and rear spar inboard landing gear attachment fittings, front spar upper and lower bathtub fittings, and the rear spar upper bathtub fitting. Due to the location of corrosion in the bathtub fittings, accurate pit depth measurements could not be obtained.

2.4.2.1 Right Wing Front Spar.

No defects were found during the microscopic examination of the right wing front spar.

2.4.2.2 Right Wing Rear Spar.

No defects were found on the right wing rear spar during the microscopic examination.

2.4.2.3 Right Wing Attachment Fittings.

Five areas of corrosion were found on the right wing attachment fittings on the front and rear spar inboard landing gear attachment fittings, front spar upper and lower bathtub fittings, and the rear spar upper bathtub fitting. Only light corrosion was found on the landing gear attachment fittings, and the severity of the corrosion on the bathtub fittings could not be assessed due to its location in the fitting.

2.4.2.3.1 Right Wing Landing Gear Attachment Fittings.

Two areas of corrosion were found on the right wing landing gear attachment fittings. Figure 51 shows a 0.765-square-inch area of corrosion on the front spar inboard landing gear attachment fitting at WS 46. This corrosion was classified as light corrosion because it caused a maximum localized thickness loss of 2.2%. Figure 52 shows an area of corrosion located on the rear spar inboard landing gear attachment fitting at WS 46. This area of corrosion encompassed a surface area of 0.675 square inch with a maximum thickness loss of 1.1%, which is classified as light corrosion.

Figure 51. Corrosion on the Right Wing Front Spar Inboard Landing Gear Attachment Fitting WS 46

Figure 52. Corrosion on the Right Wing Rear Spar Inboard Landing Gear Attachment Fitting WS 46

2.4.2.3.2 Right Wing Bathtub Fittings.

Three areas of corrosion were found on the right wing bathtub fittings. Figure 53 shows an 8.15-square-inch area of corrosion on the front spar lower bathtub fitting from WS 23 to 27. A 2.90-square-inch area of corrosion was identified on the front spar upper bathtub fitting from WS 24 to 28 and is pictured in figures 54 and 55, and another area of corrosion, shown in figure 56, was identified on the rear spar upper bathtub fitting from WS 24 to 26. This area of corrosion covered a surface area of 4.71 square inches.

Figure 53. Corrosion on the Right Wing Front Spar Lower Bathtub Fitting WS 23-27

Figure 54. Corrosion on the Right Wing Front Spar Upper Bathtub Fitting WS 24-28

Figure 55. Corrosion on the Right Wing Front Spar Upper Bathtub Fitting WS 24-28

Figure 56. Corrosion on the Right Wing Rear Spar Upper Bathtub Fitting WS 24-26

2.5 FRACTOGRAPHIC EXAMINATION.

The fractographic analysis of the left wing rear spar lower cap crack at WS 66 found on the first wing set was performed at the Center for Aircraft Structural Life Extension, United States Air Force Academy. The analysis included a macroscopic analysis, scanning electron microscope (SEM) observation, optical microstructural analysis, and a hardness measurement. All analysis work was performed by an experienced, qualified metallurgist.

Metallurgical failure analysis of the part received from a T-34A left wing rear spar lower cap at WS 66 shows extensive damage due only to high-cycle fatigue. There are two root causes for the failure of the angle: shot-peening that induced subsurface cracks and machining defects that resulted in nucleation of secondary cracks. The beach marks show the primary origin located in the clad metal interface as a result of subsurface crack nucleation resulting from the severe shot-peening. Additionally, multiple cracks nucleated from the machining grooves and propagated. The beach marks all appear to join the primary one, the crack from the shot-peening defect. Locations of all the crack nucleation sites and directions of propagation are all shown in a schematic diagram supported by microstructural analysis. Due to strong evidence that the failure mode is fatigue and the root cause for the crack nucleation was clearly evident, detailed analysis such as mechanical and electrical properties assessment were not done, with the exception of a hardness measurement. Hardness measurement was chosen because it provides a quick assessment of the temper condition of the material and, thus, is expected to provide the fundamental mechanical property. The hardness of the clad layer was found to be 85-90 Brinell Hardness (HB) and that of the bulk material was around 150-155 HB. The failure analysis confirmed the initial observation that the shot-peening methodology combined with the poor machining (drilling) caused the crack to nucleate in the interface between the clad and the bulk material. Furthermore, multiple crack nucleation sites were found on the machining grooves. Due to the lack of the material background and processing history, some assumptions are made regarding these factors. Conclusions were drawn based on these assumptions and the microstructural observation. Unfortunately, etching of the primer coating from a previous failure investigation has partially damaged the fracture surface. In the future, care has to be taken during the etching process. Unless necessary, avoid etching or removing the primer coating. For this particular failure analysis subject, the analysis could have been done without removing the primer coating.

2.5.1 Macroscopic Analysis.

The part received is a formed angle from the lower wing spar of the T-34A and is assumed to be made from aluminum alloy 7075-T6. Based on the material provided and the fracture surface, the process by which the crack was opened during the previous failure investigation is shown as a schematic in figure 57. The blue dotted line indicates the region where the crack was opened during the failure analysis. Figure 58(a) illustrates the schematic of macroscopic observation of the fracture surface. The corresponding stereomicroscopic image is shown in figure 58(b). From the macroscopic observation under the stereomicroscope, four major features were seen: (1) fatigue striations, (2) beach marks, (3) poor machining (drilling), and (4) deformation in the fastener hole.

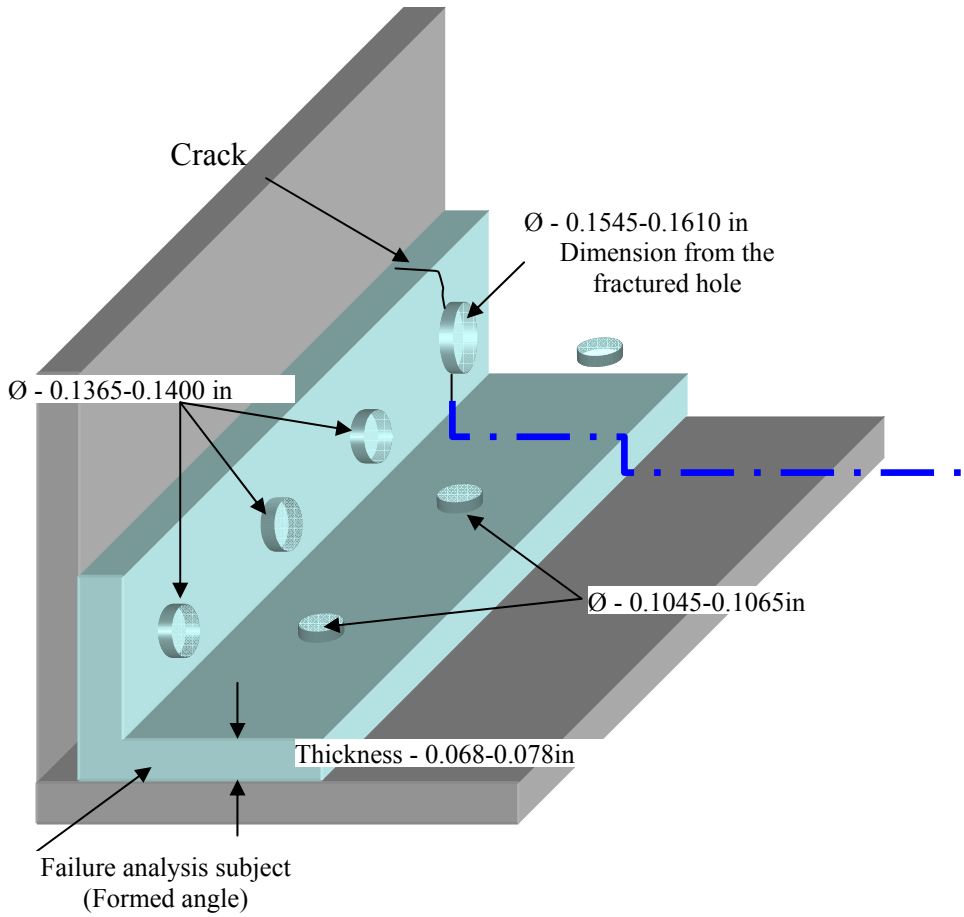

Figure 57. Schematic of the Formed Angle, Dimension, and Location of the Crack

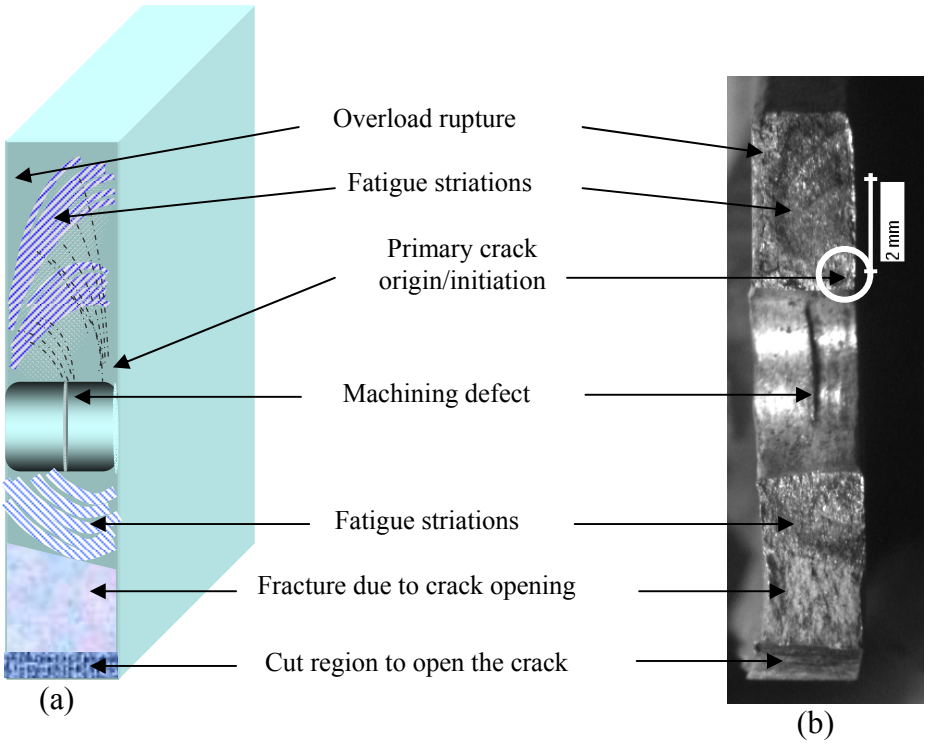

Figure 58. Schematic of the Features Observed on the Fracture Surface and Macroscopic Stereomicrograph Taken at 7X

Among the four features mentioned above, all but the beach marks can be seen in figure 58(b). In addition, the macroscopic observation of the fracture surface indicated the crack propagated first on the top side (description based on the fastener hole) by fatigue loading. The crack in the lower section of the hole had propagated half the height of the formed angle and then was possibly opened by standard techniques during the previous failure investigation. Another interesting observation is that the thin overload rupture region just on the edge of the angle, shown in figure 58(b), indicates a very small load acting on the formed angle. The beach marks indicating the origin of the crack are shown in figure 59, which is an enlargement of the upper portion of figure 58(b). An SEM micrograph of the fracture surface from the white circular region (figures 58(b) and 59) is presented in the next section under SEM observation. Distinct crack propagation curves indicate a torsion loading mode as shown in figure 59. White and yellow lines indicate the crack nucleation sites of two different beach marks.

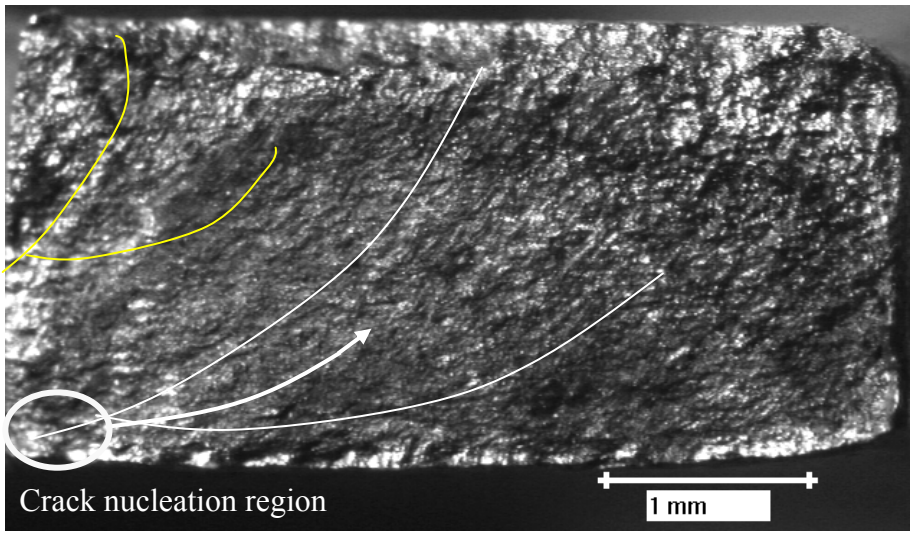

Figure 59. Stereomicrograph Showing Beach Marks, Crack Origin, and Direction of the Crack Propagation

The macroscopic observation of the specimen sides using the stereomicroscope shows the extent of damage on the fastener hole during the process of crack propagation and/or during the cracking opening, see figure 60. The deformation of the hole diameter is about 13% to 15%. In general, aluminum alloys under specific temper condition have a unique elongation at fracture, that is 8% to 11% for most of the alloys under T6 temper conditions. The observation of 13% to 15% strain in the fastener hole of this specimen suggests that after the fracture of the top portion, the part could have been subjected to higher load resulting in larger deformation. It cannot be necessarily ruled out that this large deformation of the fastener hole could have happened during crack opening process conducted during the previous failure investigation. However, considering the deformation on the rim of the fastener hole, it is more likely that the deformation should have occurred during the crack propagation. Figure 60 also shows a very rough surface, which is typical of a shot-peened surface. Subsurface microstructure analysis would reveal the processing history and type of heat treatment. This analysis will be discussed in section 2.5.3 of this report.

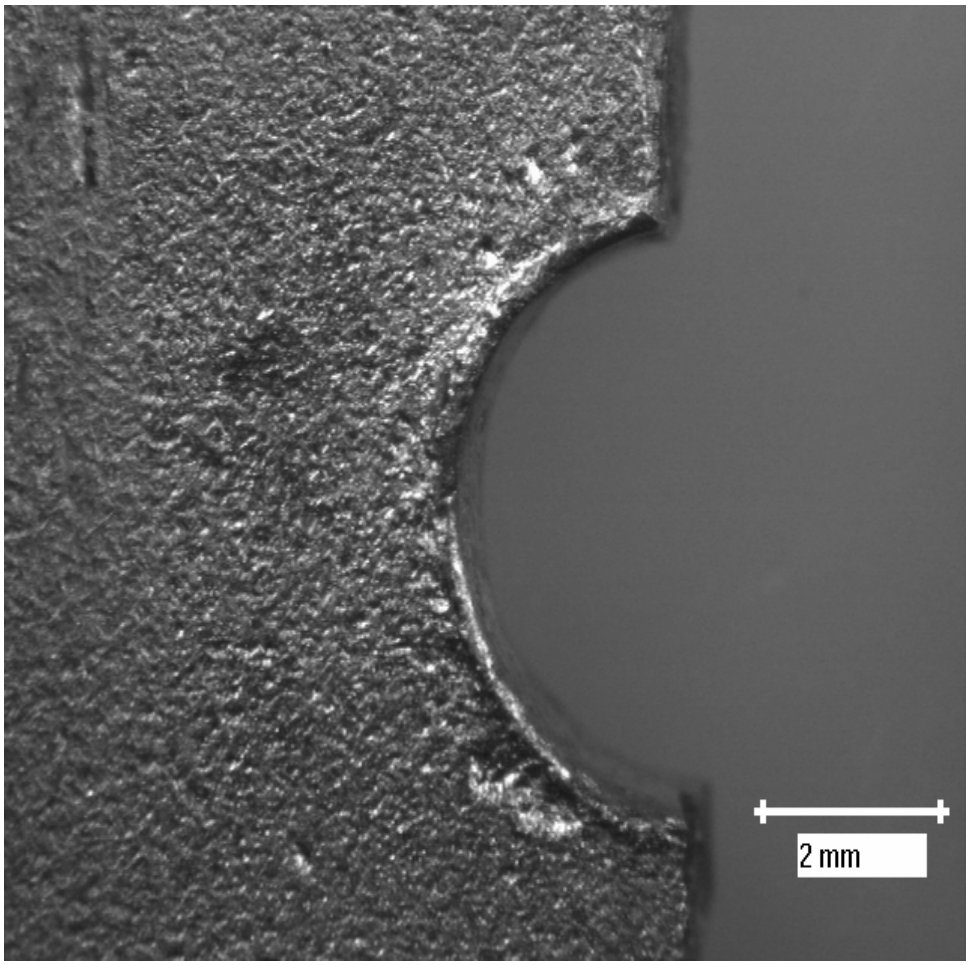

Figure 60. Stereomicrograph of the Part From the Side Shows Strain on Fastener Hole During Crack Propagation

2.5.2 The SEM Observation.

SEM analysis was done on the fracture surface using Hitachi Model S-2600N. The resulting fractrographs are shown in figures 61 through 63. Detailed observation of the fracture mode, nucleation sites, and other relevant features are discussed in this section. The arrow marks in figure 61 indicate etch pits that were induced during the cleaning process. Marker A indicates the primary crack nucleation site and a portion of a crater typical of some impingement process, which is similar to shot-peening.

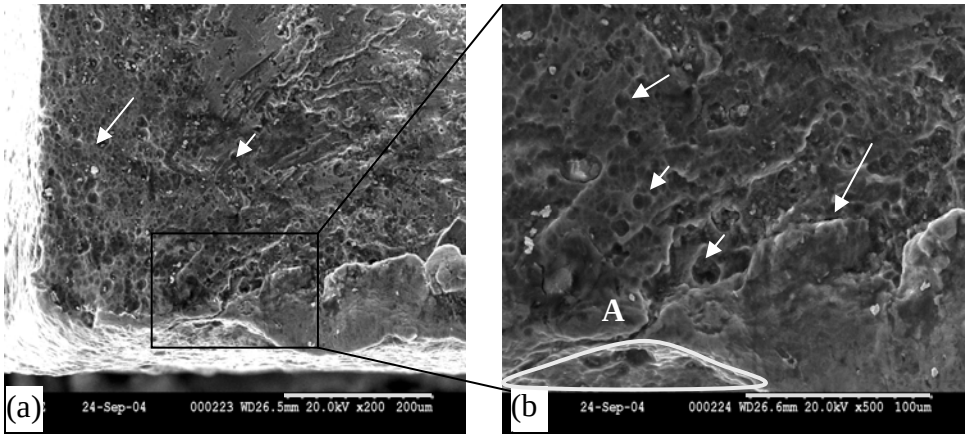

Figure 61. The SEM Micrograph of the Fracture Surface Shows the Primary Crack Nucleation Site (a) at Low-Magnification and (b) at Higher Magnification of the Rectangular Inset (a)

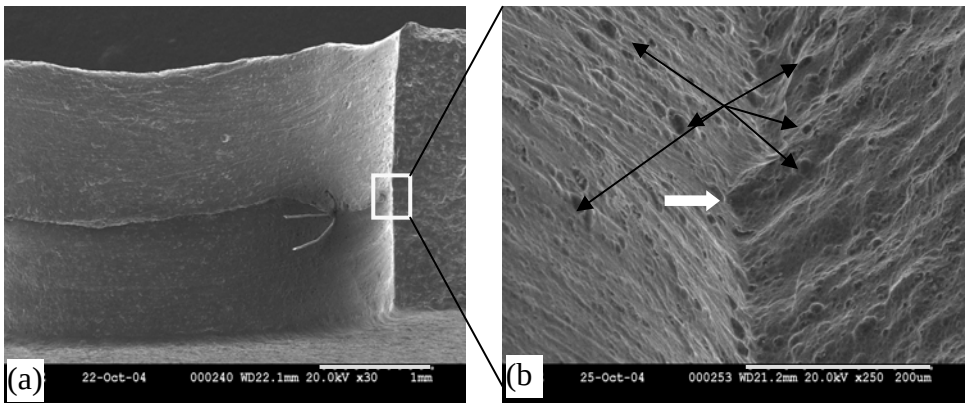

Figure 62. (a) Low-Magnification Micrograph Shows Machining Defect in the Form Rough Surface and (b) High-Magnification Micrograph of the Region From Figure 62(a)

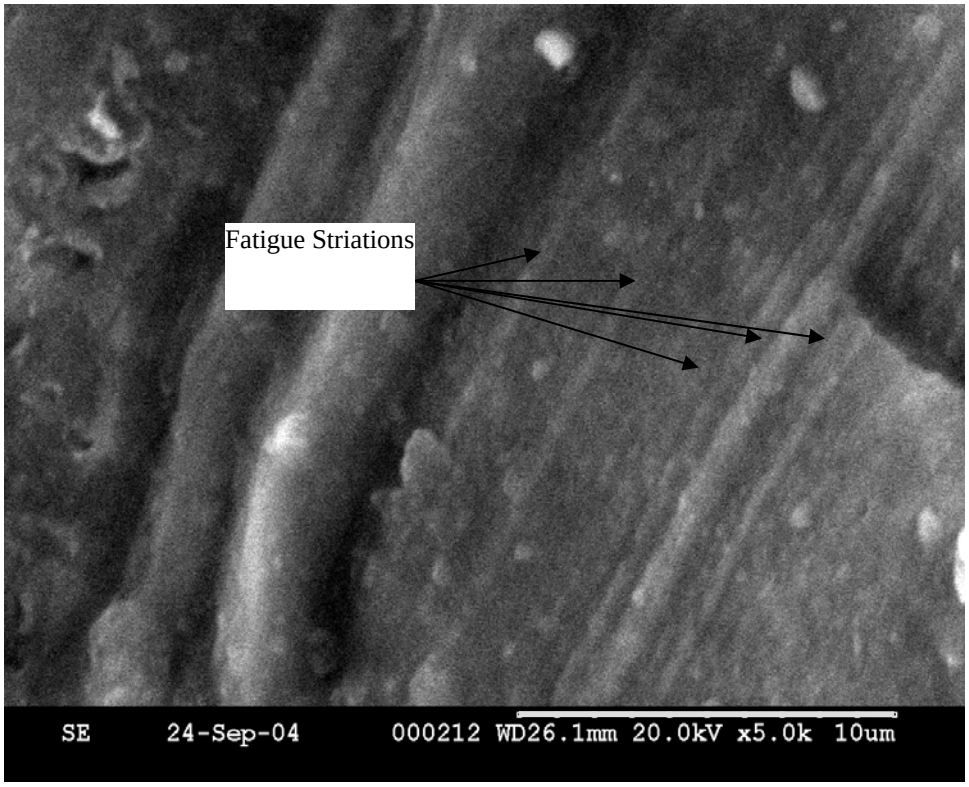

Figure 63. The SEM Micrograph of the Fracture Striations Observed on the Fracture Surface

With reference to the stereomicroscopic observation, the location of the primary crack nucleation site was identified using SEM and is shown in the micrograph in figure 61. The low-magnification image of the region is shown in figure 61(a) and that of the higher magnification of the nucleation site in figure 61(b). From the SEM observation of the fracture surface, multiple crack nucleation sites were found in both the upper and lower section of the hole, and the one shown in figure 61(a) indicates the primary one. The term "primary nucleation site" is used to indicate the faster kinetic for the crack propagation. Thus, it is possible that cracks could have first nucleated even in the lower section, but the kinetics were more favorable in the upper section, thus that crack propagated faster. The interesting part of the observation is that the crack nucleated from the region where a portion of a crater is observed or from the clad metal interface. Craters are formed during an erosion process (in general, during any particle impingement) or during pitting corrosion. Crater formation due to pitting corrosion was ruled out due to smooth surface and subsurface morphology of the crater. It would have been more obvious if the surface had not been etched. In this particular case, the crater indicates surface damage during shot-peening. The fracture surface also reveals that the surface was damaged during etching as is evident from numerous etch pits.

Figure 62 shows the machining defect with deep grooves and a rough surface. A step in the machined surface caused by a metal wire from a turning entrapped in the machining groove is shown in figure 62(a). The square box shows the region of the multiple crack nucleation sites from the rough surface. A high-magnification view of the same is shown in figure 62(b) with a crack nucleation site shown by the white arrow mark. In addition, the micrograph shows the

etching pits (marked by dark arrows) on both fracture surface and on the surface of the fastener hole.

The signature of the fatigue crack propagation is striation formation, which dominates the entire surface. A representative micrograph taken from the top part (completely fractured surface) is shown in figure 63.

SEM micrographs of the fracture surface from the lower part of the hole are shown in figure 64. Multiple crack nucleation sites in the lower section of the hole near the clad metal interface and the machining groove are shown in figure 64(a), (b), (c), and (d), respectively. Figure 64(a) shows a lower magnification of the multiple crack nucleation sites originating near the clad metal interface. At higher magnification from the same region, the fracture surface reveals fatigue striations shown by arrow marks in figure 64(b).

Figure 64(c) shows a crack nucleation site at low-magnification from the machining grooves. The crack appears to be opened by static overloading from the nature of the tearing morphology. However, at higher magnification from the circular region, figure 64(d) shows the crack nucleated by fatigue cyclic loading as evident from the striations.

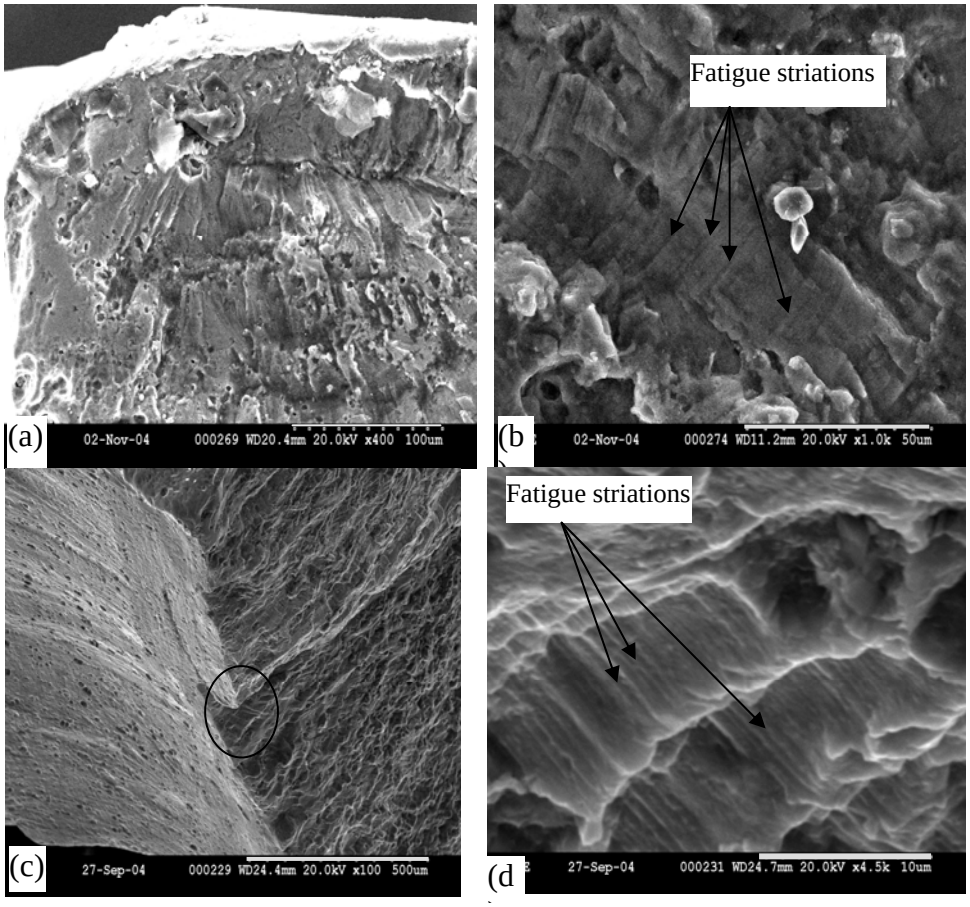

Figure 64. The SEM Micrographs of Fracture Surface From the Lower Part of the Hole

The present SEM fracture surface analysis indicates without any ambiguity that the fracture occurred by fatigue and suggests that multiple crack nucleation sites exists. The primary one (based on the kinetics) being from the upper part of the hole, near the subsurface where some kind of crater was observed (refer to figure 61(b)), and other (secondary) crack nucleation sites are from the machining grooves (Figures 62(b), 64(a), and 64(c)). However, the study to this point could not reveal the root cause for the crack nucleation. To delineate the root cause for the crack nucleation that resulted in fatigue crack growth, optical microstructural analysis was done on the subsurface to determine the processing history and how that influenced the fracture of the material subject.

A sample was cut from the angle using a low-speed saw and polished using standard metallographic techniques. A polished specimen was then observed in a Nikon Epiphot 300 inverted microscope after etching using Keller's reagent. Microstructure observation and hardness measurement were done on the polished specimen and analyzed.

2.5.3 Optical Microstructural Analysis and Hardness Measurement.

A three-dimensional (3-D) view of the microstructure of the specimen with its orientation is given in figure 65. Elongated grains and etch grain contrast (bright and dark grains) that differentiate between recrystallized grain (light gray or white) and unrecrystallized grain (dark gray) are seen, which is common in wrought products. In general, the microstructure (grain size) and intermetallic particle distribution appear homogenous, suggesting a sound material. Two important observations are made in this material: (1) the material is clad and (2) the surface is shot peened.

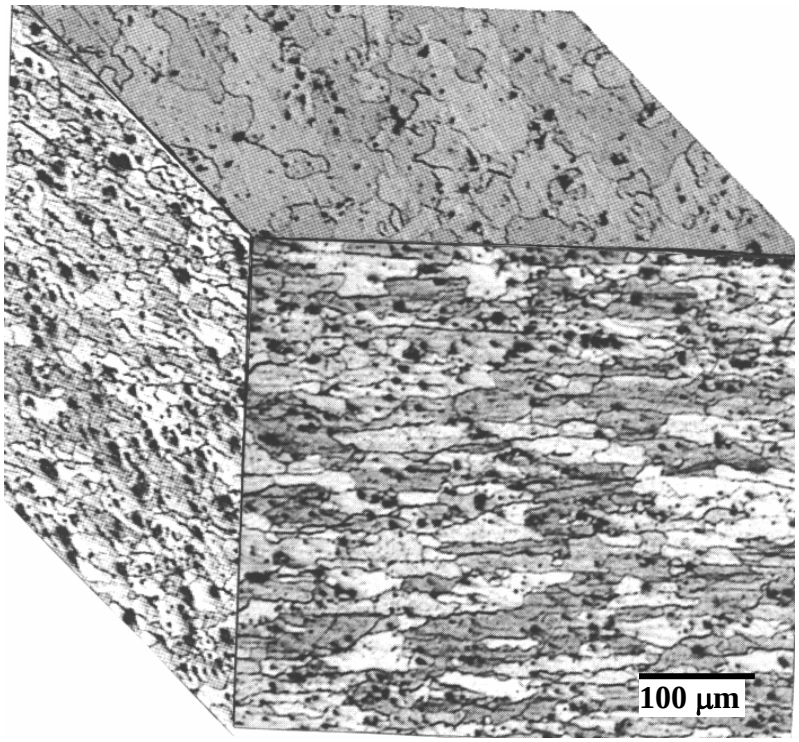

Figure 65. The 3-D Optical Microstructure View of the Specimen

Optical micrographs of the clad layer and that of the surface damage due to shot-peening are shown in figure 66. The thickness of the clad layer is 70 μm (±15 μm) [0.00275, ±0.0004 in.], which is about 4% of the section thickness 1.75 mm (0.069 in.). The observed clad thickness satisfies the specification of the Alclad 7075 sheet and plate given by Aluminum Standards and Data, the Aluminum Association, Inc. The subsurface damage due to shot-peening was found severe, and crack nucleating either at interface or slightly above the interface (in the clad layer) were observed, as shown in figure 66(a) and (b).

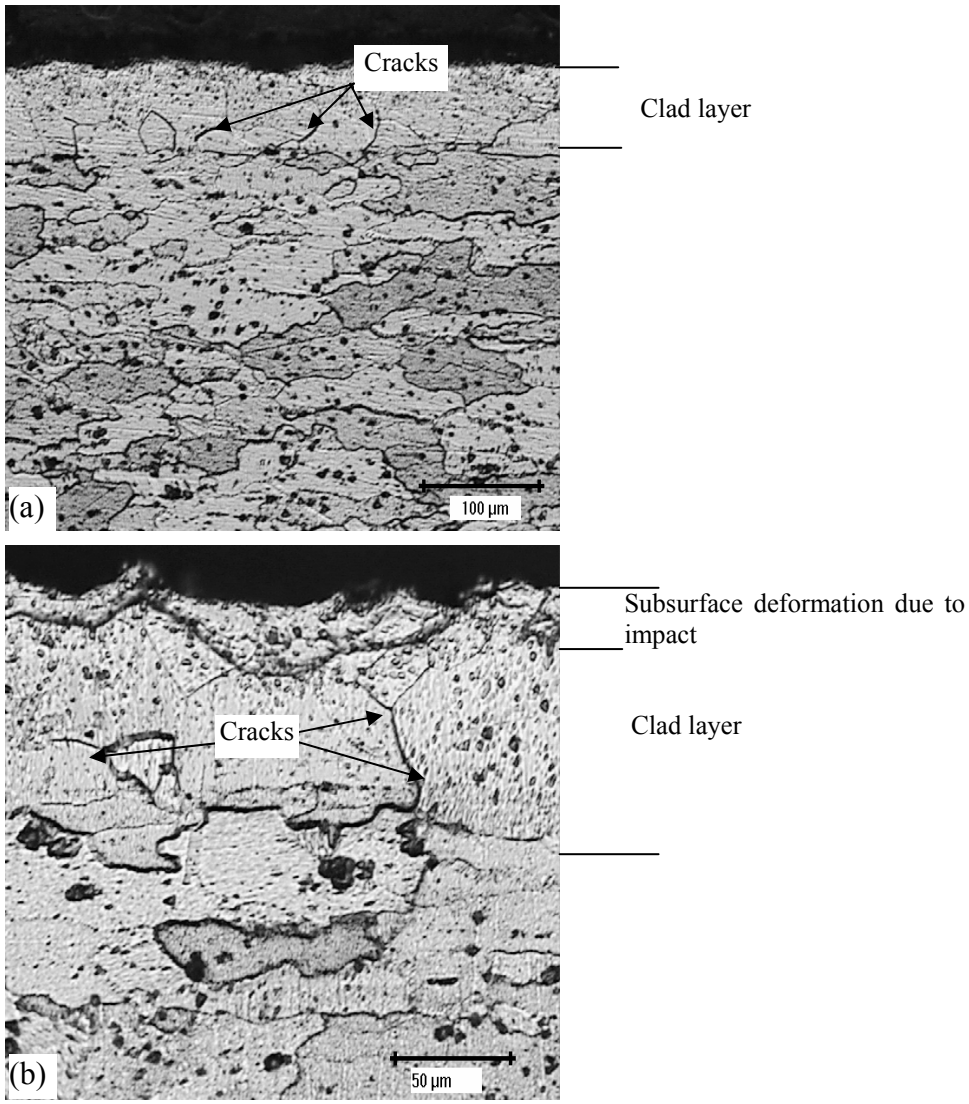

Figure 66. Optical Micrograph of (a) the Clad Layer of about 70 μm Thickness Observed on Both Sides of the Section and (b) Subsurface Deformation and Roughening Due to Shot-Peening

It may be argued that the cracks marked in figure 66 could be the grain boundary, but considering the fact that grain boundary follows certain rules, such as specific surface or grain boundary energy concepts that are different from that of the cracks, it was concluded these are

cracks. To illustrate the severity of the shot-peening on the subsurface of the clad layer, a composite micrograph showing a damage site with a subsurface crack running parallel to surface is shown in figure 67.

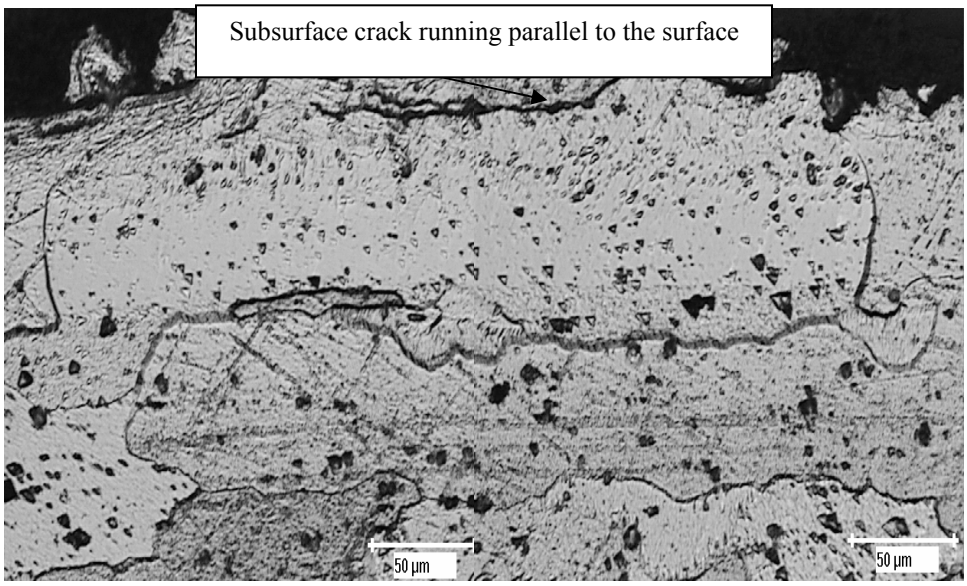

Figure 67. Composite Optical Micrograph Showing Subsurface Crack Running Parallel to the Surface on the Clad Layer

Shot-peening is a process in which the surface is impinged with steel shots to induce residual compressive stress on the surface. However, if the stresses are too high, it could cause damage on the subsurface. This damage is similar to damage or crack nucleation during an erosion process under normal impact. Impingement of hard particles (such as steel shots) on ductile surface (like aluminum) causes the surface to plastically deform. If the plastic deformation exceeds a critical strain value, then the crack nucleates at the subsurface and propagates parallel to the surface and detaches as platelets. The observation of a crack running parallel to the surface, as seen in figure 67, indicates the shot-peening was done more than the recommended time or at higher velocity. This indication could be one possible reason for the observed crack nucleation near the clad layer. Further discussion of this observation is beyond the scope of this investigation because the surface was already deeply etched during the previous failure analysis.

Based on the microstructural analysis, the processing history of the subject formed angle was manufactured by the following process. An aluminum alloy was clad rolled and then bent in the hot or warm condition. Elemental analysis was not done to determine the composition, but it appears as aluminum alloy 7075. Initially, the angle was thought to be an extruded product, but microstructural analysis shows that the material is clad rolled and then bent. The conclusion is based on the fact the grains are coarser near the bent region, where localized strain caused the grain to grow during the bending and heat treatment process. Grain coarsening in the bent region could also occur during the precipitation hardening treatment after cold forming. Optical micrograph of the grain size variation near the bent region is shown in figure 68.

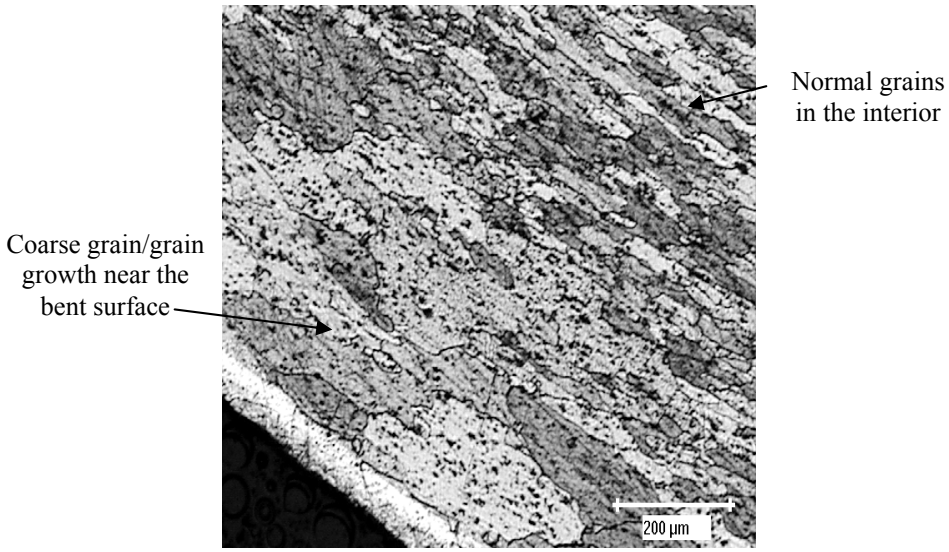

Figure 68. Optical Micrograph of the Cross Section of the Angle Showing Grain Coarsening Near Bent Surface

Hardness measurement was carried out on the polished specimens to determine the type of heat treatment done on the formed angle. Measured hardness across the thickness shows a value of about 85-90 HB on the clad layer and about 150-155 HB on the core material. These values were normal for aluminum alloy 7075-T6 tempered condition.

2.5.4 Conclusion.

Failure analysis of a formed angle from the lower wing spar of a T-34A aircraft was successfully carried out. The mode of fracture shows predominant high cycle fatigue failure. The primary crack nucleation site was from the clad metal interface layer and another secondary crack originated from the machining defects (rough surface and deep grooves associated with poor drilling). It appears that the crack nucleated at the clad metal interface due to severe shot-peening.

In addition, the processing history was also determined. The material appears to be made of aluminum alloy 7075-T6 with processing by clad rolling followed by the bending and heat treatment process. The bent structure was then subjected to precipitation hardening treatment. EDX or other means of compositional analysis would provide the definitive details regarding the type of aluminum alloy. However, for this particular failure investigation, the material type was immaterial.

2.5.5 Suggestions.

Based on the observations made during the fractographic examination, the following suggestions were made.

- Improved control of the shot-peening process should be used in the present angle material to induce residual compressive stress. Exceeding the time limit of the shot-peening process, or using a higher velocity, will induce subsurface damage that will cause detrimental effects to the clad layer property.

- Drilling is a simple process even in a production environment, and defects could be easily avoided in this machining process.

- An etching process, or removal of primer coating during a failure investigation, should be avoided as much as possible. In the present material, the surface is deep etched and could be easily noticed from the SEM observation. If etching is necessary, application of a lacquer coating on the fracture surface prior to etching would protect the fracture surface from pitting.

2.6 SUMMARY OF FIRST WS FINDINGS.

Table 1 provides a summary of all findings on the initial set of T-34A wings.

Table 1. Summary of Findings for T-34A WS 1

Part Description	Defect Location NDI	Defect Location Microscopic Examination	Flaw Type	Flaw Extent NDI	Flaw Extent Microscopic Examination
Left Wing Front Spar Forward Upper Cap	WS 37.5-39 WS 49-57.5	WS 40, 50, 52	Corrosion	1.84 square inches	8.71 square inches 23.5% thickness loss
Left Wing Front Spar Aft Upper Cap	WS 38-40 WS 48.75-54.5	WS 38-40 WS 48.75-54.5	Corrosion	1.24 square inches	21.66 square inches 19.4% thickness loss
Left Wing Rear Spar Web	WS 168.75	None	Crack	0.1 inch	None
Left Wing Rear Spar Web	None	WS 123-191	Corrosion	None	14.23 square inches 15% thickness loss
Left Wing Rear Spar Lower Cap	WS 66	WS 66	Crack	0.17 inch	0.172 inch
Left Wing Rear Spar Lower Doubler	WS 66	WS 66	2 Cracks	0.12 inch 0.07 inch	0.128 inch 0.078 inch

Table 1. Summary of Findings for T-34A WS 1 (Continued)

Part Description	Defect Location NDI	Defect Location Microscopic Examination	Flaw Type	Flaw Extent NDI	Flaw Extent Microscopic Examination
Left Wing Front Spar Inboard Landing Gear Attachment Fitting	WS 46	WS 46	Corrosion	0.38 square inch	0.20 square inches 1.1% thickness loss
Left Wing Rear Spar Inboard Landing Gear Attachment Fitting	WS 46	WS 46	Corrosion	2.57 square inches	2.32 square inches 0.5% thickness loss
Left Wing Front Spar Upper Bathtub Fitting	WS 23.5-25.75	WS 24-28	Corrosion	4.48 square inches	1.82 square inches, percent thickness loss not measurable
Left Wing Front Spar Lower Bathtub Fitting	WS 23-27.5	WS 23-27.5	Corrosion	6 square inches	4 square inches, percent thickness loss not measurable
Left Wing Rear Spar Lower Bathtub Fitting	WS 24.75-26	WS 25	Corrosion	1.56 square inches	1.54 square inches, percent thickness loss not measurable
Right Wing Front Spar Inboard Landing Gear Attachment Fitting	WS 46	WS 46	Corrosion	0.99 square inch	0.765 square inch 2.2% thickness loss

Table 1. Summary of Findings for T-34A WS 1 (Continued)

Part Description	Defect Location NDI	Defect Location Microscopic Examination	Flaw Type	Flaw Extent NDI	Flaw Extent Microscopic Examination
Right Wing Rear Spar Inboard Landing Gear Attachment Fitting	WS 46	WS 46	Corrosion	0.88 square inch	0.675 square inch 1.1% thickness loss
Right Wing Front Spar Lower Bathtub Fitting	WS 23-27.75	WS 23-27	Corrosion	4.71 square inches	8.15 square inches, percent thickness loss not measurable
Right Wing Front Spar Upper Bathtub Fitting	WS 23.5-28	WS 24-28	Corrosion	3.05 square inches	2.90 square inches, percent thickness loss not measurable
Right Wing Rear Spar Upper Bathtub Fitting	WS 23.5-27	WS 24-26	Corrosion	5.12 square inches	4.71 square inches, percent thickness loss not measurable

3. SECOND WING SET.

In June 2004, a second set of wings from a high-time T-34A became available for teardown examination. Instead of repairing the wings, which had known cracks on the rear spars, the maintenance facility elected to replace the wings, providing the damaged wings to the FAA and NIAR to conduct a teardown evaluation. Raytheon's SB 57-3329 was performed in its entirety on this set of wings, resulting in three crack indications and two visually verified cracks. Figure 69 shows the second set of T-34A wings as received.

Three cracks were found on the left wing of the second set, located on the leading-edge aft lower cap, rear spar lower doubler, and the rear spar lower cap. On the right wing, four cracks were found on the leading-edge forward lower spar cap, and one crack was found on the leading-edge aft lower spar cap. Nine areas of pitting corrosion were observed on the left wing, and five areas of pitting corrosion were found on the right wing. Pitting corrosion was also found on the left and right wing front spar webs, left and right wing front spar upper caps, left wing leading-edge aft upper and lower spar caps, and the left and right wing rear spar upper bathtub fittings. Three areas of mechanical damage were also noted on the left wing front spar upper cap. Seven areas of exfoliation corrosion occurred on the left wing front spar upper cap. Nine areas of

intergranular corrosion were detected on the left wing front spar upper cap, and seven areas were found on the right wing front spar upper cap. One area of intergranular corrosion was found on the left wing rear spar upper bathtub fitting.

Figure 69. Second Set of T-34A Wings as Received

3.1 THE SB 57-3329 INSPECTIONS.

As shown previously in figure 3, Raytheon SB 57-3329 prescribes bolthole eddy-current inspections at the following locations:

- Five fasteners on the aft lower reinforcement of the front spar inboard of WS 34
- Four fasteners on the lower side of the front spar at WS 34
- Two fasteners on the lower leading-edge hinge angle outboard of WS 63
- Forward trunnion fastener location
- Two aft trunnion fasteners

The following locations required eddy-current surface scan:

- Front spar lower cap outside of each fastener row from the attachment fittings to the wing tips

- Step tang in the lower aft bathtub fittings

- Aft reinforcement on the front spar

- Aft flange of the leading-edge access panel at WS 63

- Aft flange of the leading-edge fuel cell access panel

Two cracks were found visually on the right wing. A crack, shown in figure 70, was found visually at WS 29 in the right wing stiffener panel in the wheel well bay common to the upper skin. Another crack, pictured in figure 71, was found visually in the leading-edge aft lower spar cap at WS 64. Three crack indications were found with bolthole eddy-current inspections. Two of these crack indications were found on the right wing at WS 36 in the upper inboard hole of the aft reinforcement and on the front spar lower cap. The third crack indication was found on the left wing also at WS 36 on the front spar lower cap. These three indications are acceptable per the SB due to the orientation of the indication.

Figure 70. Crack in the Right Wing Stiffener Panel in Wheel Well Common to the Upper Skin WS 29

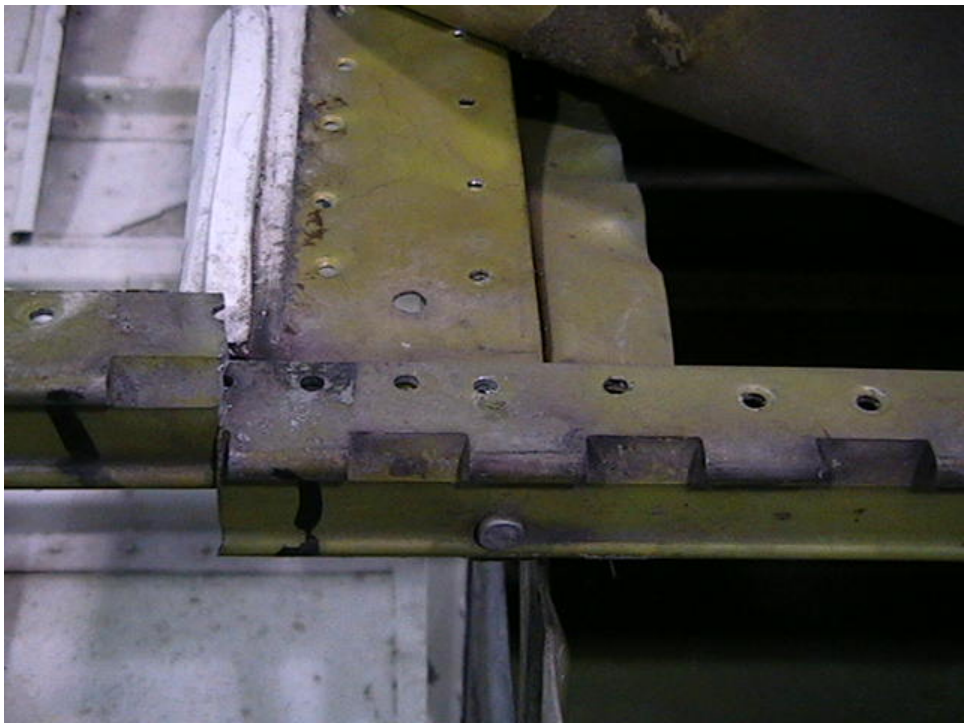

Figure 71. Crack in the Right Wing Leading-Edge Aft Lower Spar Cap WS 64

3.2 DISASSEMBLY PHASE.

The wings were disassembled to gain access to the primary wing structure to evaluate pre-existing damage. All details were fully disassembled, paint stripped, and etched for enhancing damage detection. Disassembly methods were selected to minimize potential damage to the underlying structure. Following the disassembly, all structural details were paint stripped using plastic media blasting and etched with a sodium hydroxide base to enhance damage detection during the post-disassembly NDI and microscopic examination.

3.3 POST-DISASSEMBLY NDIs.

Following the disassembly of the second set of T-34A wings, a comprehensive fluorescent liquid penetrant inspection was performed on all primary structure including the components of the spars and all attachment fittings. The post-disassembly NDI was performed to aid in the identification of all defects present in the structure. At least one defect was found on each of the following wing components: the left and right wing front spars, the left and right wing leading-edge spars, left wing rear spar, and the left and right wing rear spar upper bathtub fittings.

3.3.1 Left Wing.

Three areas of mechanical damage, three cracks, and twenty areas of corrosion were observed on the left wing. Five areas of pitting corrosion were found, and eight areas of intergranular corrosion and seven areas of exfoliation corrosion were also documented on the left wing during

the post-disassembly fluorescent liquid penetrant inspections. The structural stackup for the front spar is provided in figures 72 and 73, and the stackup for the rear spar is provided in figure 74.

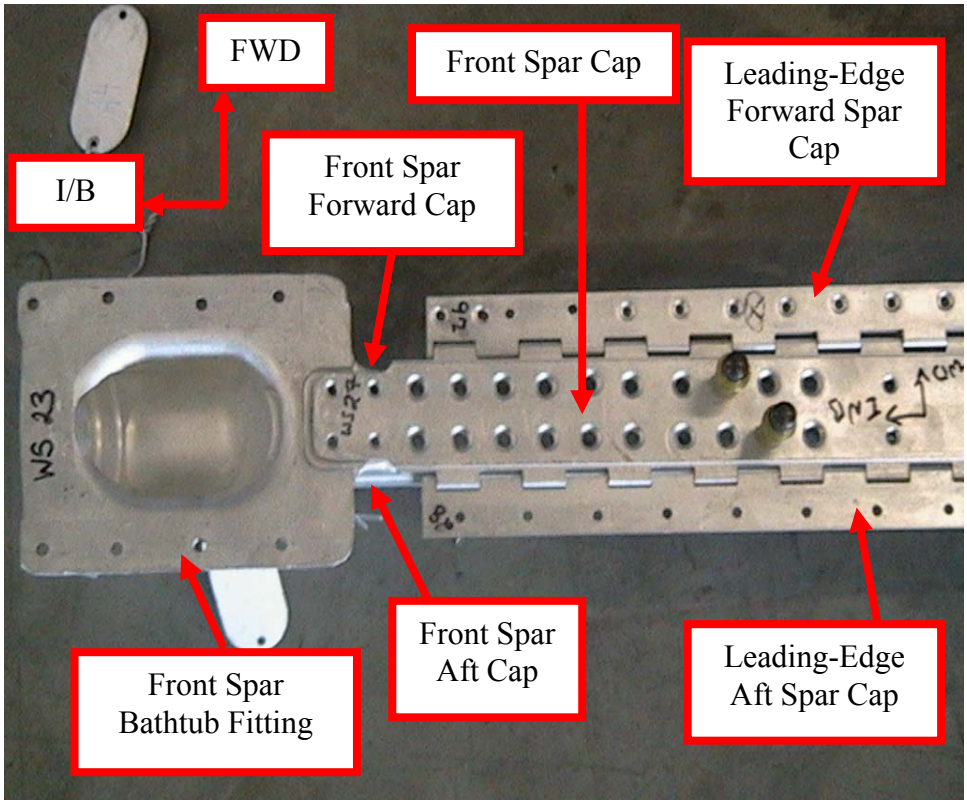

Figure 72. Front Spar Structural Stackup

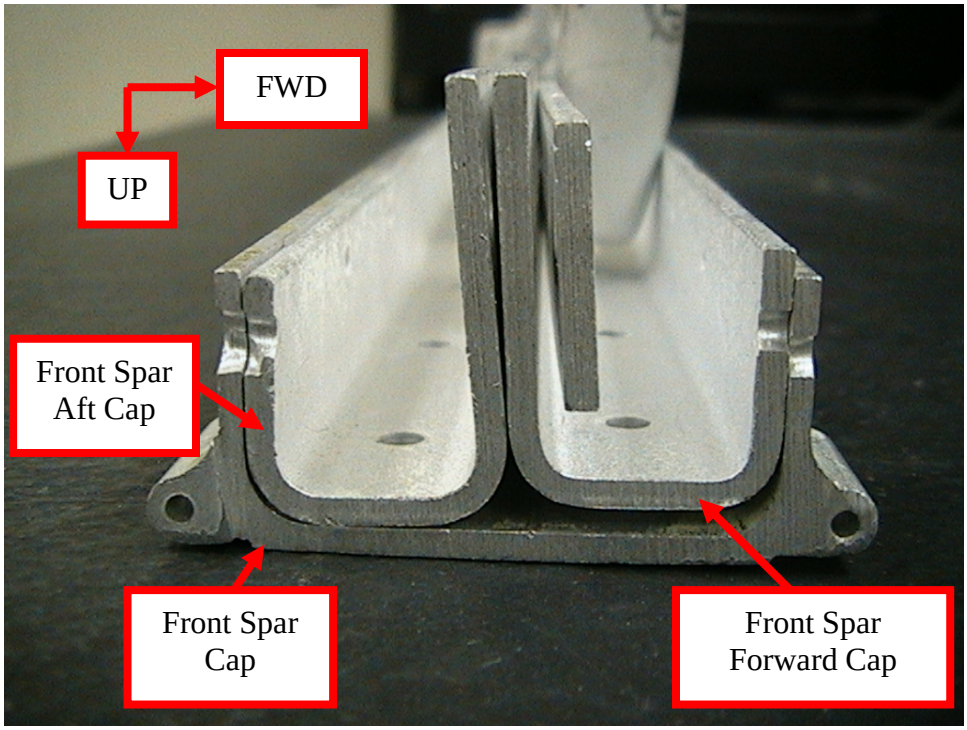

Figure 73. Front Spar Forward and Aft Cap Structural Stackup

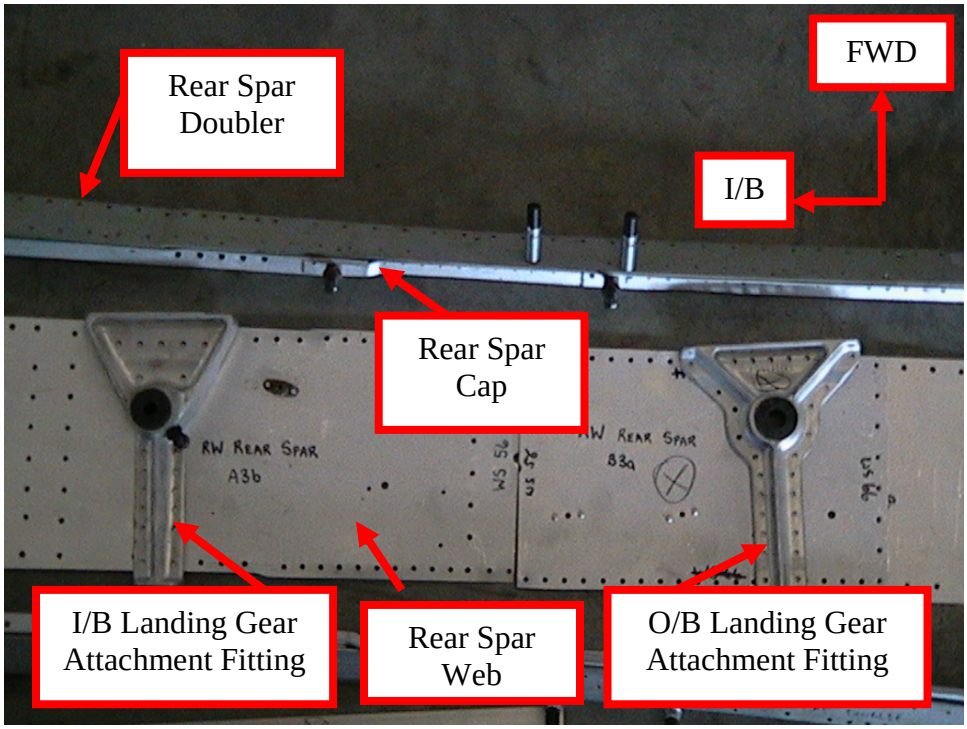

Figure 74. Rear Spar Structural Stackup

3.3.1.1 Left Wing Front Spar.

A 0.8-square-inch area of pitting corrosion was observed on the left wing front spar web, pictured in figure 75, from WS 37 to 42, as shown in figure 76. The left wing front spar upper cap is shown in figure 77. On the left wing front spar upper cap at WS 39.5, a 0.2-inch area of mechanical damage, shown in figure 78, was noted.

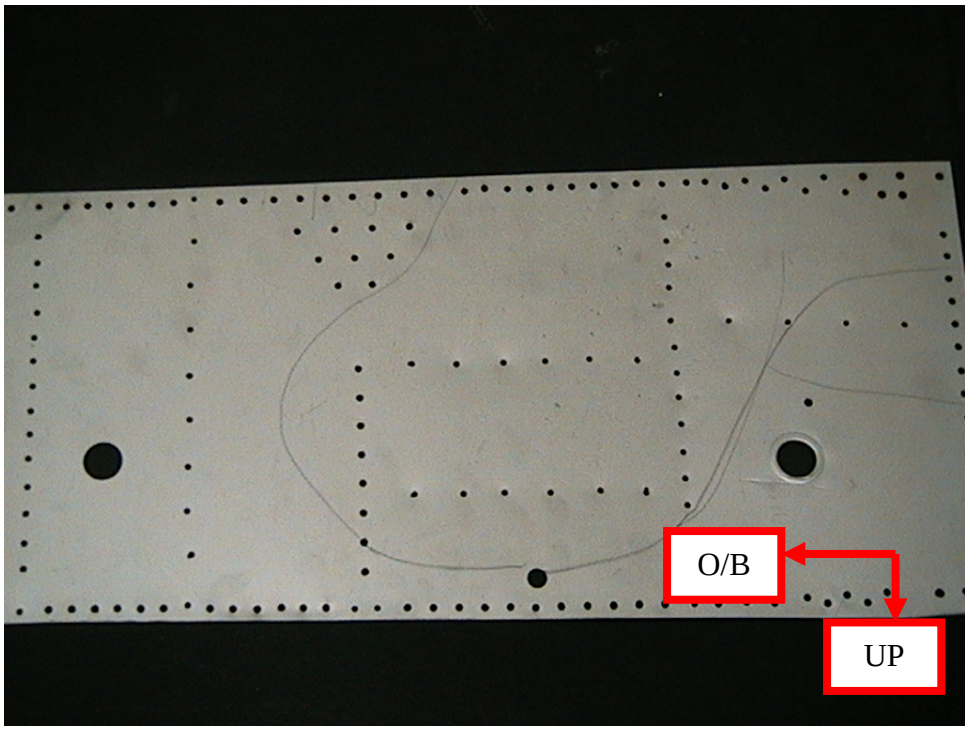

Figure 75. Left Wing Front Spar Web

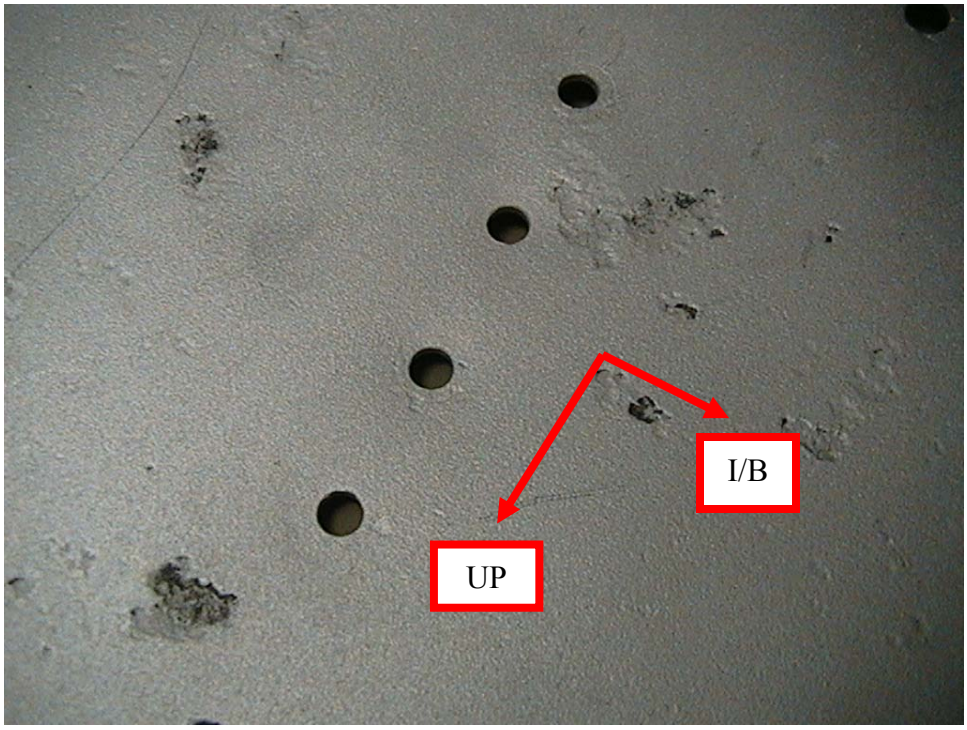

Figure 76. Corrosion on the Left Wing Front Spar Web WS 37-42

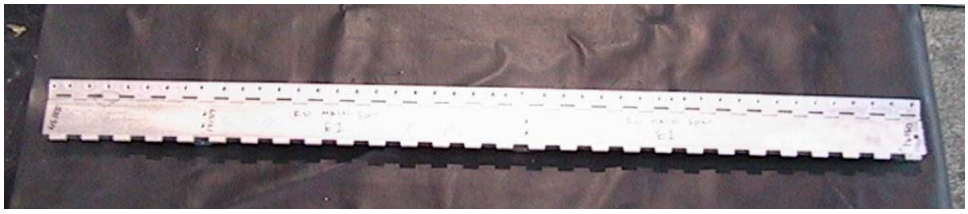

Figure 77. Left Wing Front Spar Upper Cap

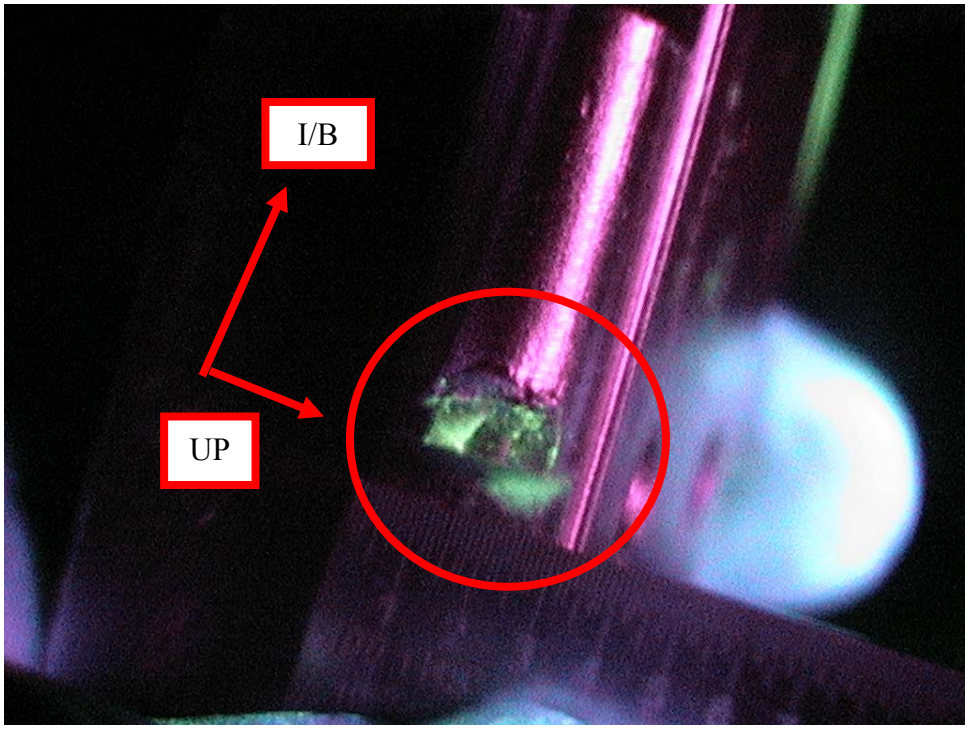

Figure 78. Damage on the Left Wing Front Spar Upper Cap WS 39.5

Two areas of exfoliation corrosion spanning 3.5 and 6.3 inches were observed on the upper spar cap and are shown in figures 79 and 80, respectively. These areas of corrosion were located from WS 118 to 122.5 and WS 136 to 142.75. Intergranular corrosion was documented on the upper cap at WS 139. This corrosion, shown in figure 81, measures 0.6 inch in length.

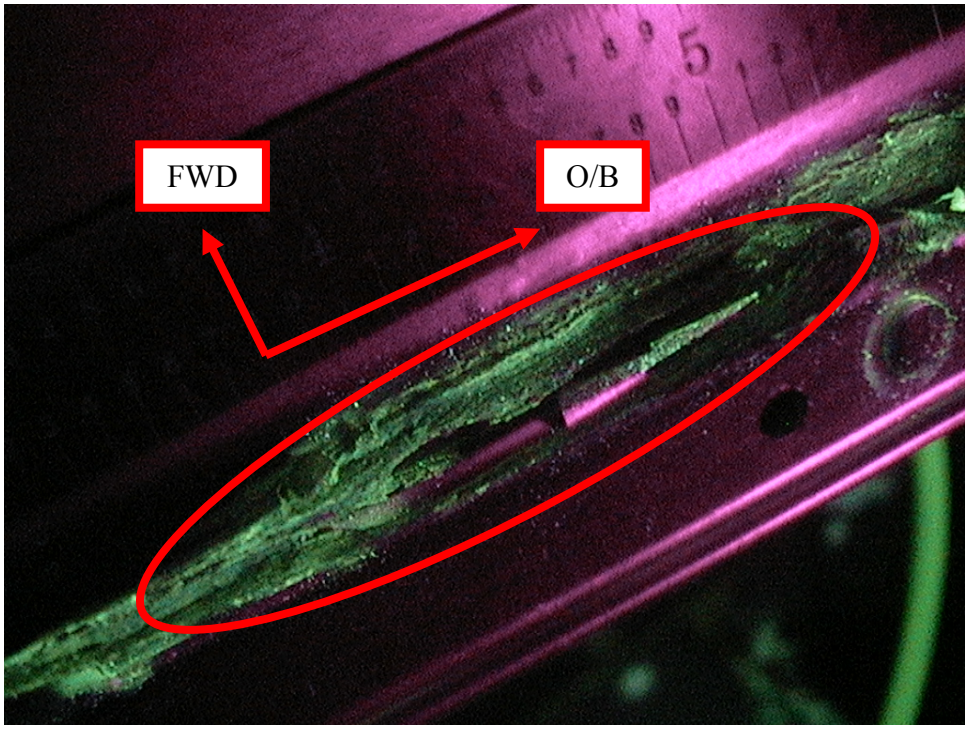

Figure 79. Exfoliation Corrosion on the Left Wing Front Spar Upper Cap WS 118-122.5

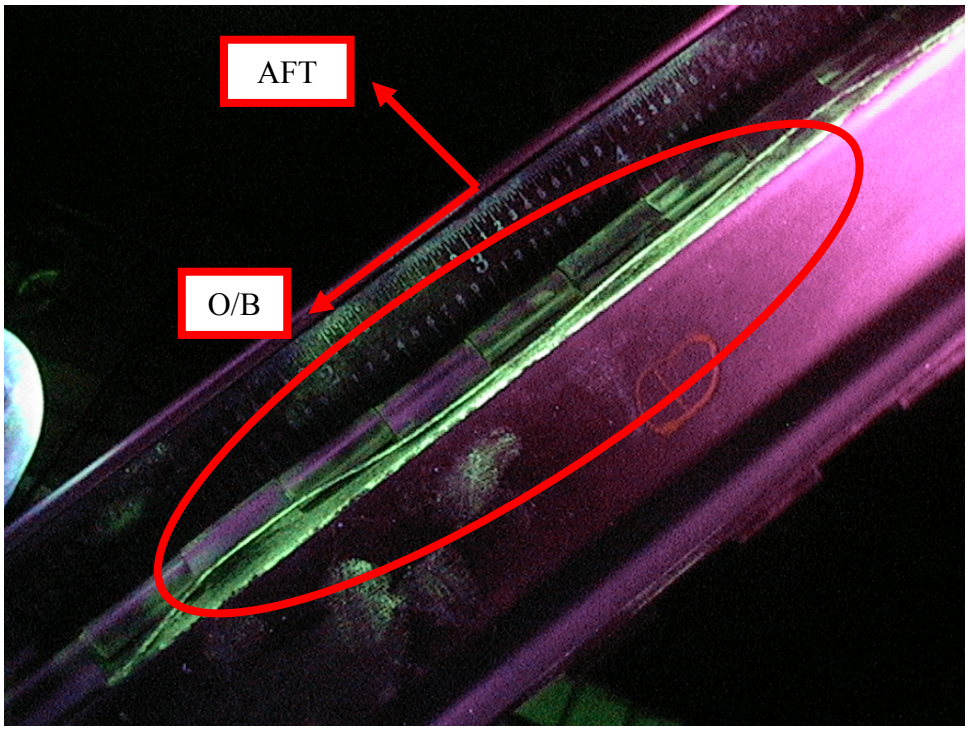

Figure 80. Exfoliation Corrosion on the Left Wing Front Spar Upper Cap WS 136-142.75

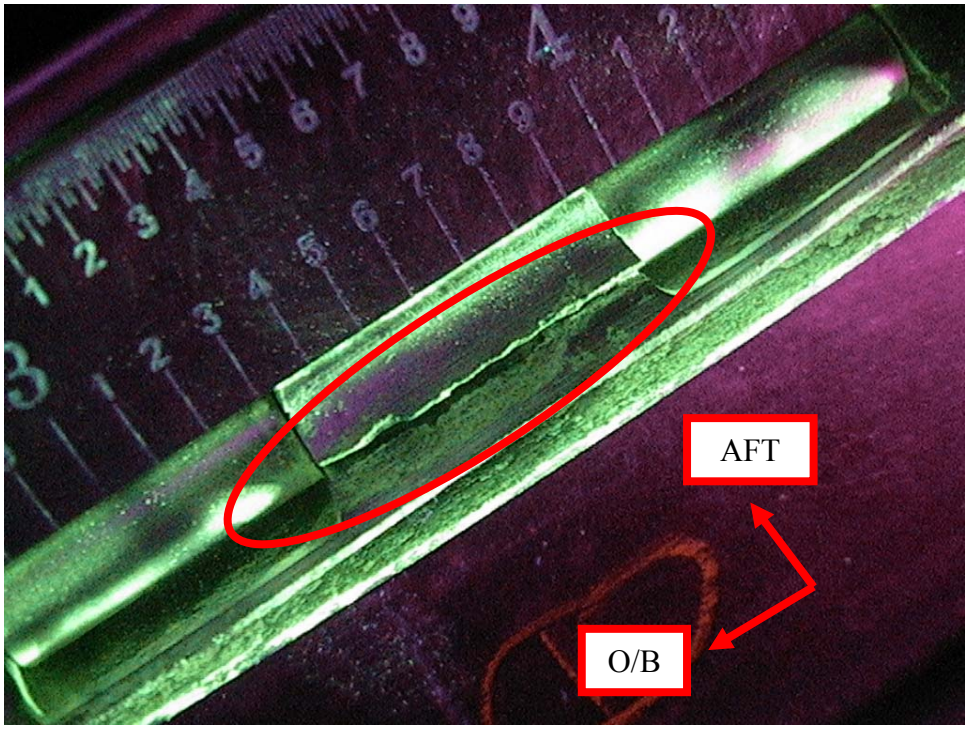

Figure 81. Intergranular Corrosion on the Left Wing Front Spar Upper Cap WS 139

Figure 82 shows an area of exfoliation corrosion, measuring 0.75 inch, located from WS 156.25 to 157.25. Damage observed on the left wing front spar upper cap at WS 156.75 is pictured in figure 83. This area of mechanical damage measured 0.6 inch in length.

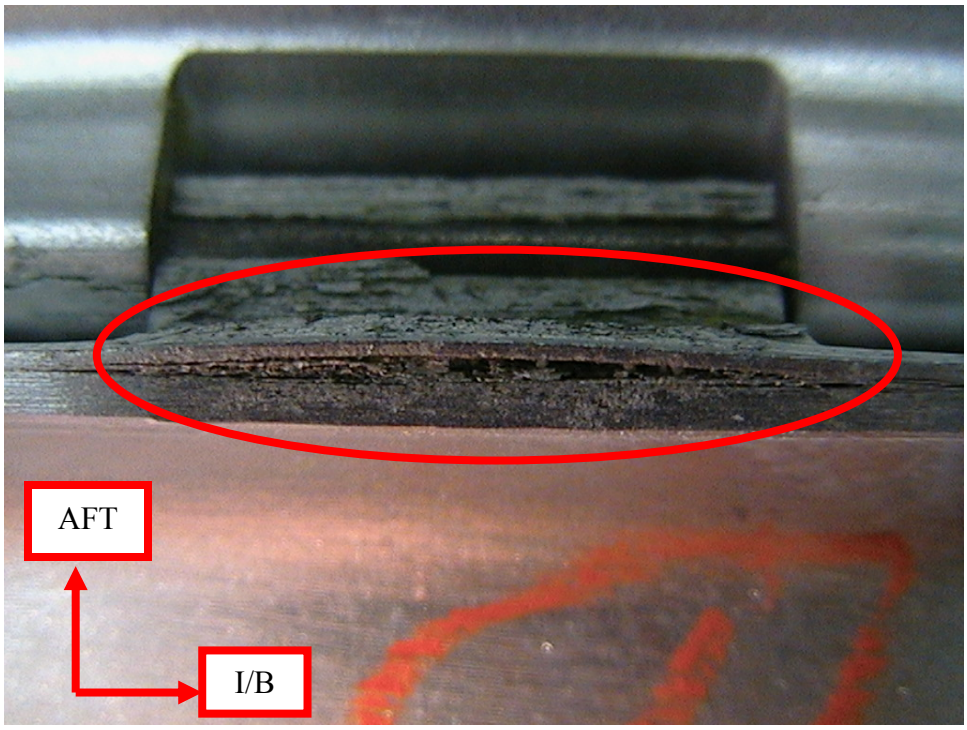

Figure 82. Exfoliation Corrosion on the Left Wing Front Spar Upper Cap WS 156.25-157.25

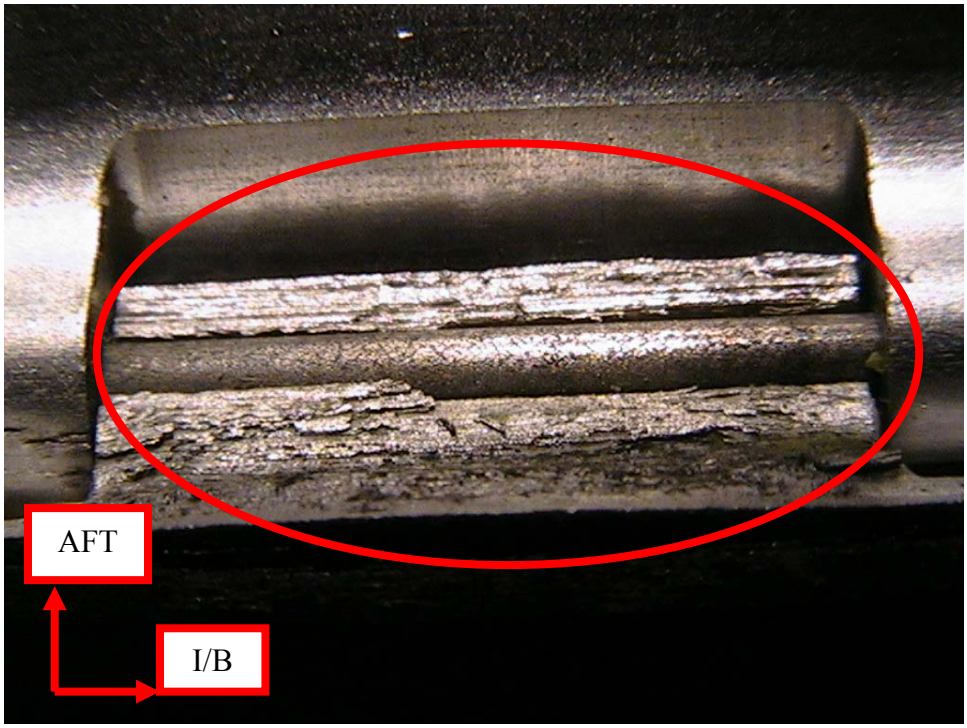

Figure 83. Damage on the Left Wing Front Spar Upper Cap WS 156.75

Three areas of intergranular corrosion were observed on the left wing front spar upper cap, two at from WS 157.25 and one at WS 163.75. These areas of corrosion measured 0.31, 0.35, and 0.25 inch and are shown in figures 84 to 86, respectively. The exfoliation corrosion, located at WS 164, measured 0.8 inch and is shown in figure 87. A 0.6-inch area of damage, also located at WS 164, is pictured in figure 88.

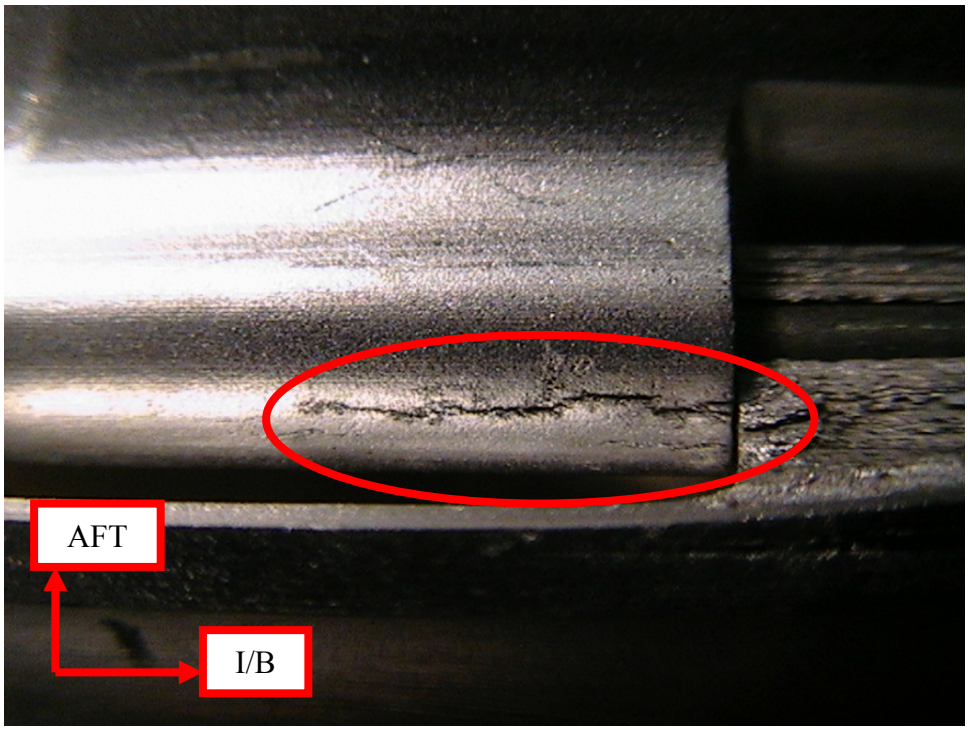

Figure 84. Intergranular Corrosion on the Left Wing Front Spar Upper Cap
WS 157.25 Bottom View

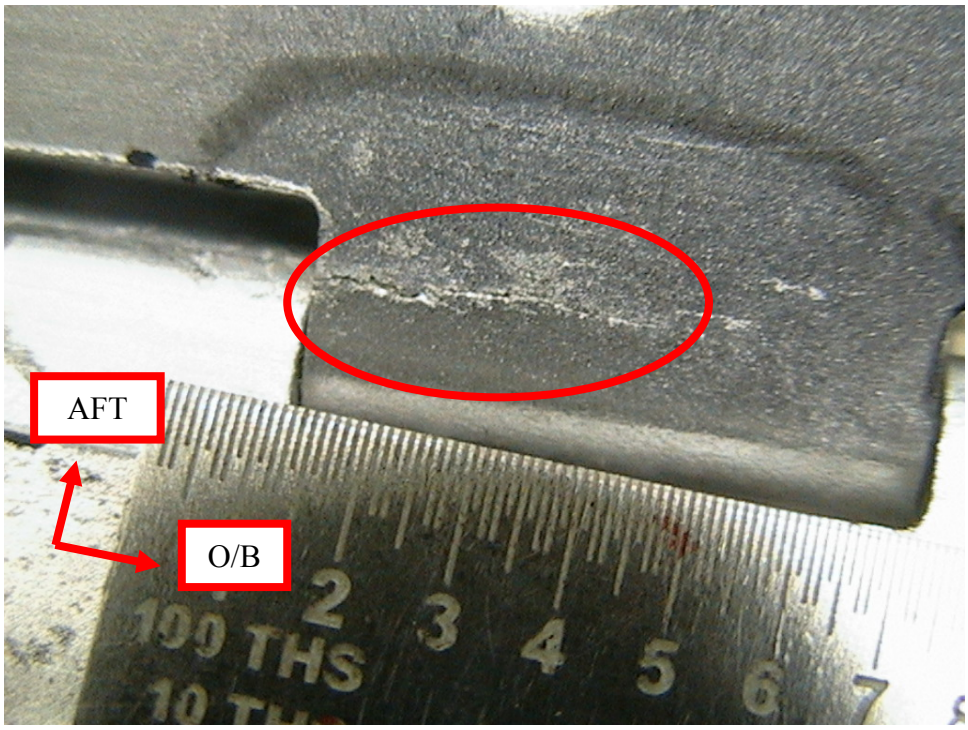

Figure 85. Intergranular Corrosion on the Left Wing Front Spar Upper Cap WS 157.25 Top View

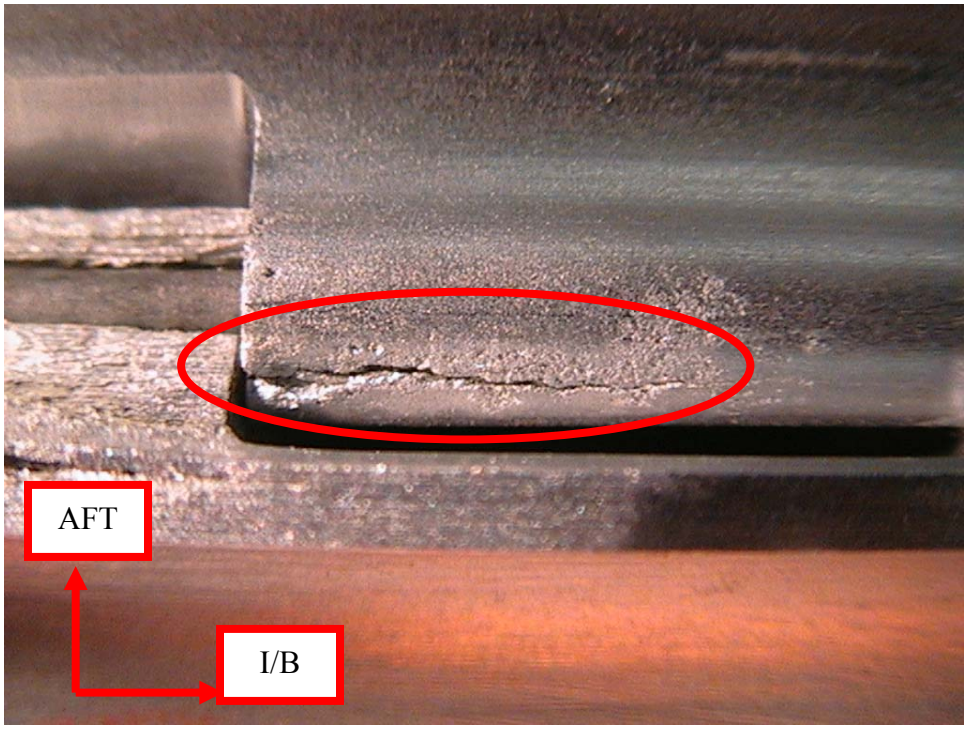

Figure 86. Intergranular Corrosion on the Left Wing Front Spar Upper Cap WS 163.75

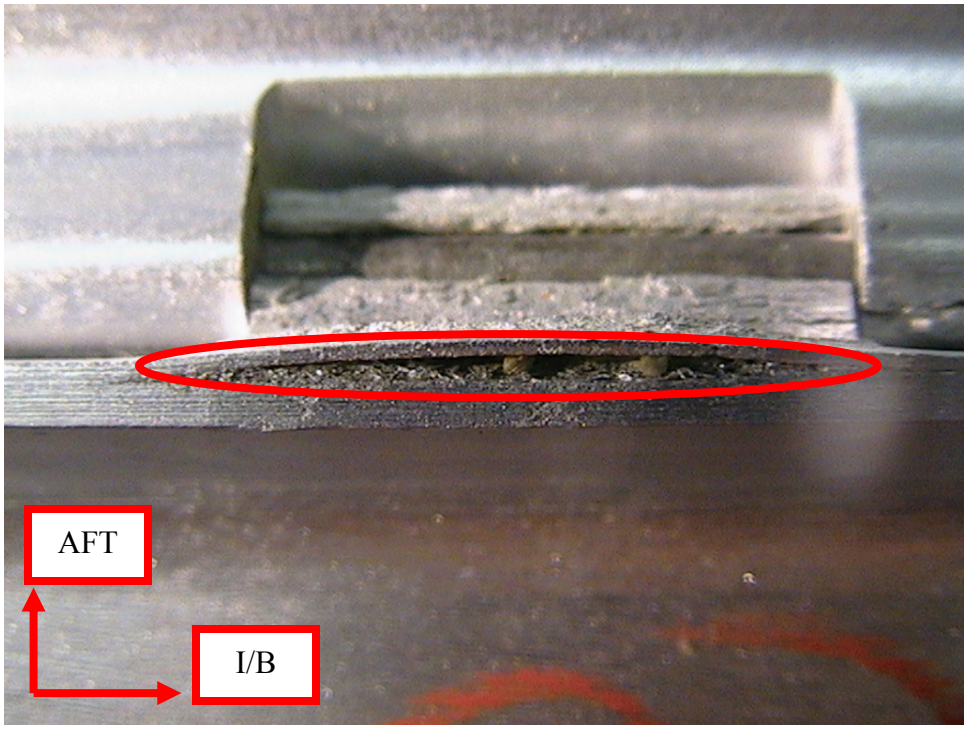

Figure 87. Exfoliation Corrosion on the Left Wing Front Spar Upper Cap WS 164

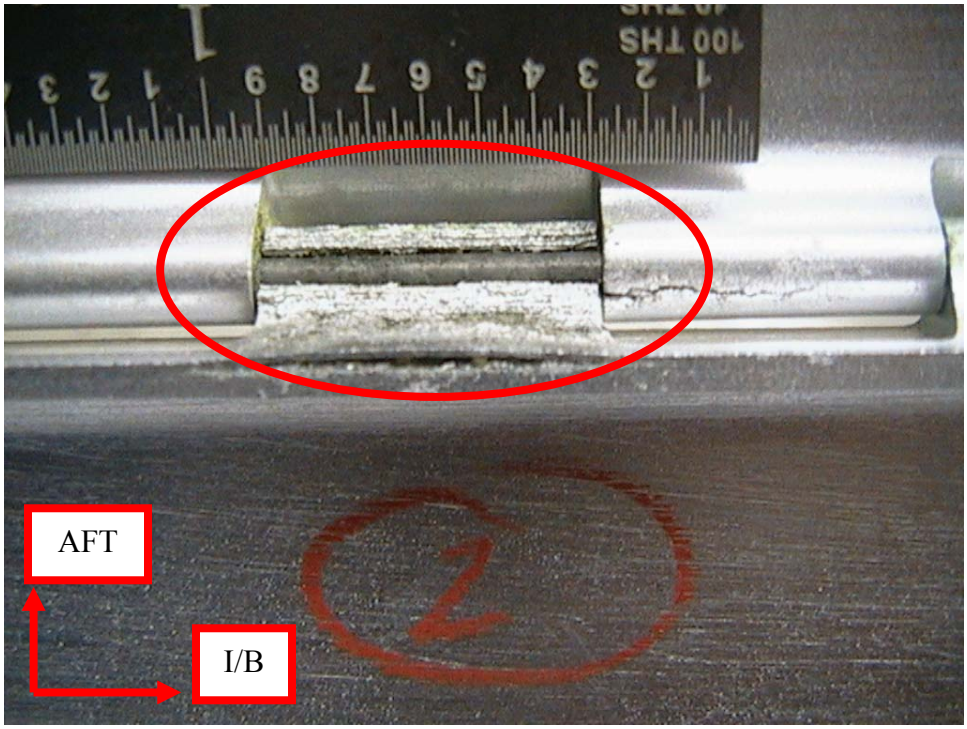

Figure 88. Damage on the Left Wing Front Spar Upper Cap WS 164

Figure 89 shows a 0.25-inch area of exfoliation corrosion located at WS 166.5, and figure 90 shows a 0.6-inch area of intergranular corrosion located at WS 166.75 on the left wing front spar upper cap. A 0.7-inch area of exfoliation corrosion and a 0.07-inch area of intergranular corrosion are pictured in figure 91 and were located on the front spar upper cap at WS 170.25.

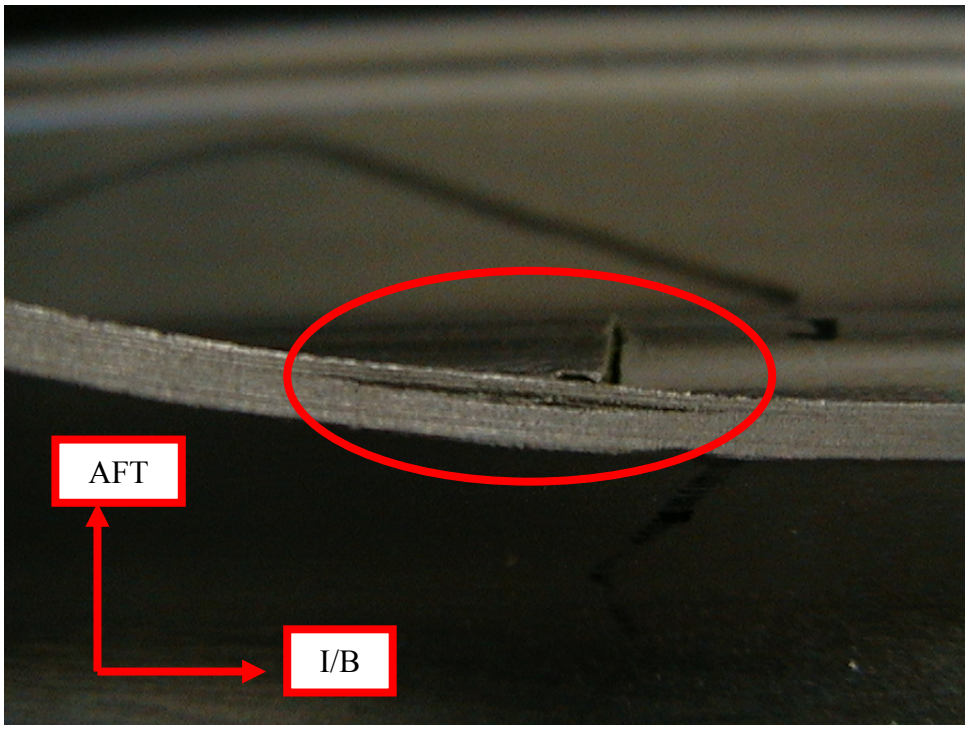

Figure 89. Exfoliation Corrosion on the Left Wing Front Spar Upper Cap WS 166.5

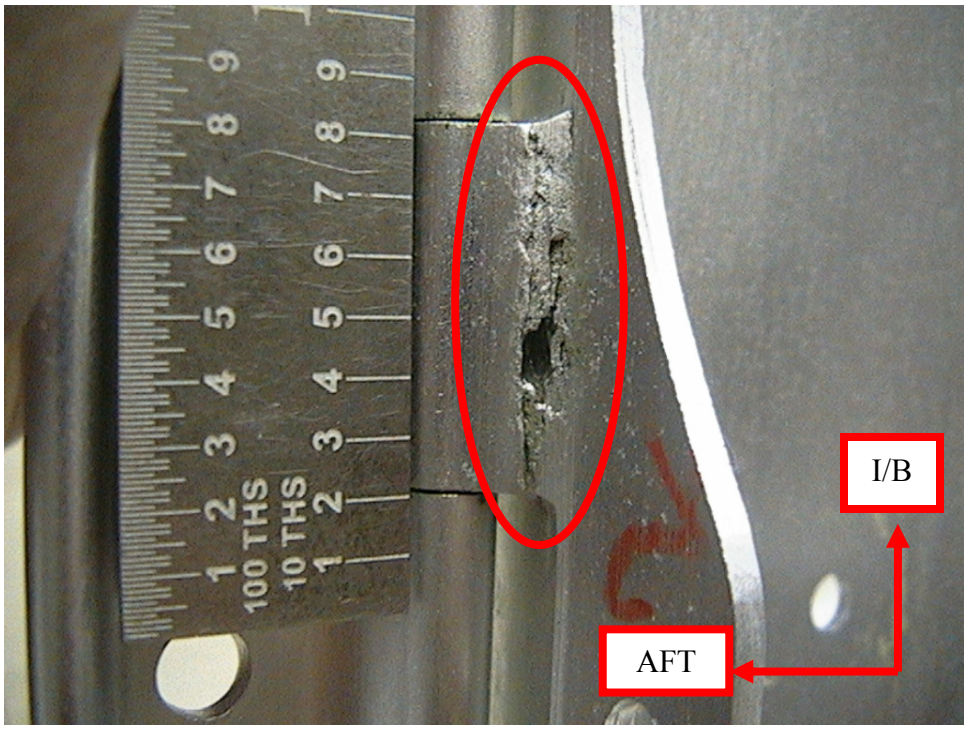

Figure 90. Intergranular Corrosion on the Left Wing Front Spar Upper Cap WS 166.75

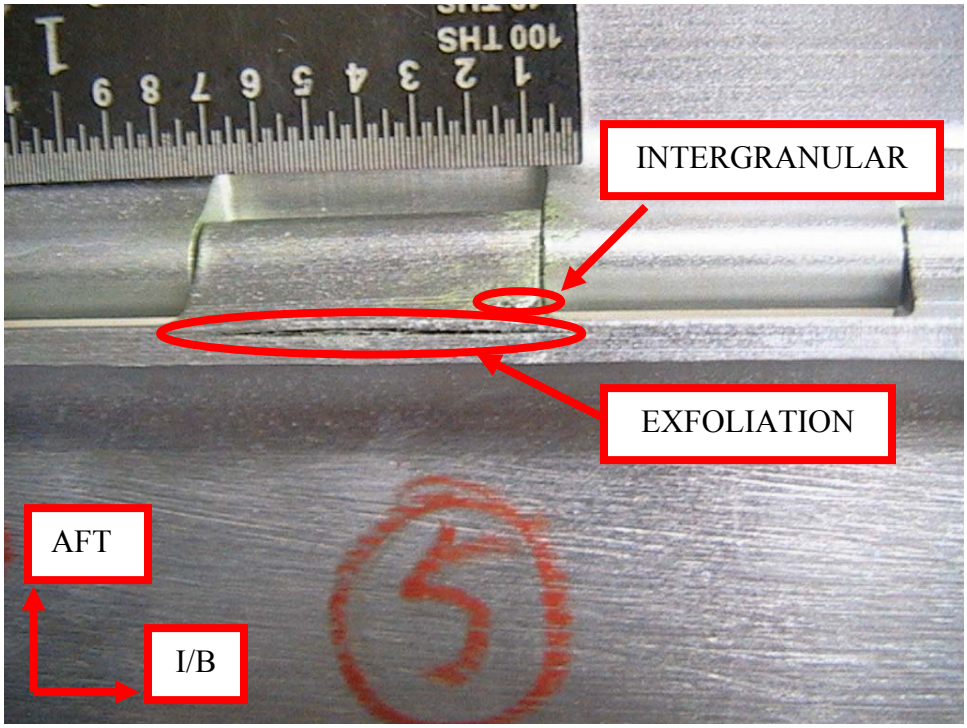

Figure 91. Exfoliation and Intergranular Corrosion on the Left Wing Front Spar Upper Cap WS 170.25

A 1-inch area of exfoliation corrosion, located at WS 171.25, and a 0.6-inch area of intergranular corrosion, located at WS 171.5, are shown in figure 92. Two areas of pitting corrosion were observed on the left wing front spar upper cap at WS 174 and 174.25. These areas of corrosion covered 0.008 and 0.013 square inch and are shown in figure 93.

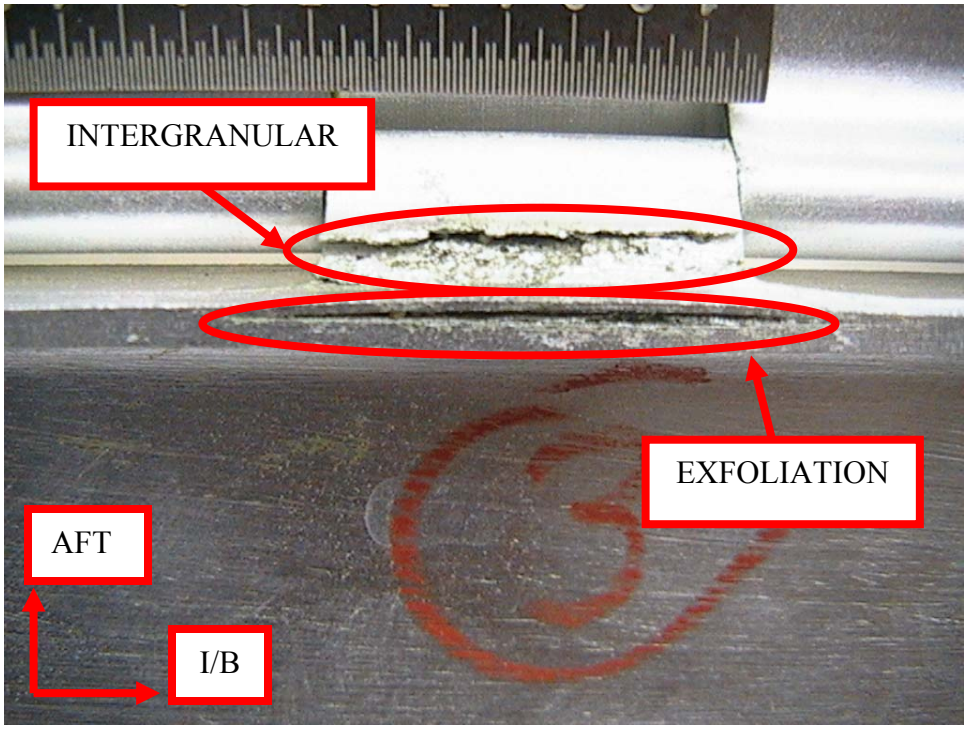

Figure 92. Exfoliation and Intergranular Corrosion on the Left Wing Front Spar Upper Cap WS 171.25 and 171.5

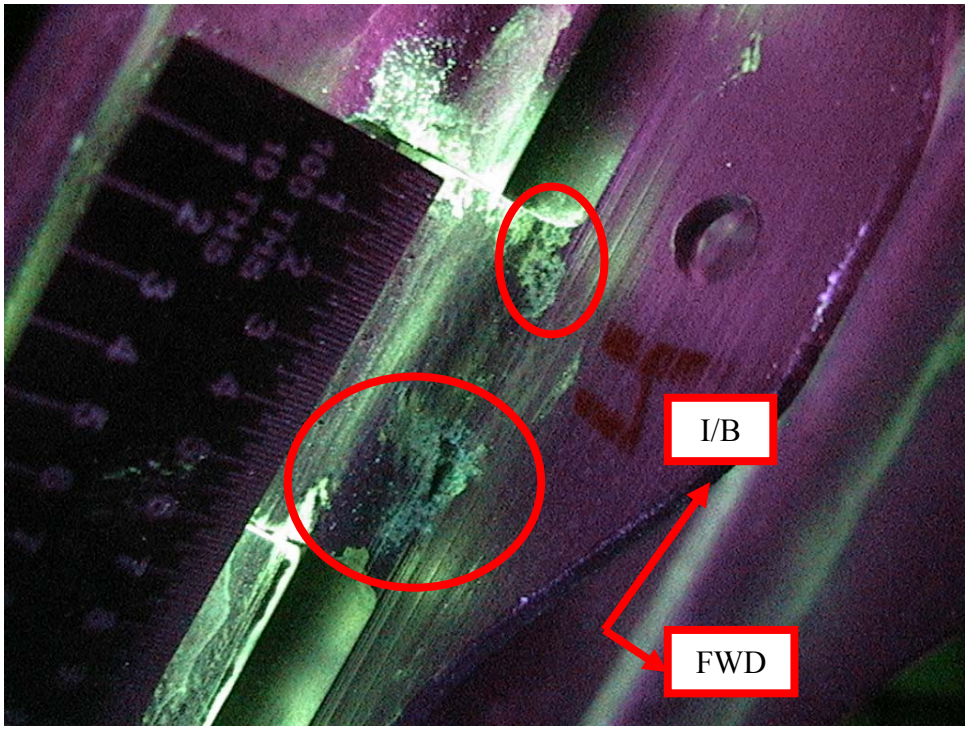

Figure 93. Pitting Corrosion on the Left Wing Front Spar Upper Cap
WS 174 and 174.25

3.3.1.2 Left Wing Leading-Edge Spar.

The left wing leading-edge aft lower spar cap is shown in figure 94. Figure 95 shows a 1.3-inch crack observed on the left wing leading-edge aft lower spar cap at WS 64. Pitting corrosion was also observed on the aft lower spar cap from WS 57 to 69. This area of corrosion encompassed a surface area of 1.6 square inches and is shown in figure 96. Another area of pitting corrosion was observed on the aft upper cap, shown in figure 97, from WS 100.5 to 102.5, covering a surface area of 0.8 square inch. This area of pitting corrosion is pictured in figure 98.

Figure 94. Left Wing Leading-Edge Aft Lower Spar Cap

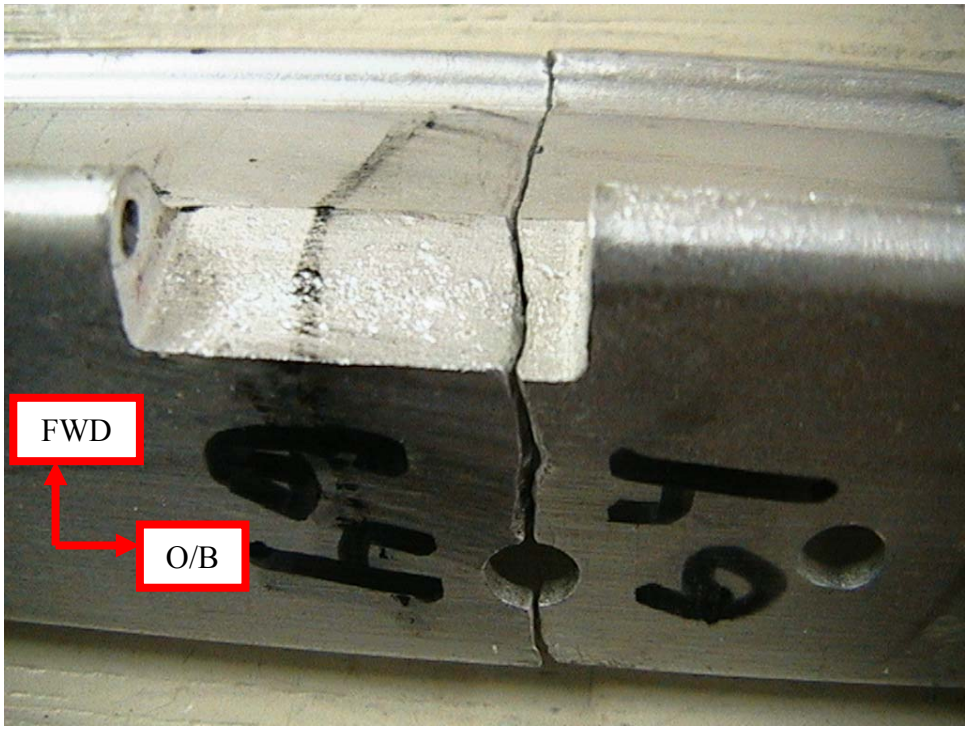

Figure 95. Crack in the Left Wing Leading-Edge Aft Lower Spar Cap WS 64

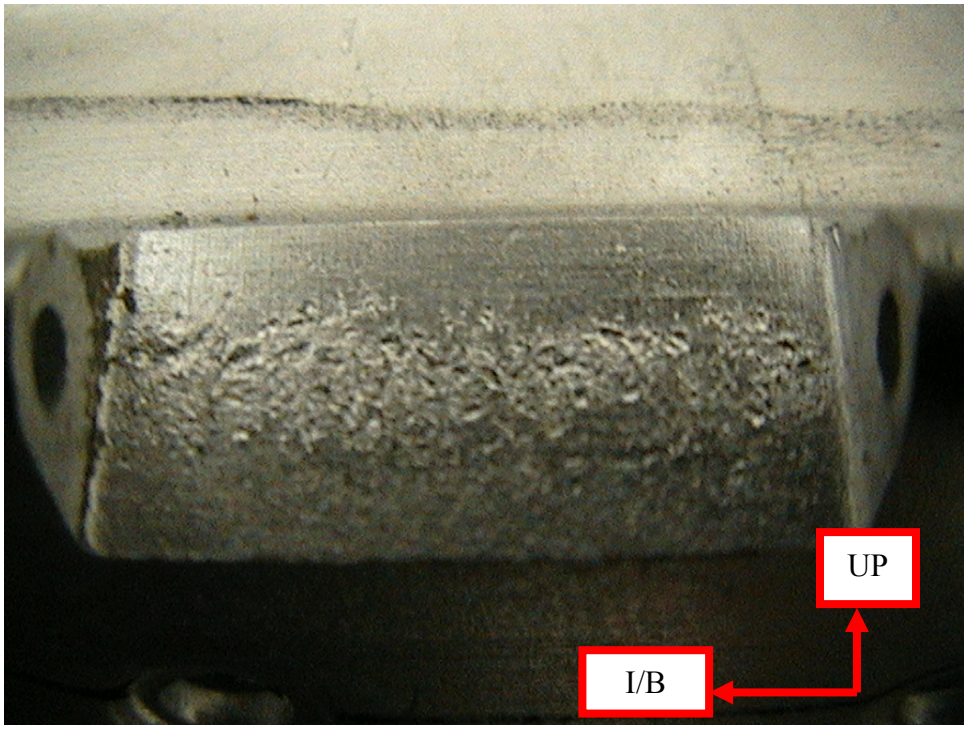

Figure 96. Pitting Corrosion on the Left Wing Leading-Edge Aft Lower Spar Cap WS 57-69

Figure 97. Left Wing Leading-Edge Forward Upper Spar Cap

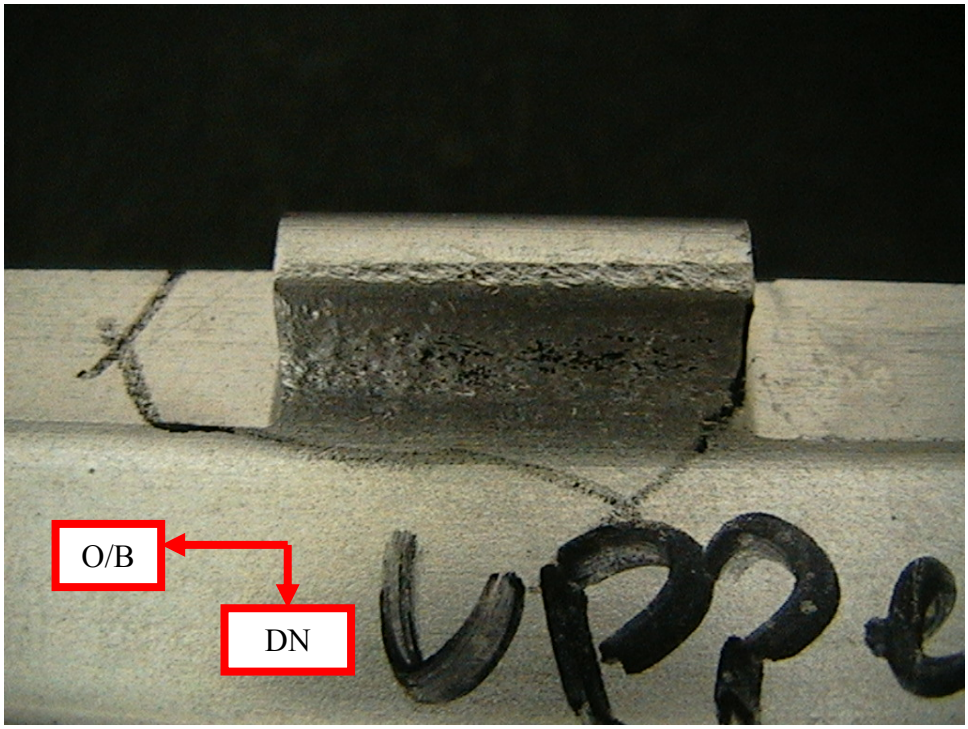

Figure 98. Pitting Corrosion on the Left Wing Leading-Edge Forward Upper Spar Cap
WS 100.5-102.5

3.3.1.3 Left Wing Rear Spar.

A 0.8-inch crack was observed on the rear spar lower doubler, shown in figure 99 at WS 64. This crack, which was detected during the post-disassembly NDI, is shown in figure 100. Another crack, with a length of 0.6 inch, was found on the rear spar lower cap, shown in figure 101 at WS 64 and is pictured in figure 102.

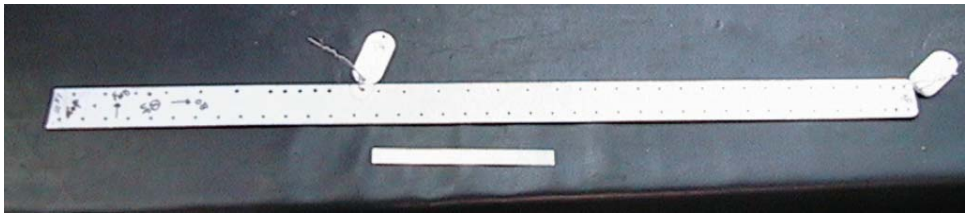

Figure 99. Left Wing Rear Spar Lower Doubler

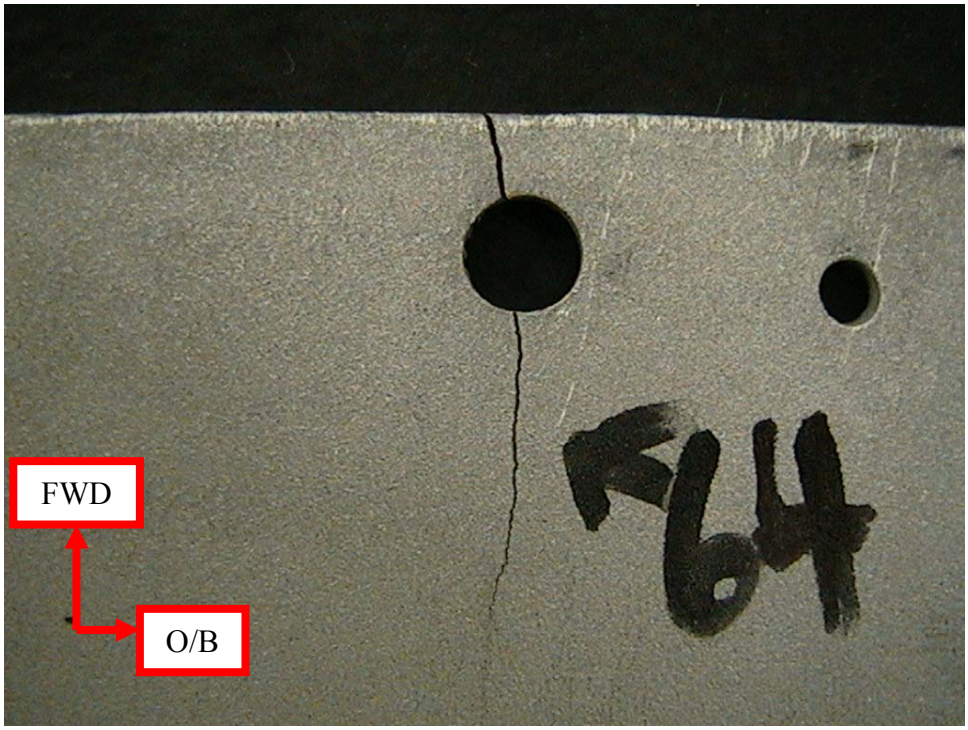

Figure 100. Crack in the Left Wing Rear Spar Lower Doubler WS 64

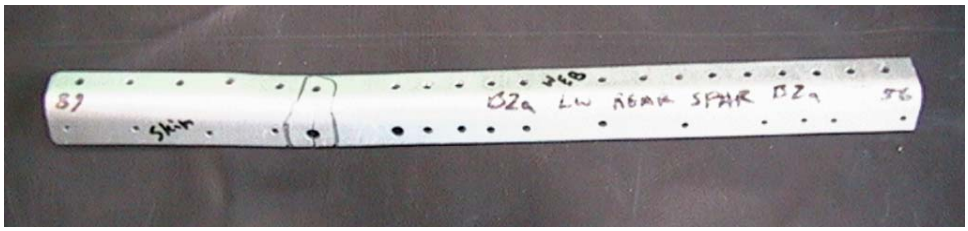

Figure 101. Left Wing Rear Spar Forward Lower Spar Cap

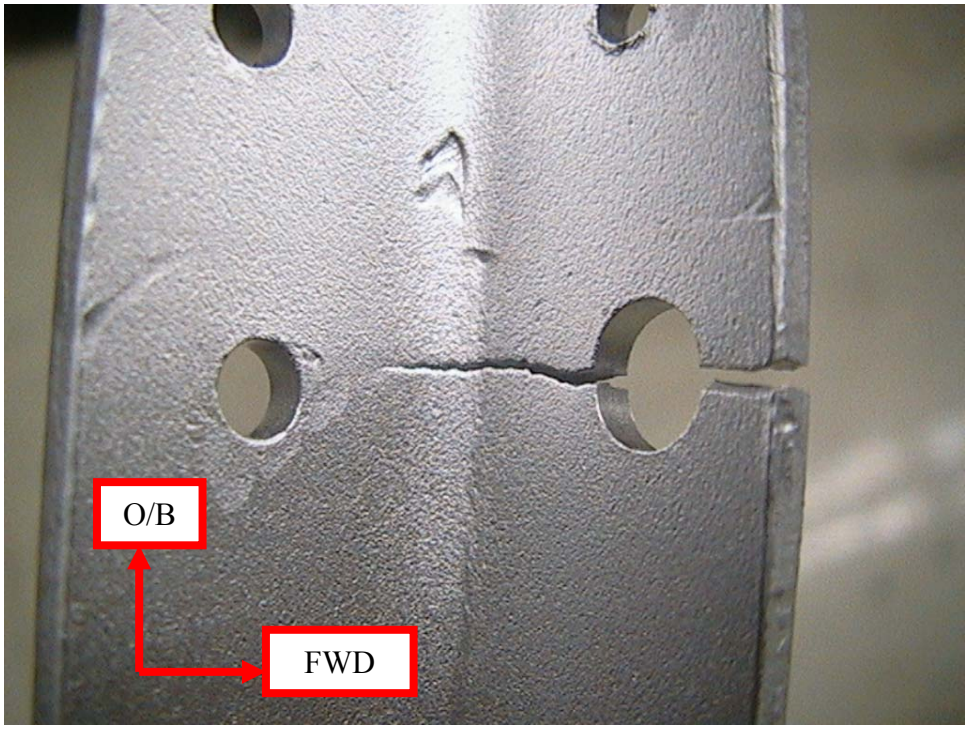

Figure 102. Crack in the Left Wing Rear Spar Forward Lower Cap WS 64

3.3.1.4 Left Wing Attachment Fittings.

No defects were noted on the left wing landing gear attachment fittings during the post-disassembly NDI. The only defect observed on any of the left wing attachment fittings was one area of intergranular corrosion on the left wing rear spar upper bathtub fitting. The left wing rear spar upper bathtub fitting is shown in figure 103. The one area of intergranular corrosion, covering a surface area of 0.1 square inch, was located at WS 27, and it is shown in figure 104.

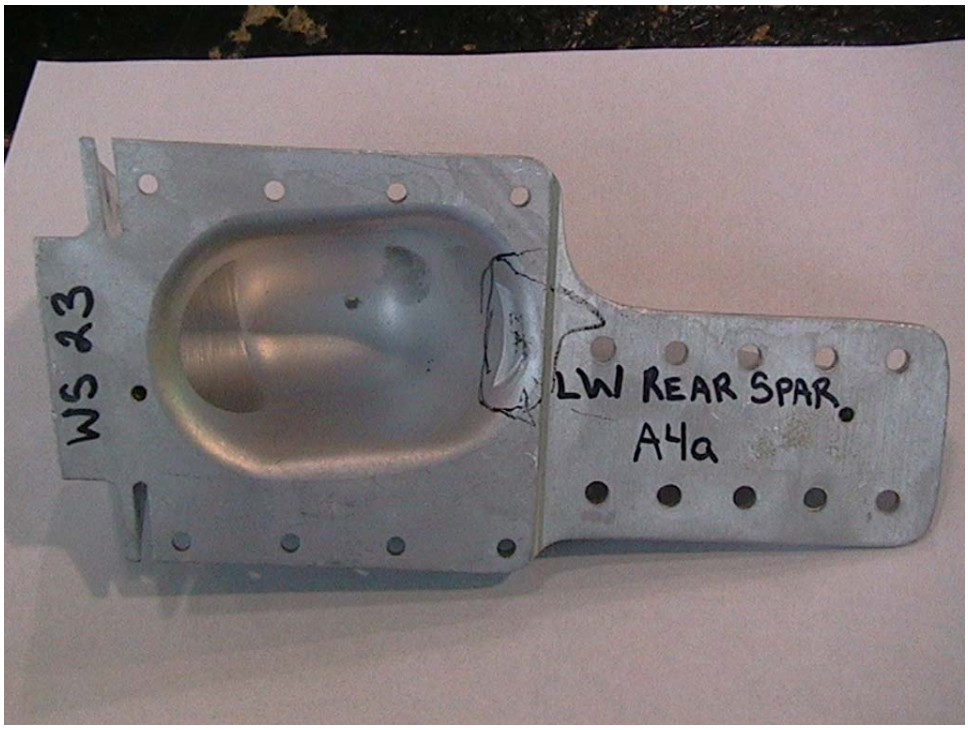

Figure 103. Left Wing Rear Spar Upper Bathtub Fitting

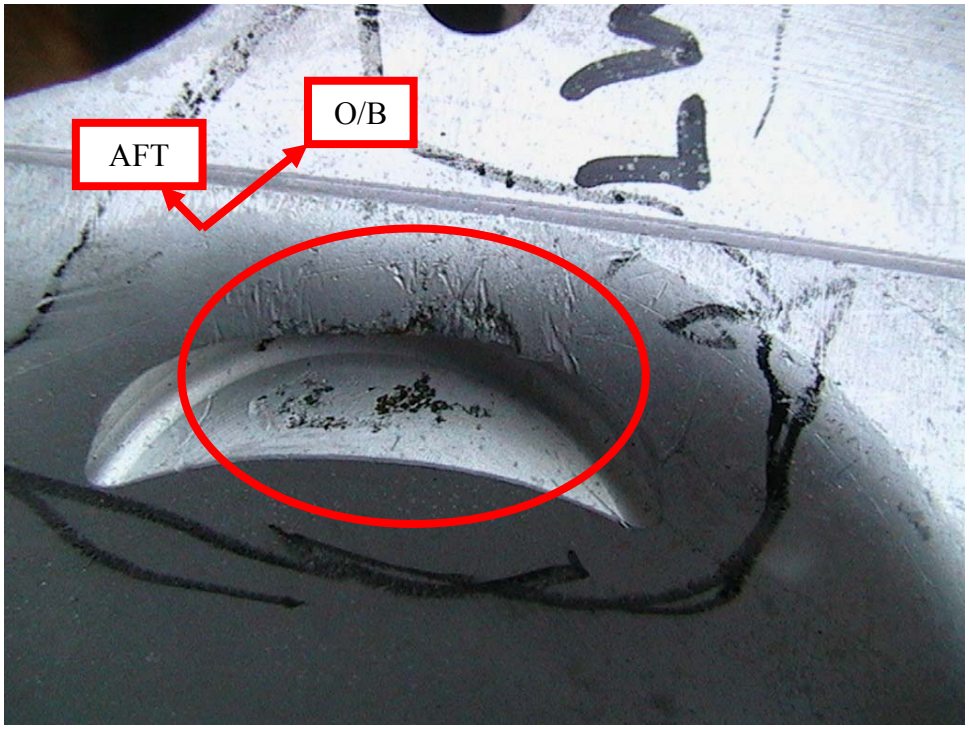

Figure 104. Intergranular Corrosion on the Left Wing Rear Spar Upper Bathtub Fitting WS 27

3.3.2 Right Wing.

Five cracks and eleven areas of corrosion were reported on the right wing. Three instances of pitting corrosion, seven areas of intergranular corrosion, and one area of exfoliation corrosion were observed.

3.3.2.1 Right Wing Front Spar.

Pitting corrosion was observed on the right wing front spar web, shown in figure 105. This corrosion, pictured in figure 106, covered a surface area of 0.13 square inch, was scattered from WS 36 to 48. The right wing front spar upper cap is shown in figure 107. Two areas of intergranular corrosion, each measuring 0.65 inch, were discovered on the right wing front spar upper cap from WS 89.5-90 and at WS 109.5. These areas of corrosion are pictured in figures 108 and 109, respectively.

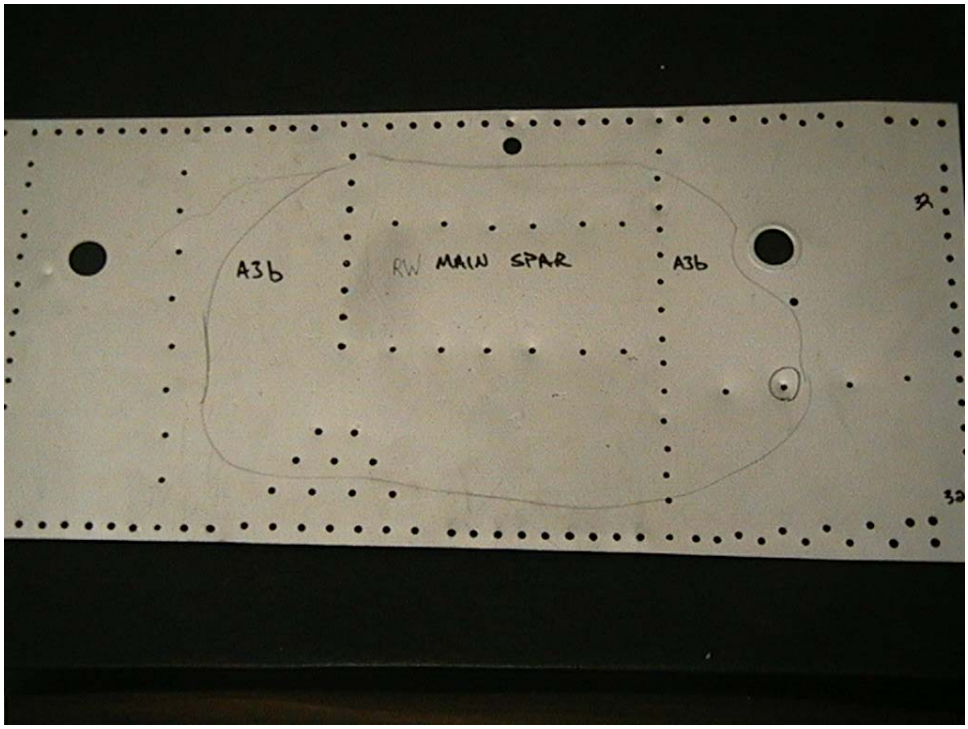

Figure 105. Right Wing Front Spar Web

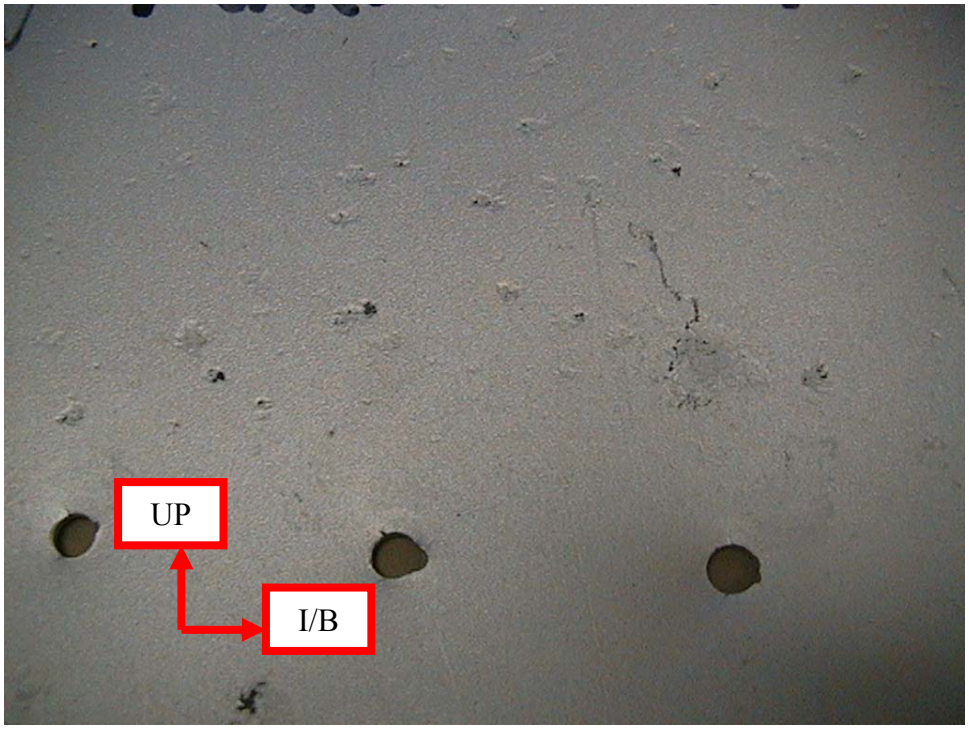

Figure 106. Pitting Corrosion on the Right Wing Front Spar Web WS 36-48

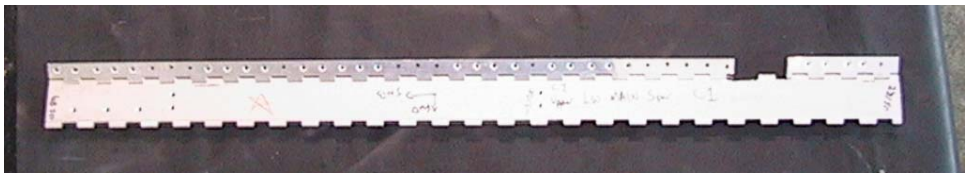

Figure 107. Right Wing Front Spar Upper Cap

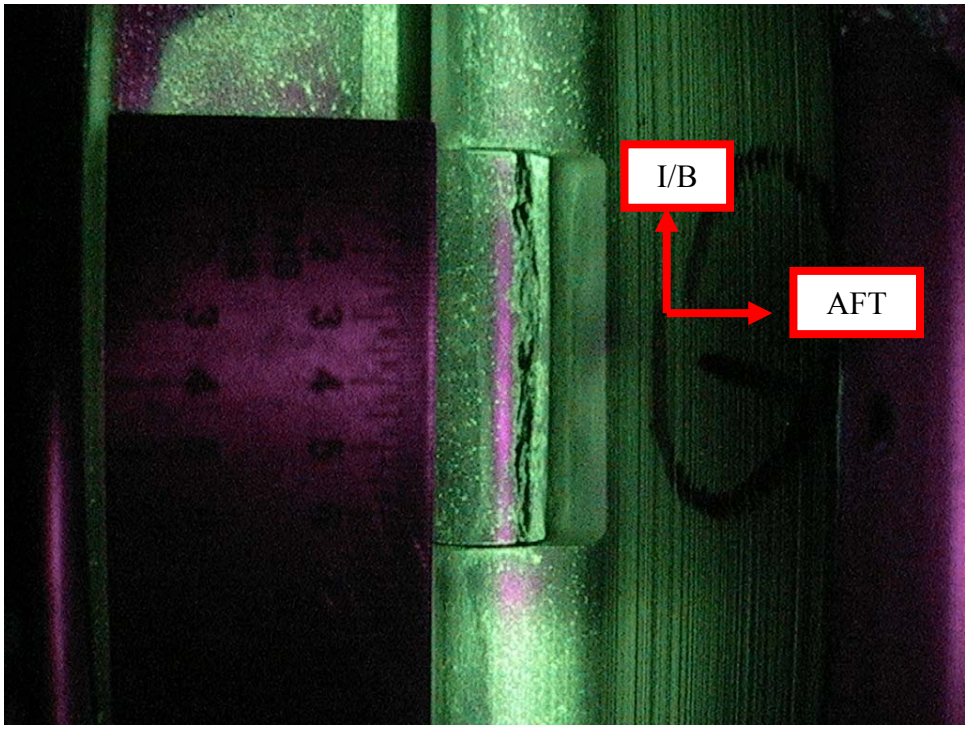

Figure 108. Intergranular Corrosion on the Right Wing Front Spar Upper Cap WS 89.5-90

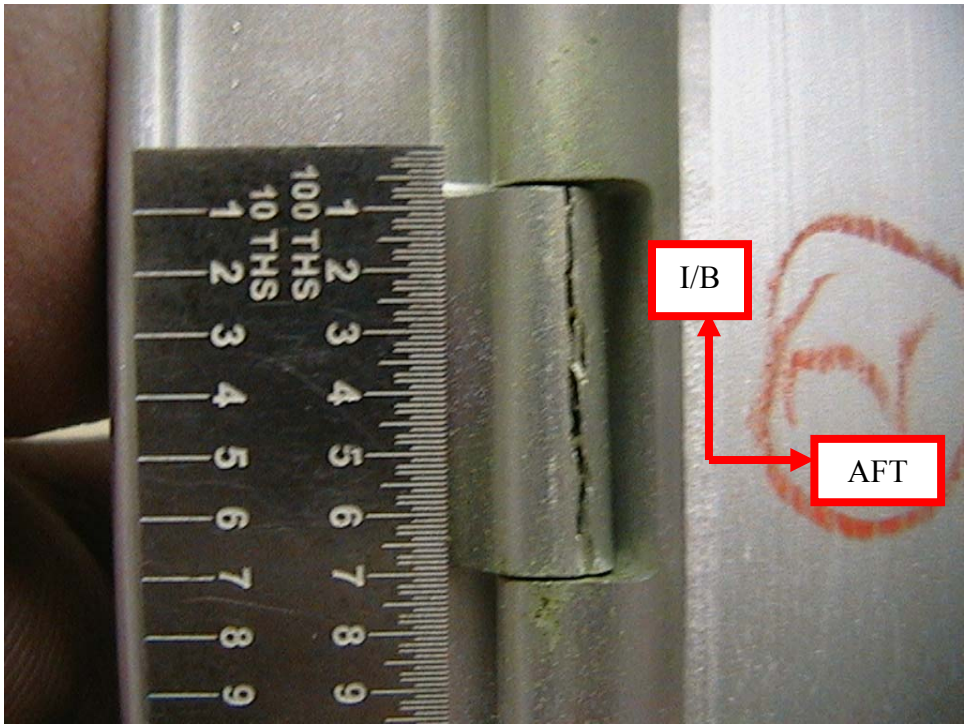

Figure 109. Intergranular Corrosion on the Right Wing Front Spar Upper Cap WS 109.5

A 1-inch area of exfoliation corrosion, located at WS 183.5, was observed on the upper cap and is shown in figure 110. Three areas of intergranular corrosion, located from WS 184 to 185.25, ranged in size from 0.4 to 0.6 inch. These three areas of corrosion are shown in figures 111 and 112. An area of intergranular corrosion was found on both sides of the upper spar cap at WS 187, shown in figures 113 and 114. This area of corrosion measured 0.4 inch in length.

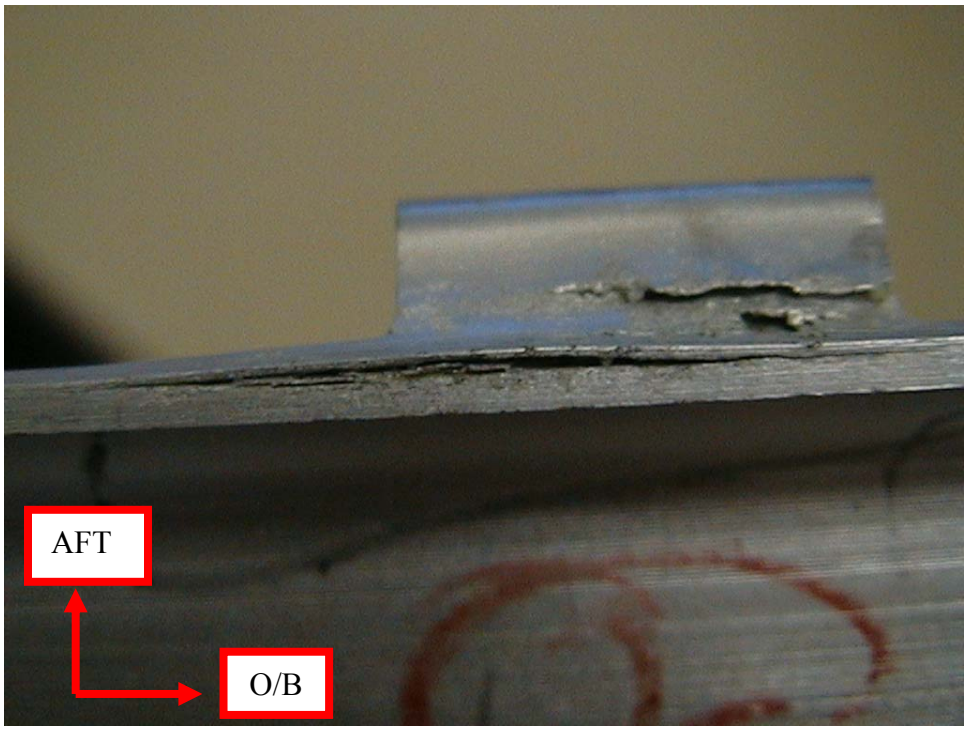

Figure 110. Exfoliation Corrosion on the Right Wing Front Spar Upper Cap WS 183.5

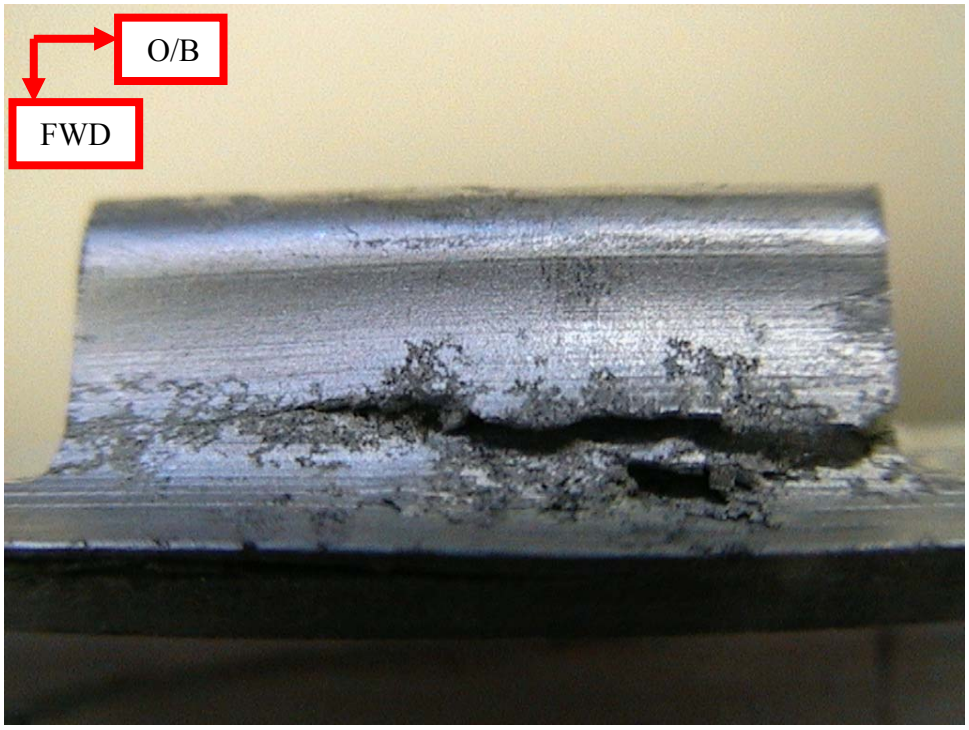

Figure 111. Intergranular Corrosion on the Right Wing Front Spar Upper Cap WS 184

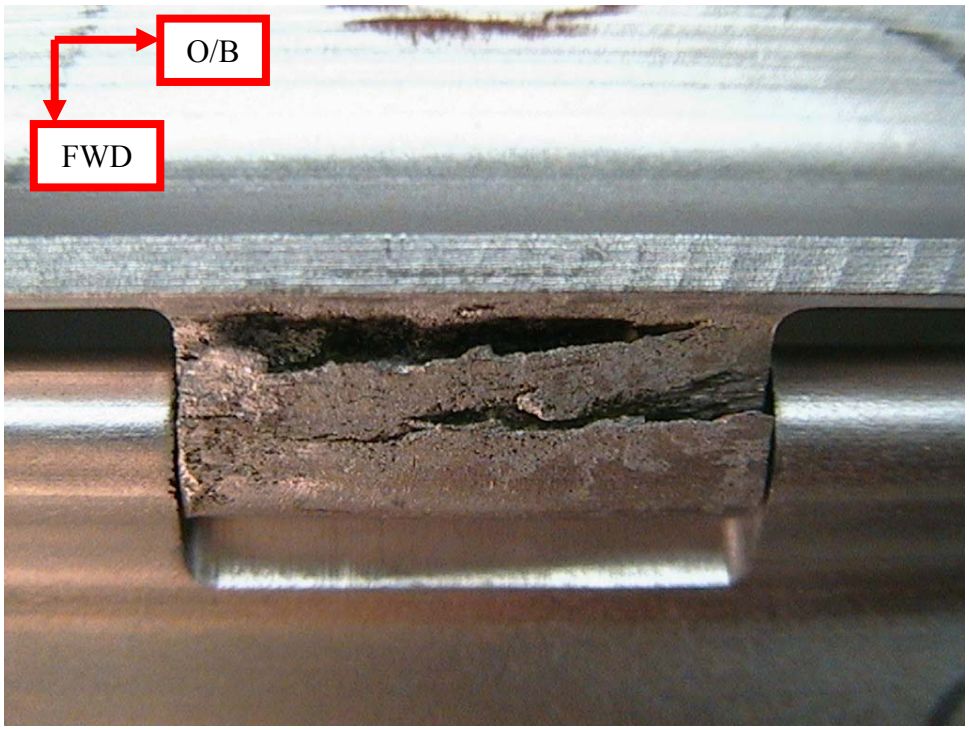

Figure 112. Intergranular Corrosion on the Right Wing Front Spar Upper Cap WS 185.25

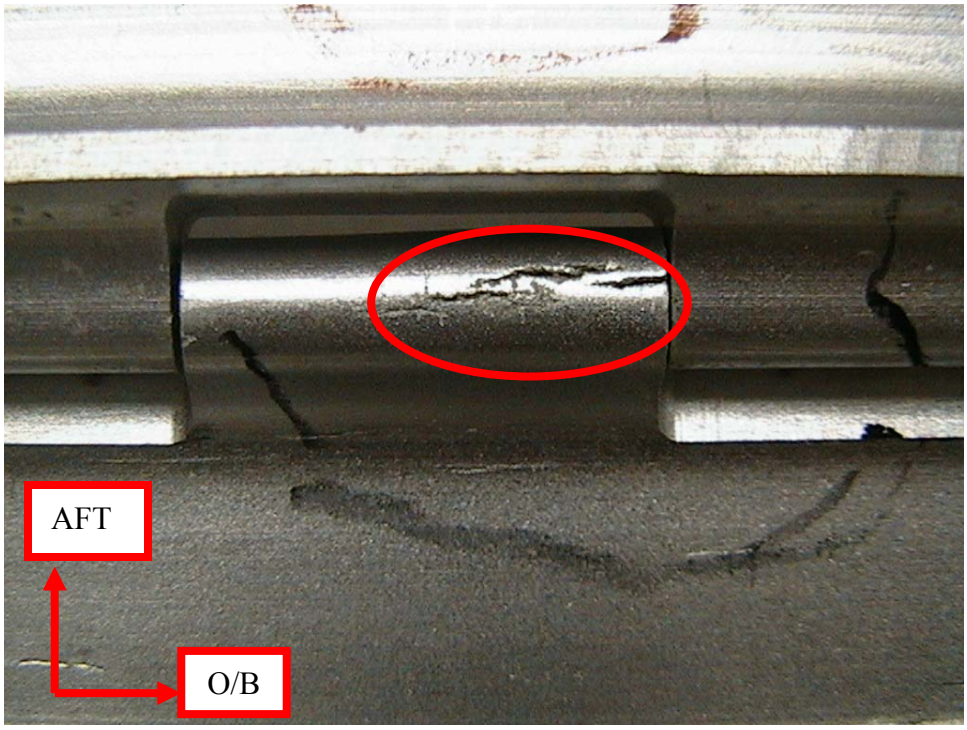

Figure 113. Intergranular Corrosion on the Right Wing Front Spar Upper Cap WS 187 Bottom View

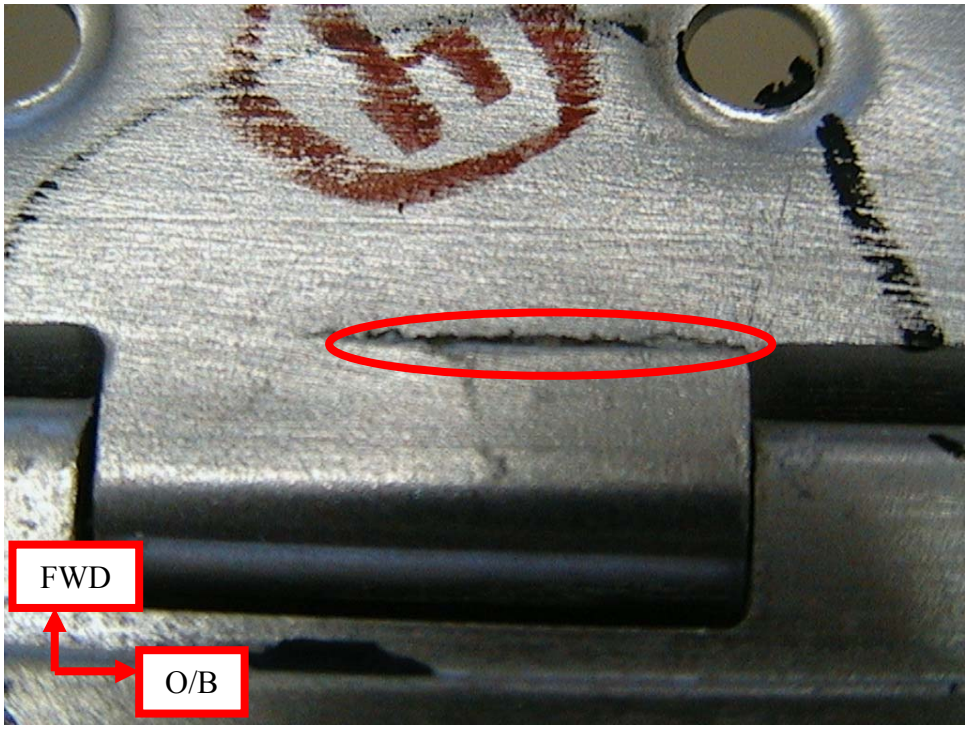

Figure 114. Intergranular Corrosion on the Right Wing Front Spar Upper Cap WS 187 Top View

3.3.2.2 Right Wing Leading-Edge Spar.

The right wing leading-edge spar forward upper cap is shown in figure 115, which is representative of the forward lower cap and the aft upper and lower caps. A 1.05-inch crack, observed at WS 47.5 on the right wing forward lower cap, is pictured in figure 116. Another crack, measuring 1.3 inches, was found on the aft lower cap at WS 64. This crack is shown in figure 117. Figure 118 shows a 0.6-inch crack observed on the forward lower cap at WS 65.25, while a 0.4-inch crack, shown in figure 119, was located on the forward lower cap at WS 65.5. Another crack, measuring 0.5 inch, was found on the forward lower cap at WS 68.25, and it is pictured in figure 120.

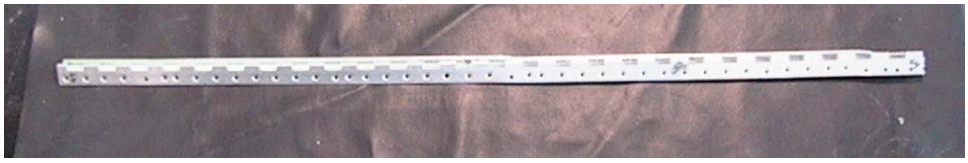

Figure 115. Right Wing Leading-Edge Forward Lower Cap

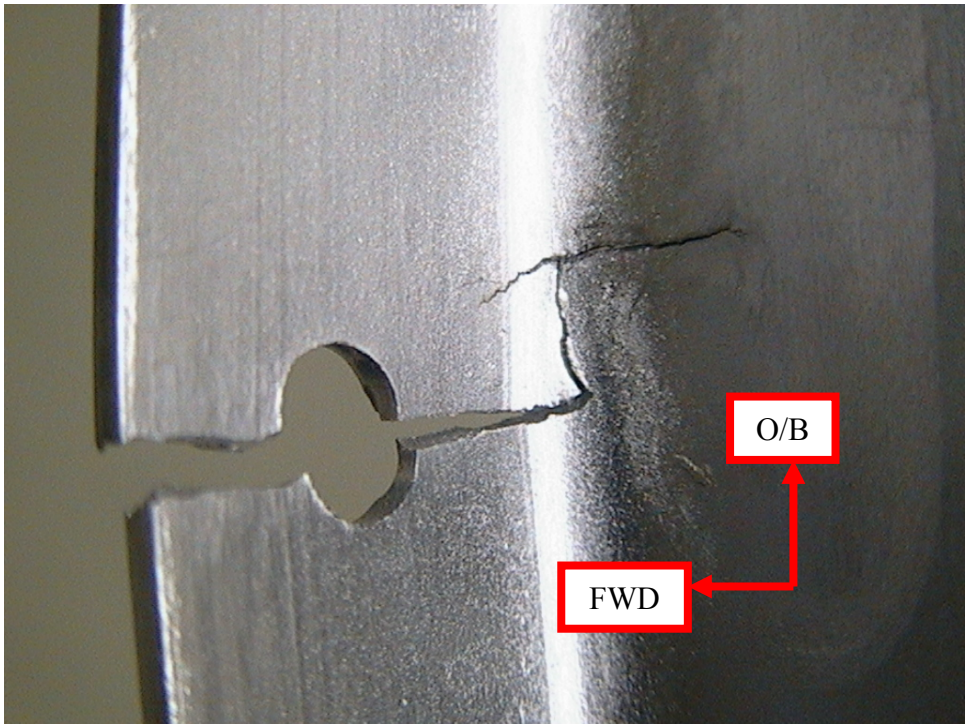

Figure 116. Crack in the Right Wing Leading-Edge Forward Lower Spar Cap WS 47.5

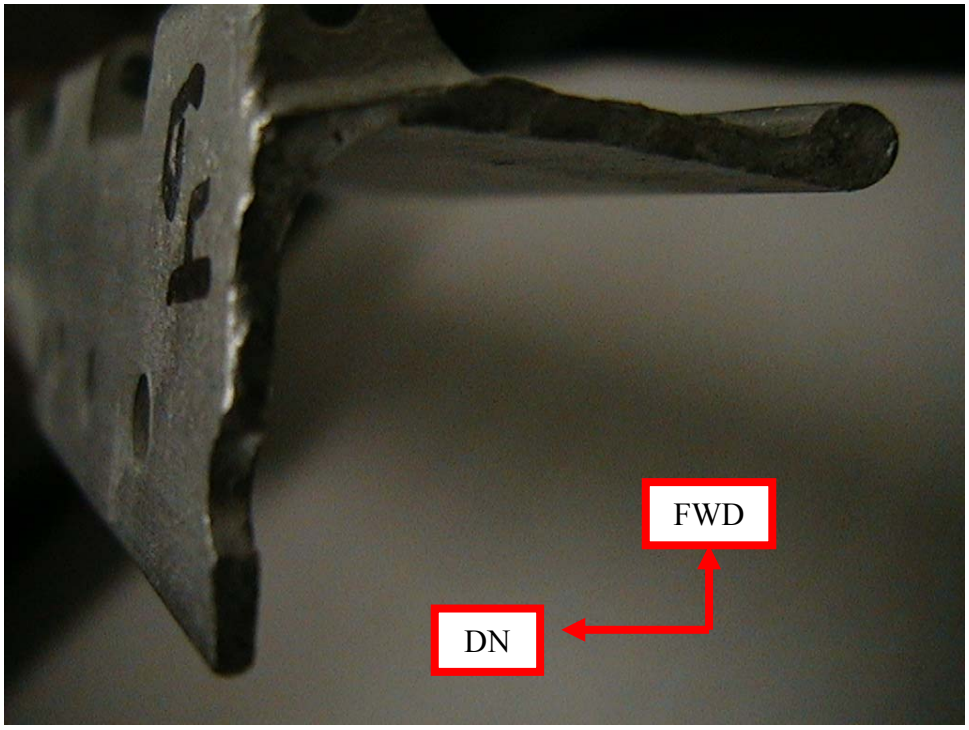

Figure 117. Crack in the Right Wing Leading-Edge Aft Lower Spar Cap WS 64

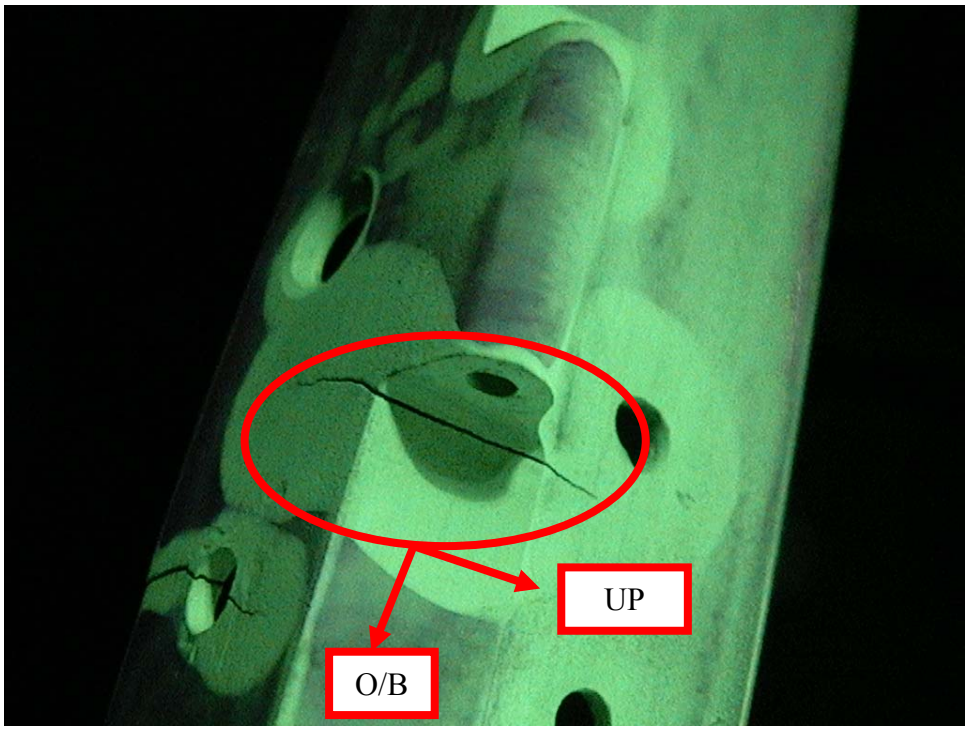

Figure 118. Crack in the Right Wing Leading-Edge Forward Lower Spar Cap WS 65.25

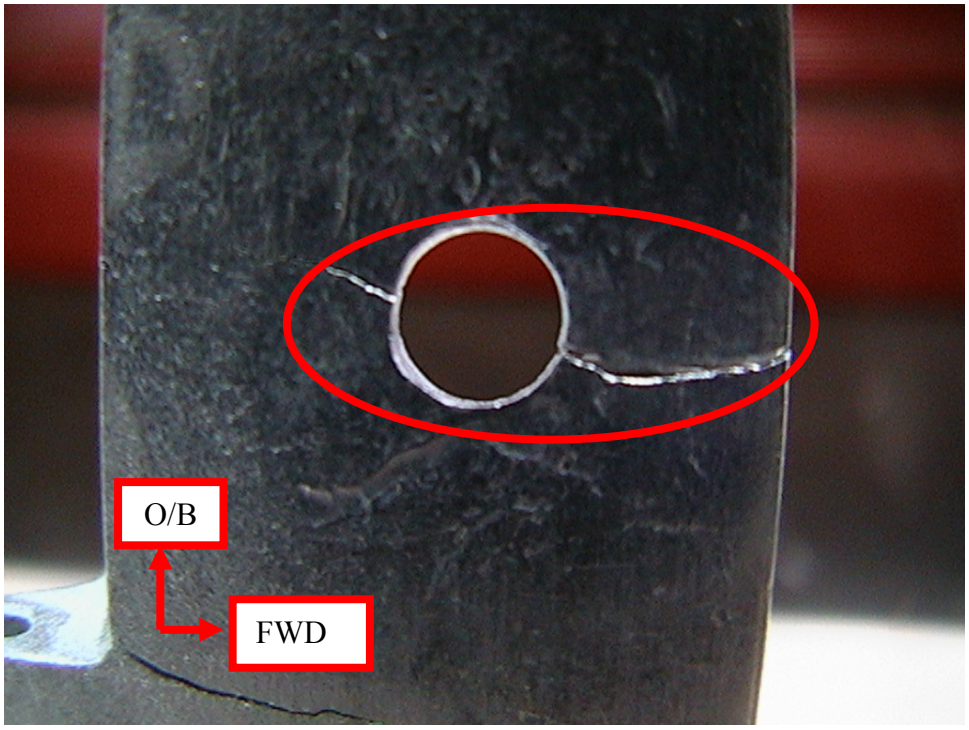

Figure 119. Crack in the Right Wing Leading-Edge Forward Lower Spar Cap WS 65.5

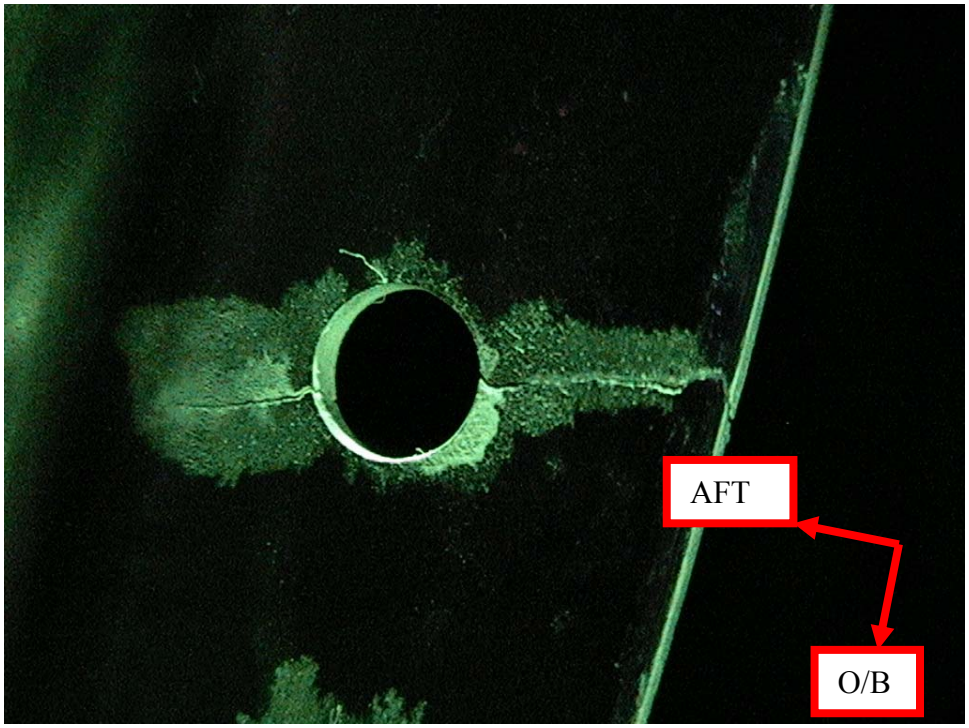

Figure 120. Crack in the Right Wing Leading-Edge Forward Lower Spar Cap WS 68.25

3.3.2.3 Right Wing Rear Spar.

No defects were observed on the right wing rear spar during the post-disassembly NDI.

3.3.2.4 Right Wing Attachment Fittings.

No defects were noted on the right wing landing gear attachment fittings. The only defects observed on the right wing attachment fittings were two areas of pitting corrosion on the right wing rear upper bathtub fitting. The right wing rear spar upper bathtub fitting is shown in figure 121. A 0.02-square-inch area of pitting corrosion was observed at WS 25, and it is pictured in figure 122. Another area of pitting corrosion, shown in figure 123, covered a surface area of 0.08 square inch at WS 27.

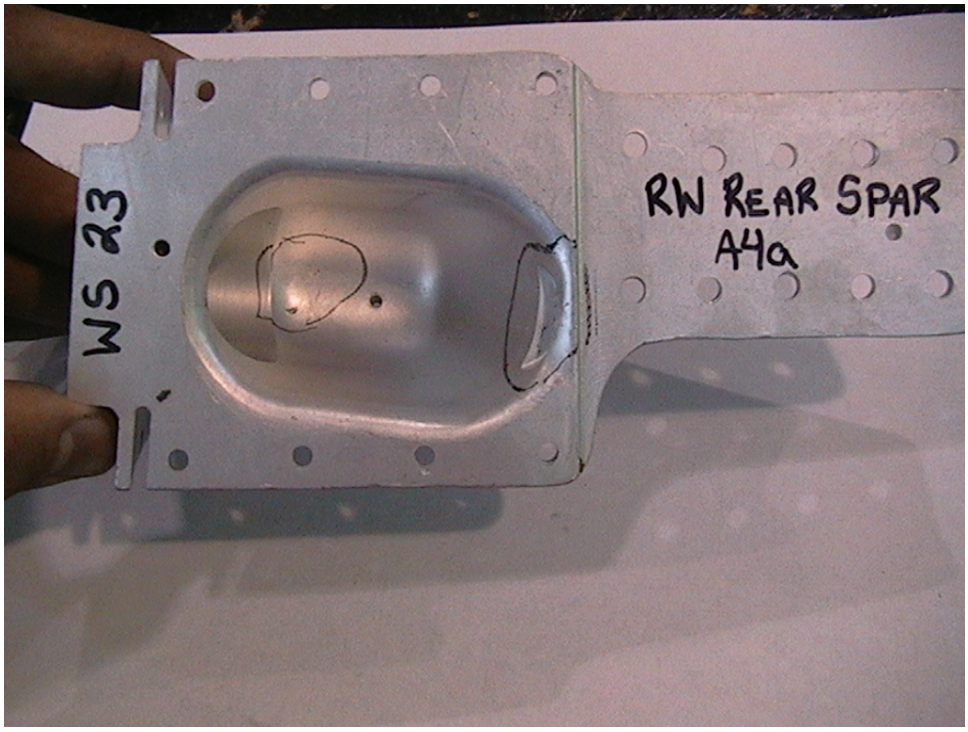

Figure 121. Right Wing Rear Spar Upper Bathtub Fitting

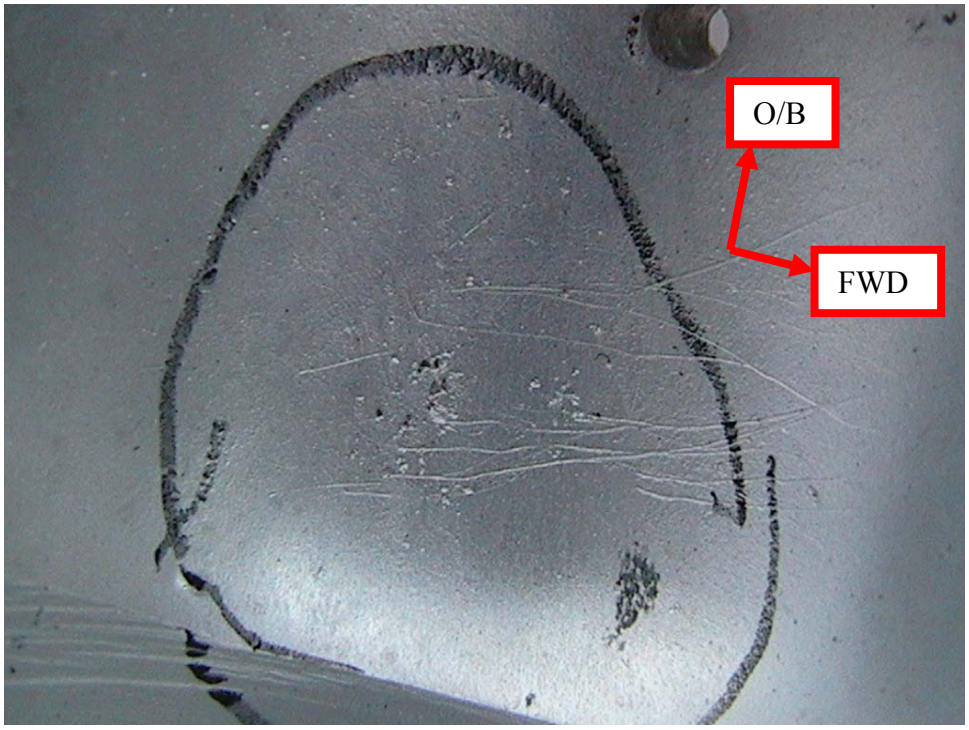

Figure 122. Pitting Corrosion on the Right Wing Rear Spar Upper Bathtub Fitting WS 25

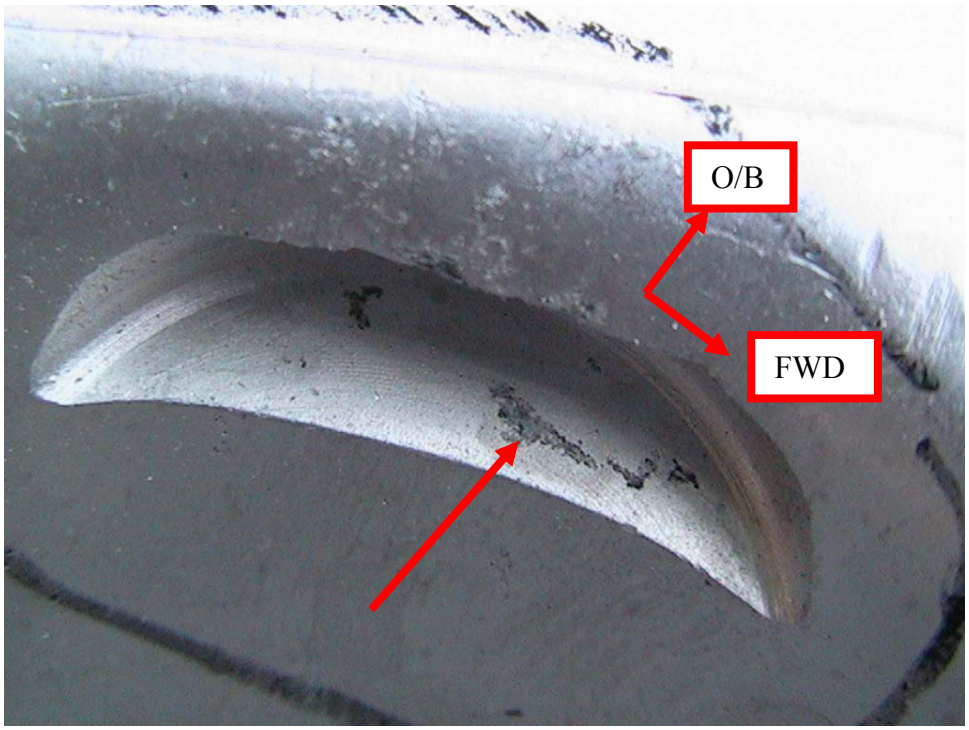

Figure 123. Pitting Corrosion on the Right Wing Rear Spar Upper Bathtub Fitting WS 27

3.4 MICROSCOPIC EXAMINATION.

All primary structure was examined with the aid of a 7-45 power optical microscope following the post-disassembly NDI. The lengths of all cracks were noted as well as the surface area and depth of each area of corrosion. The severity of the corrosion was classified by the percentage of the thickness loss due to corrosion as follows:

- Light = 0%-2% thickness loss
- Light-Moderate = 2%-5% thickness loss
- Moderate = 5%-7% thickness loss
- Moderate-Severe = 7%-10% thickness loss
- Severe = >10% thickness loss

Corrosion effects were classified by percentage of thickness loss because it seemed most representative of the actual damage done by corrosion. Typically, corrosion is classified by pit depth; however, for the purposes of this study, pit depth would not be representative of the severity of damage caused. The different classification levels used in this program are unique to this research and are not representative of other studies. NIAR recommends that these classification levels be used for future studies. It is important to note that corrosion is not assumed as uniform throughout the entire area, but that it represents the maximum depth of corrosion in that area.

Not all defects were identified and characterized in both the post-disassembly NDI and microscopic examinations. Light corrosion is often difficult to detect with a fluorescent liquid penetrant inspection because the inclusions are not deep enough to hold penetrant. All NDI indications were verified during the microscopic examination; however, some areas of corrosion were grouped together and classified as one finding during the microscopic examination. Mechanical damage and characterization was not performed during the microscopic examination, since it was previously documented by during post-disassembly NDI.

3.4.1 Left Wing.

Three cracks and fourteen areas of corrosion were examined on the left wing. Seven occurrences of pitting corrosion, three locations of exfoliation corrosion, and four areas of intergranular corrosion were documented on the left wing ranging in severity from light to severe. The cracks were found on the leading-edge aft lower spar cap, rear spar lower doubler, and the rear spar forward lower spar cap. Corrosion was found on the front spar web, front spar upper cap, leading-edge aft lower spar cap, rear spar upper bathtub fitting, and the front spar lower bathtub fitting.

3.4.1.1 Left Wing Front Spar.

The left wing front spar web was found to have areas of severe pitting corrosion. Figure 124 shows a 0.08-square-inch area of pitting corrosion located on the left wing front spar web from WS 23 to 56. This area of corrosion was classified as severe since it caused a localized maximum thickness loss of 30%. Another area of severe corrosion, shown in figure 125, was

observed on the front spar web at WS 30.5. This area of corrosion covered 0.04 square inch and resulted in a localized thickness loss of 13.3%.

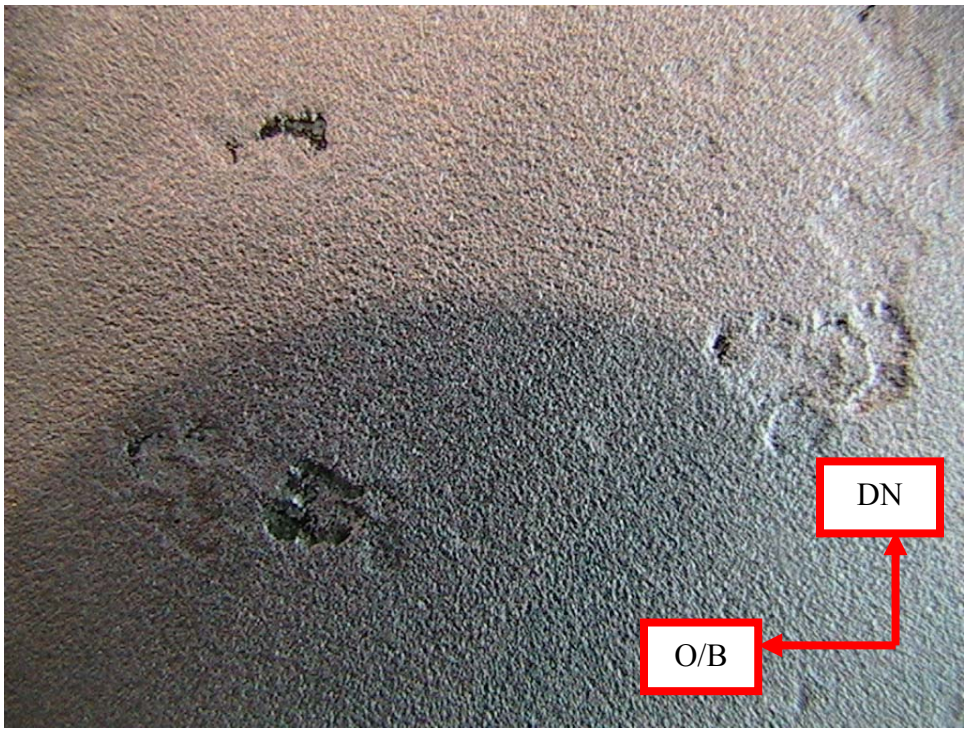

Figure 124. Pitting Corrosion on the Left Wing Front Spar Web WS 23-56

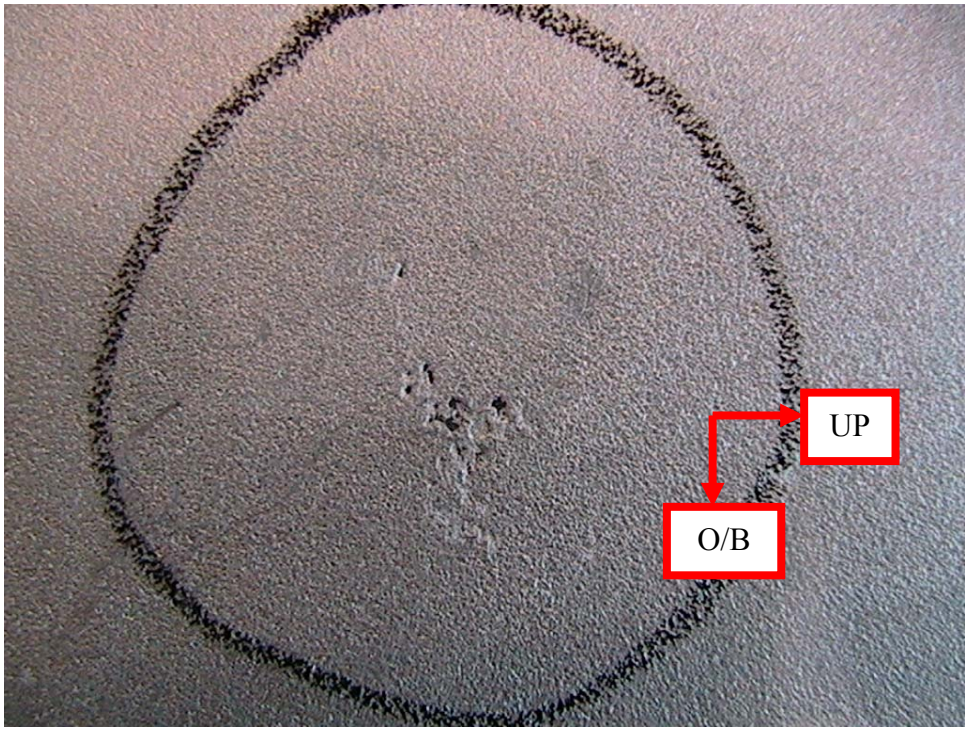

Figure 125. Pitting Corrosion on the Left Wing Front Spar Web WS 30.5

The left wing front spar upper cap had areas of through-thickness corrosion. Exfoliation corrosion, shown in figures 126 and 127, was observed at WS 120, covering a surface area of 2.07 square inches. Figures 128 through 130 show intergranular and exfoliation corrosion covering 1.16 square inches. This corrosion was located from WS 136 to 142.75.

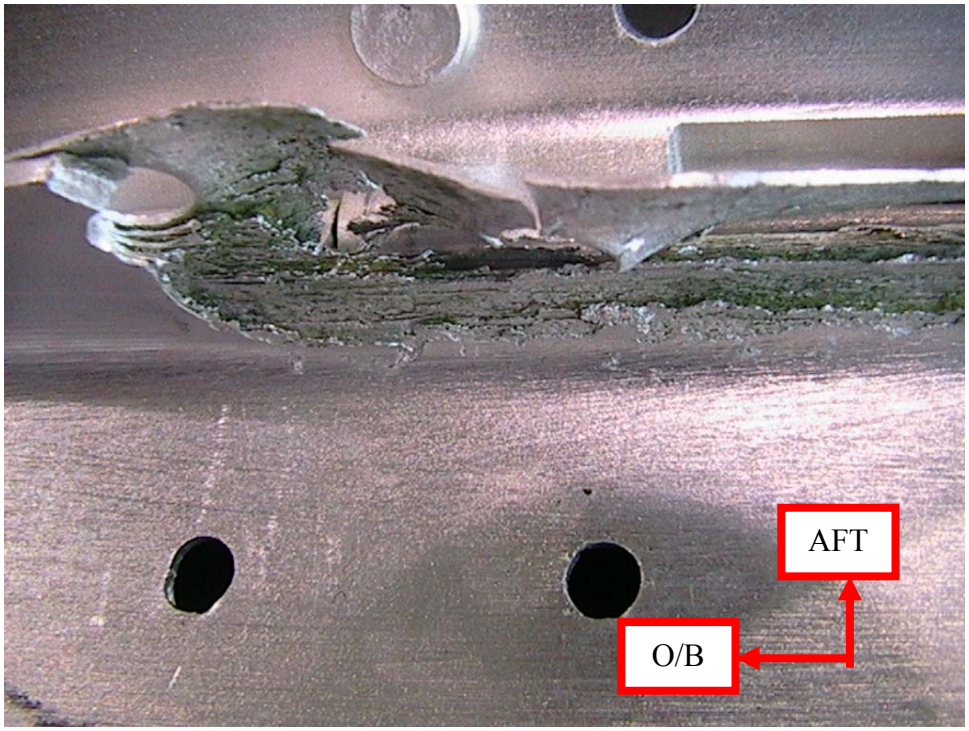

Figure 126. Exfoliation Corrosion on the Left Wing Front Spar Upper Cap
WS 120 Outboard View

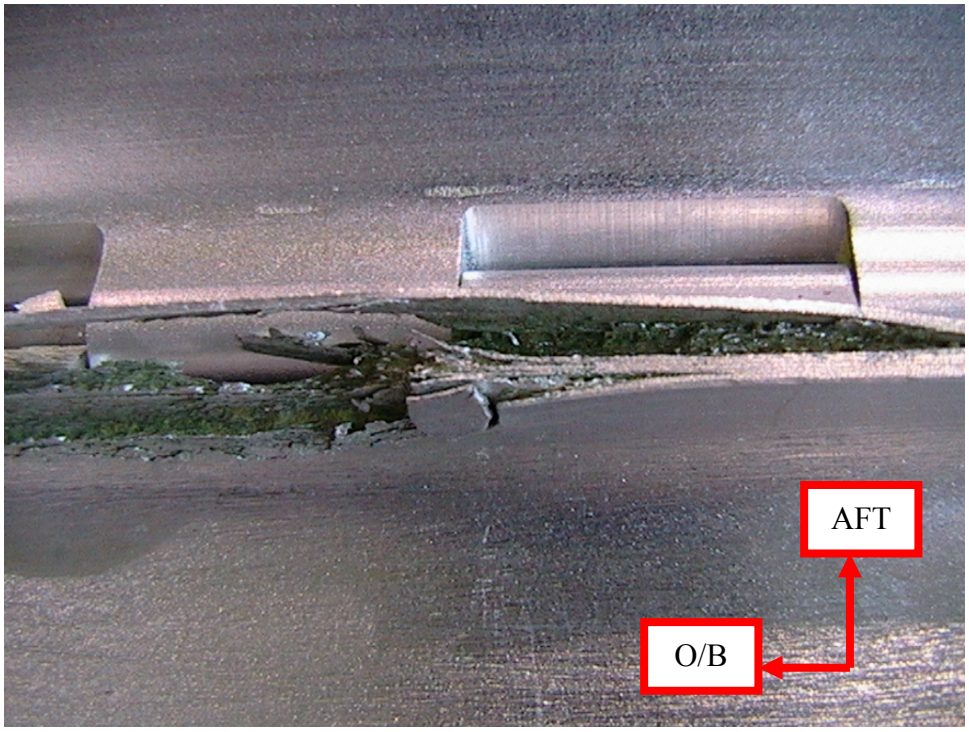

Figure 127. Exfoliation Corrosion on the Left Wing Front Spar Upper Cap WS 120 Inboard View

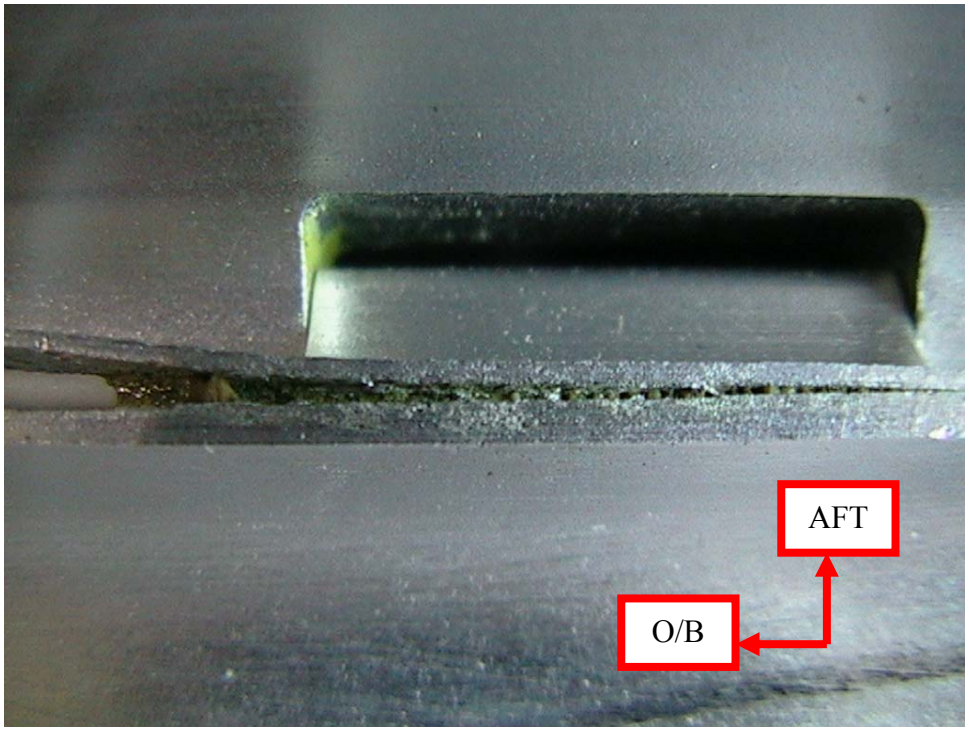

Figure 128. Intergranular Corrosion on the Left Wing Front Spar Upper Cap WS 136-142.75

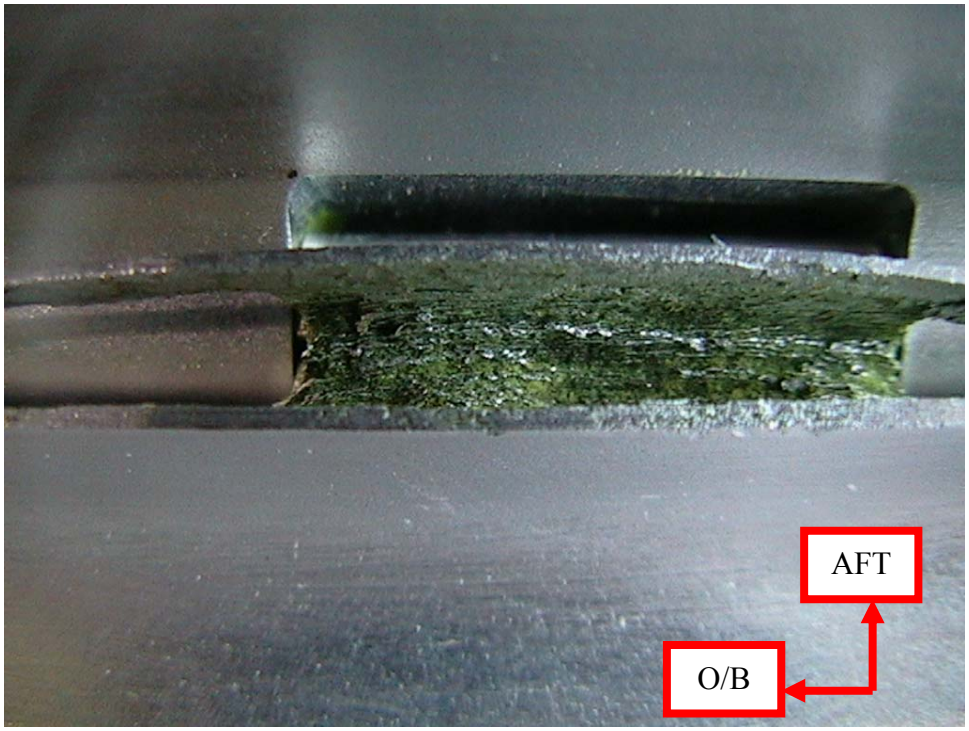

Figure 129. Exfoliation Corrosion on the Left Wing Front Spar Upper Cap WS 136-142.75 Inboard View

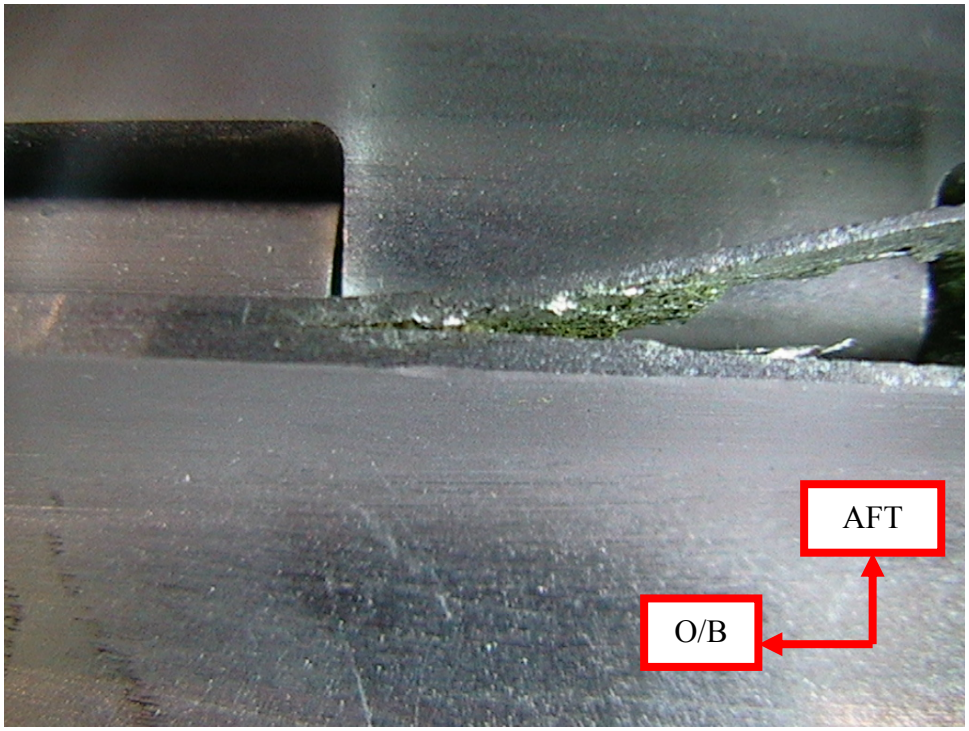

Figure 130. Exfoliation Corrosion on the Left Wing Front Spar Upper Cap WS 136-142.75 Outboard View

A 0.95-inch area of exfoliation corrosion was observed from WS 156.25 to 157.25. This corrosion resulted in 100% localized thickness loss, and it is shown in figure 131. Figure 132 shows a 0.613-inch through-thickness area of intergranular corrosion located at WS 158.25. Exfoliation corrosion, shown in figure 133, was observed on the left wing front spar upper cap. This area of corrosion measured 0.95 inch, located at WS 164, and resulted in 100% localized thickness loss.

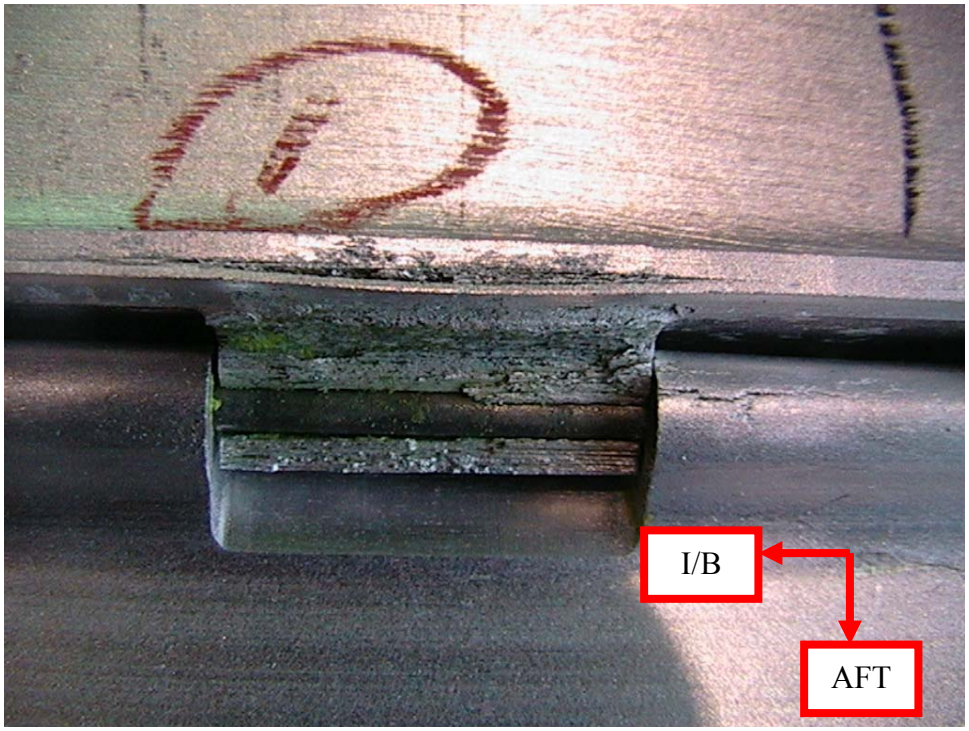

Figure 131. Exfoliation Corrosion on the Left Wing Front Spar Upper Cap
WS 156.5-157.25

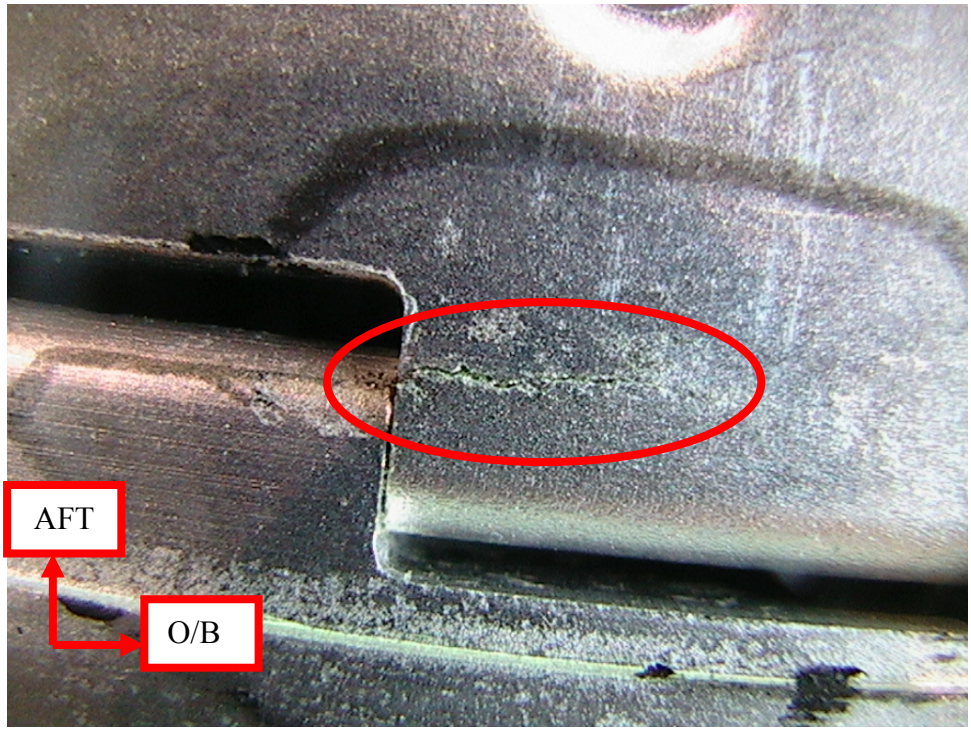

Figure 132. Intergranular Corrosion on the Left Wing Front Spar Upper Cap WS 158.25

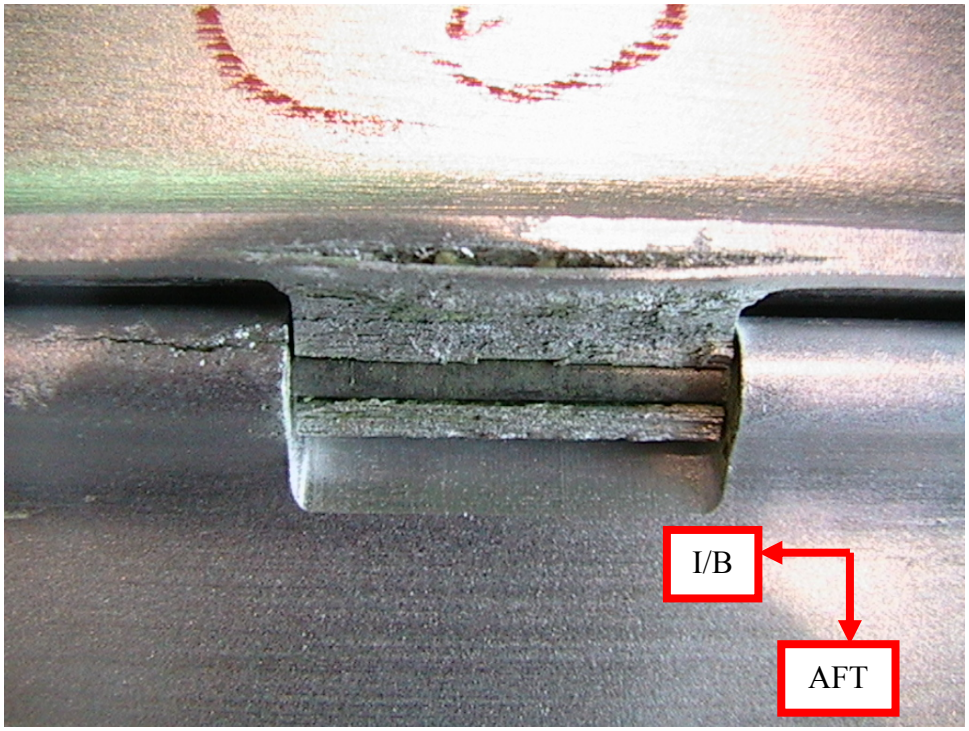

Figure 133. Exfoliation Corrosion on the Left Wing Front Spar Upper Cap WS 164

Figure 134 shows a 0.76-inch area of intergranular corrosion, which resulted in a thickness loss of 100%, and figure 135 shows a 0.96-inch through-thickness area of intergranular corrosion. Pitting corrosion, pictured in figure 136, was observed at WS 174.5. This corrosion covered 0.013 square inch with a maximum pit depth of 0.0432 inch, which resulted in an 80% thickness loss.

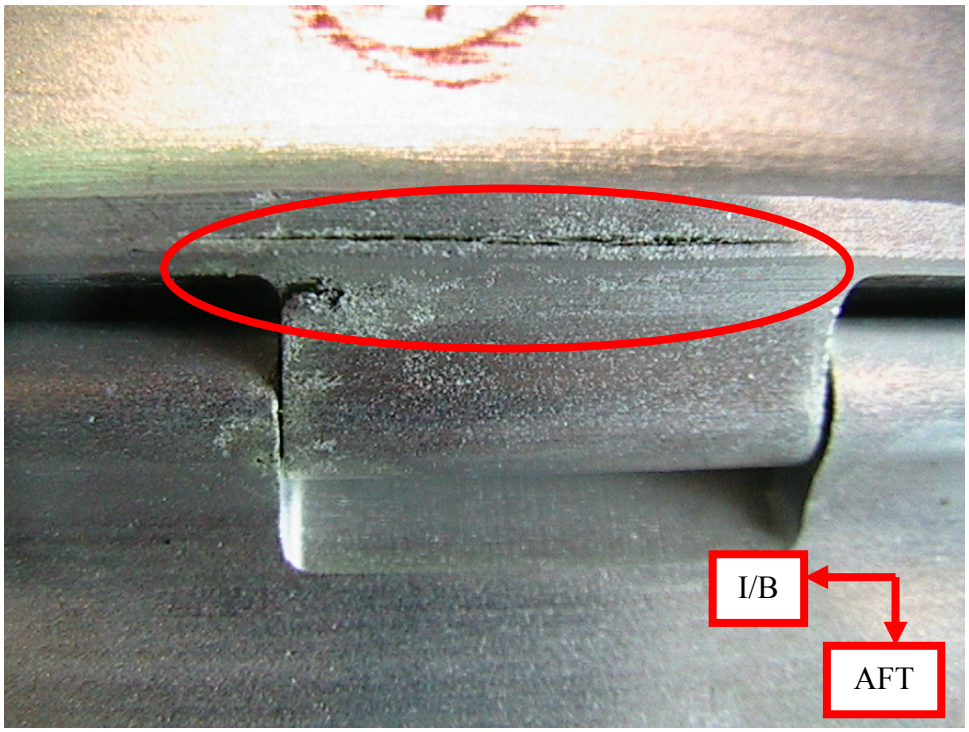

Figure 134. Intergranular Corrosion on the Left Wing Front Spar Upper Cap WS 170.25

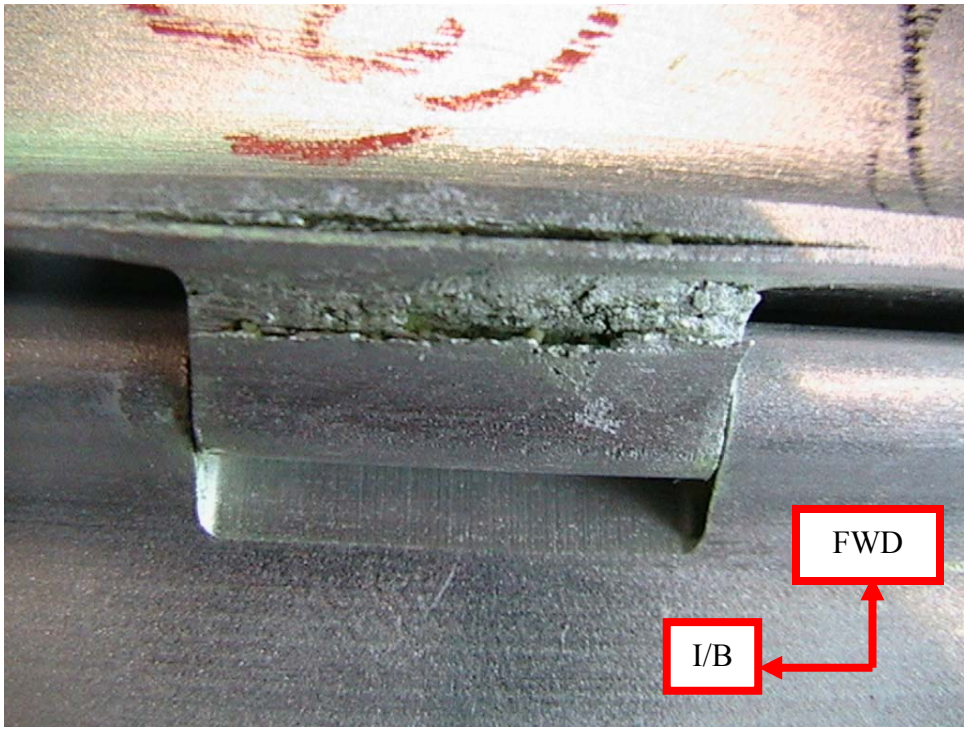

Figure 135. Intergranular Corrosion on the Left Wing Front Spar Upper Cap WS 170.5

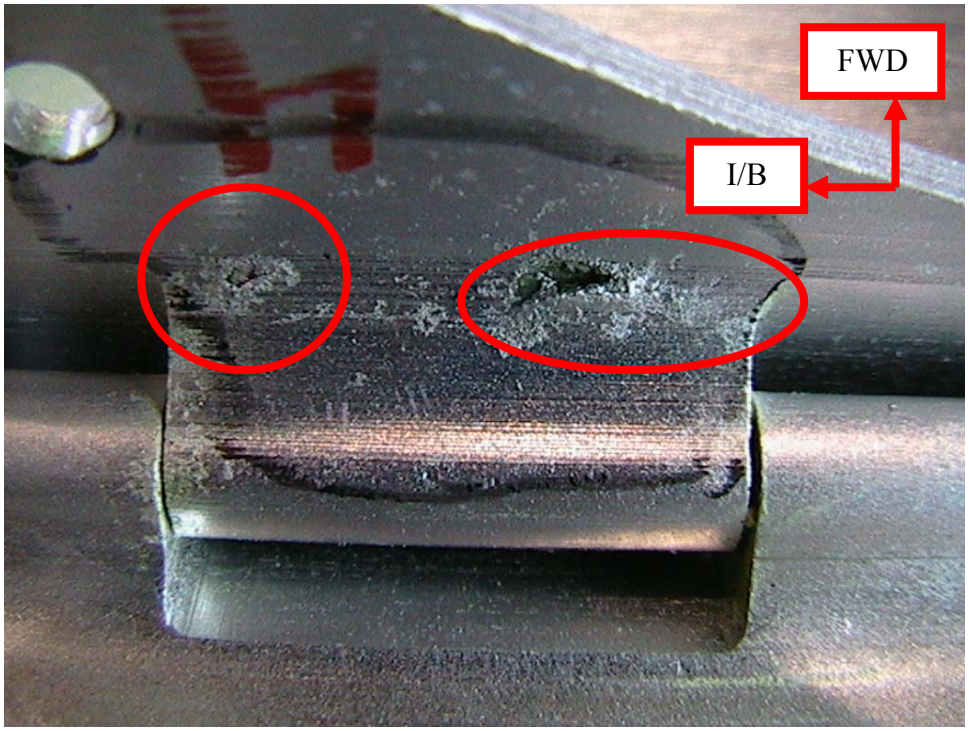

Figure 136. Pitting Corrosion on the Left Wing Front Spar Upper Cap WS 174.5

3.4.1.2 Left Wing Leading-Edge Spar.

A 1.325-inch crack, shown in figures 137 and 138, was observed on the leading-edge aft lower cap at WS 64.5. This crack was opened, and the crack face, pictured in figure 139, was examined. The failure mode of the entire crack was fatigue. A 1.62-square-inch area of pitting corrosion was observed on the aft lower cap from WS 59 to 64, and it is shown in figure 140. A maximum pit depth of 0.005 inch was recorded, yielding a maximum thickness loss of 7.2%, which is classified as moderate-severe. An area of severe corrosion was observed on the aft upper spar cap from WS 100.5 to 101, as shown in figure 141. This severe corrosion encompassed an area of 0.08 square inch, with a maximum pit depth of 0.006 inch, which resulted in a maximum thickness loss of 10.3%.

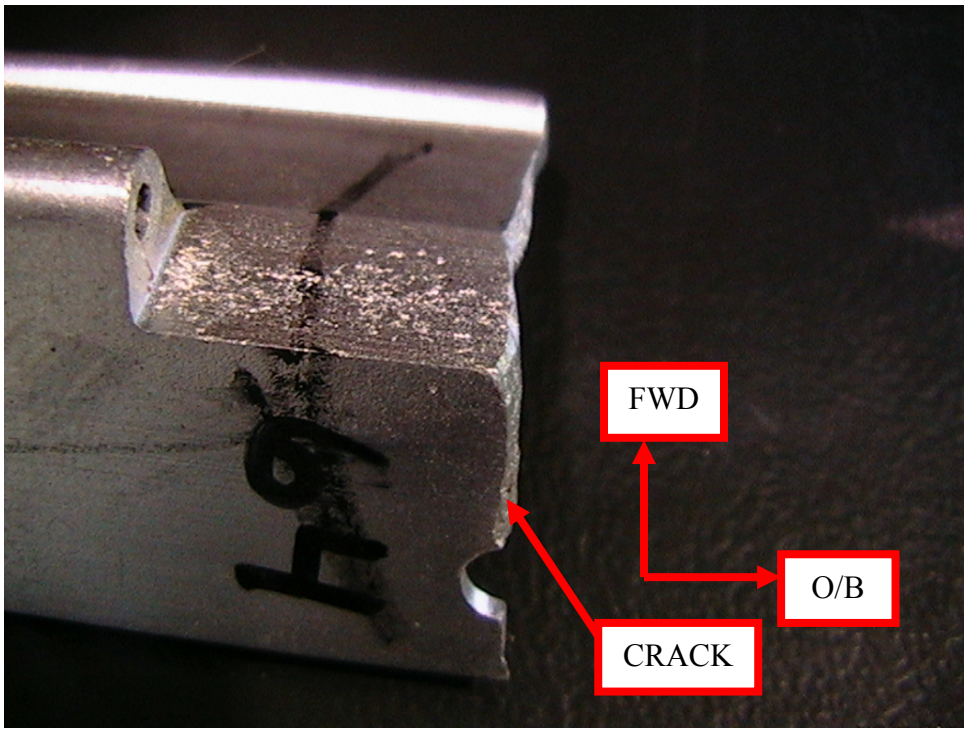

Figure 137. Crack in the Left Wing Leading-Edge Aft Lower Spar Cap WS 64.5 Bottom View

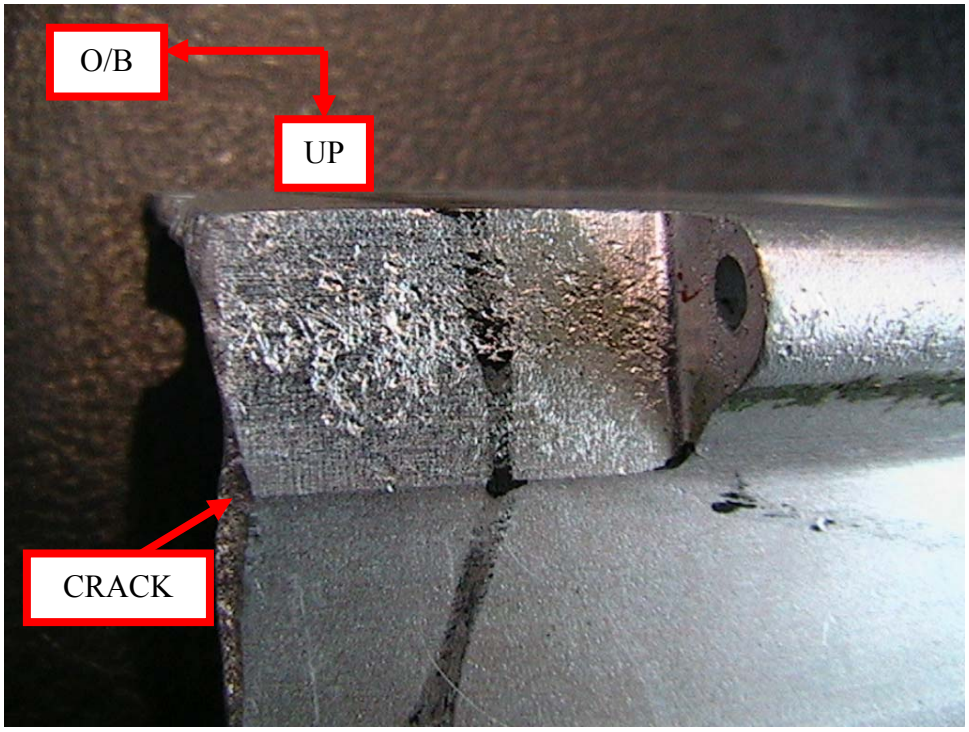

Figure 138. Crack in the Left Wing Leading-Edge Aft Lower Spar Cap WS 64.5

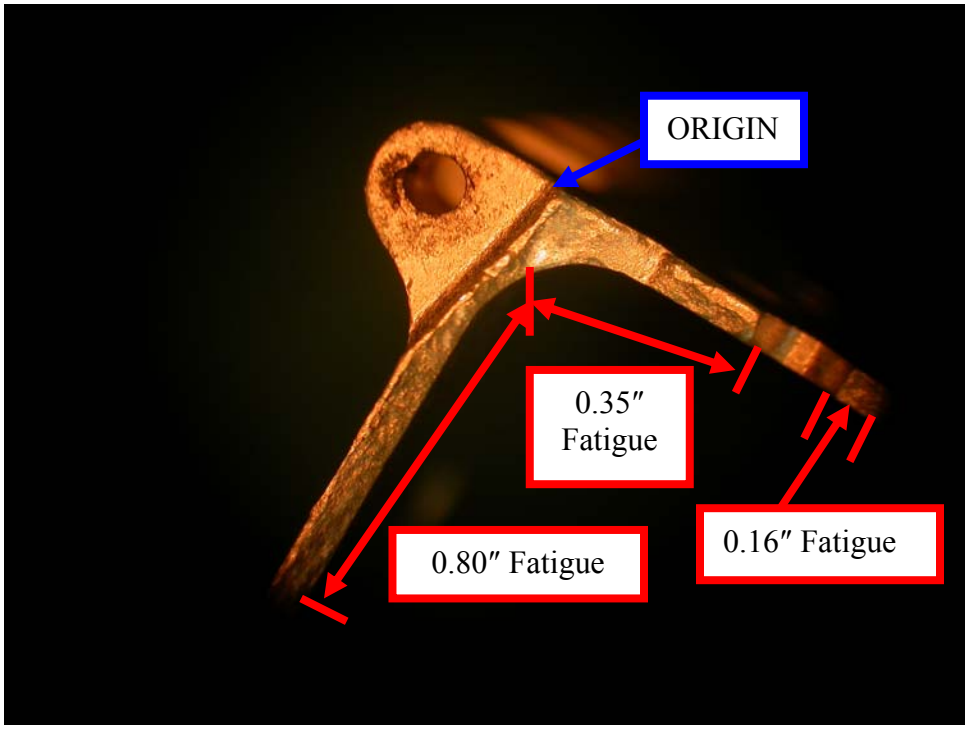

Figure 139. Crack Face of Crack in the Left Wing Leading-Edge Aft Lower Spar Cap WS 64.5

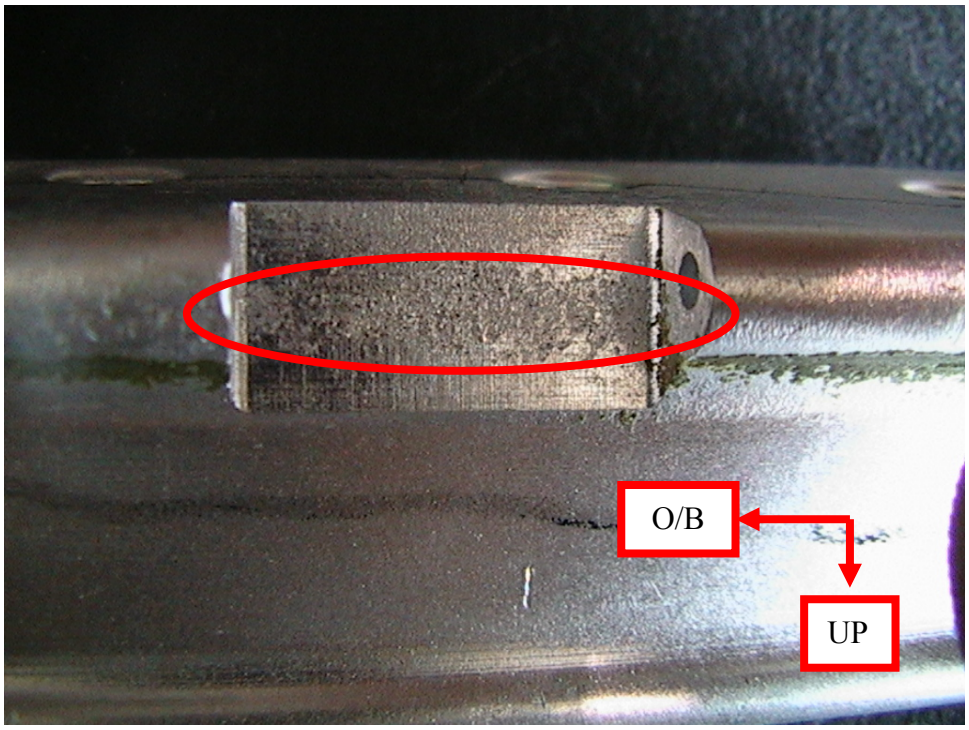

Figure 140. Pitting Corrosion on the Left Wing Leading-Edge Aft Lower Spar Cap WS 59-64

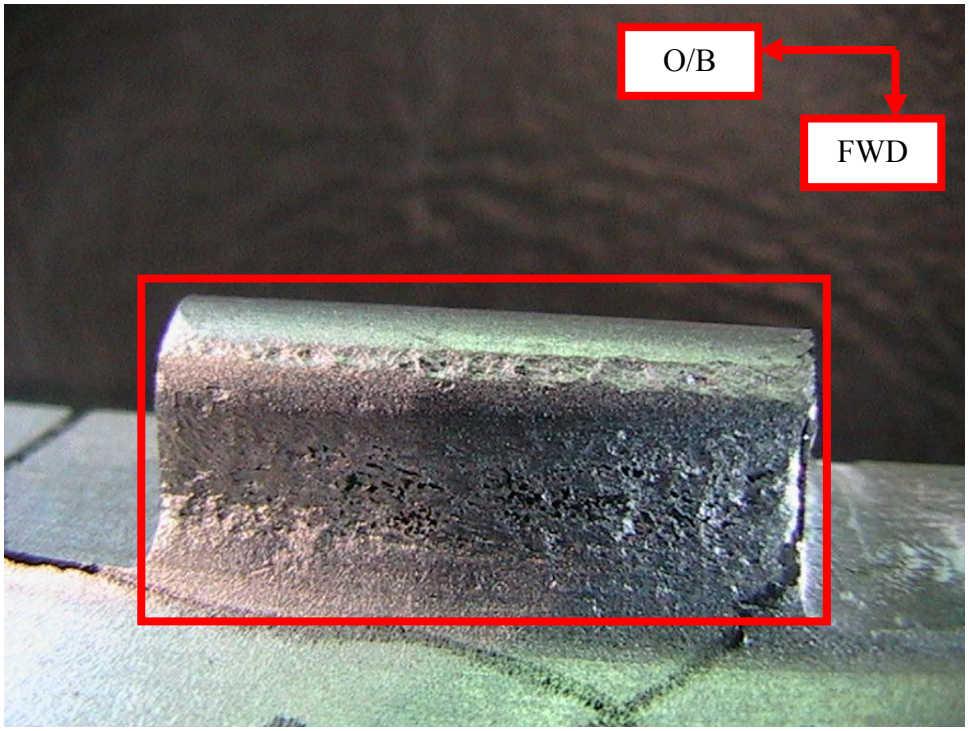

Figure 141. Pitting Corrosion on the Left Wing Leading-Edge Aft Upper Spar Cap WS 100.5-101

3.4.1.3 Left Wing Rear Spar.

A 0.8-inch crack was found on the rear spar lower doubler at WS 64, and it is shown in figure 142. This crack location corresponds to a crack on the forward lower spar cap, which measured 0.722 inch in length and is pictured in figure 143. Both crack faces, shown in figures 144 and 145, respectively, were examined and found to be caused by fatigue.

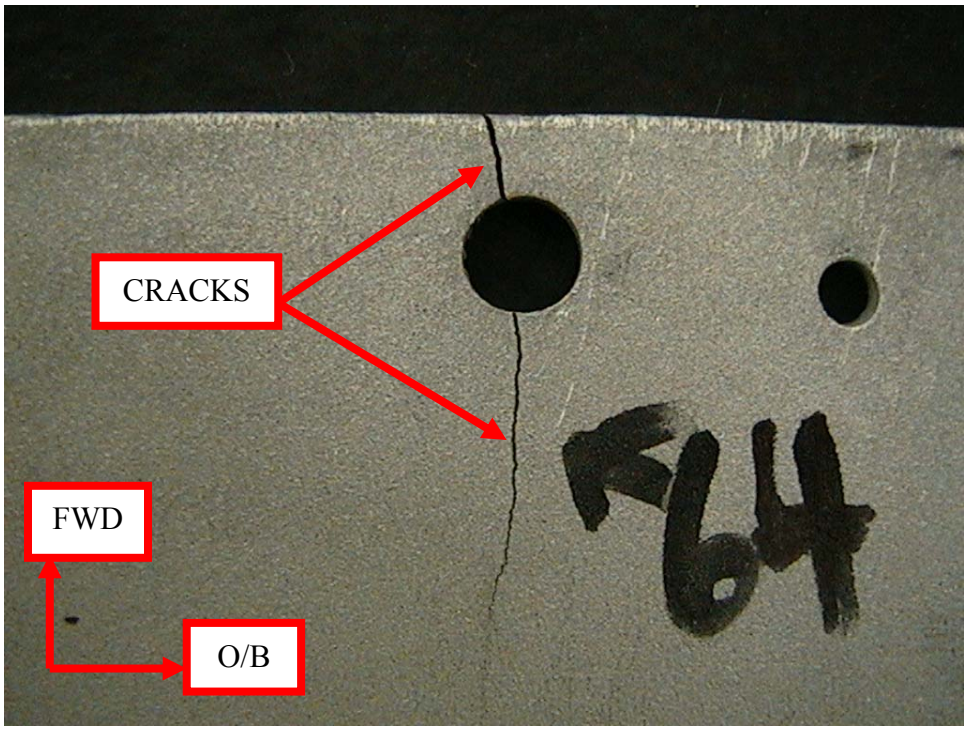

Figure 142. Crack in the Left Wing Rear Spar Lower Doubler WS 64

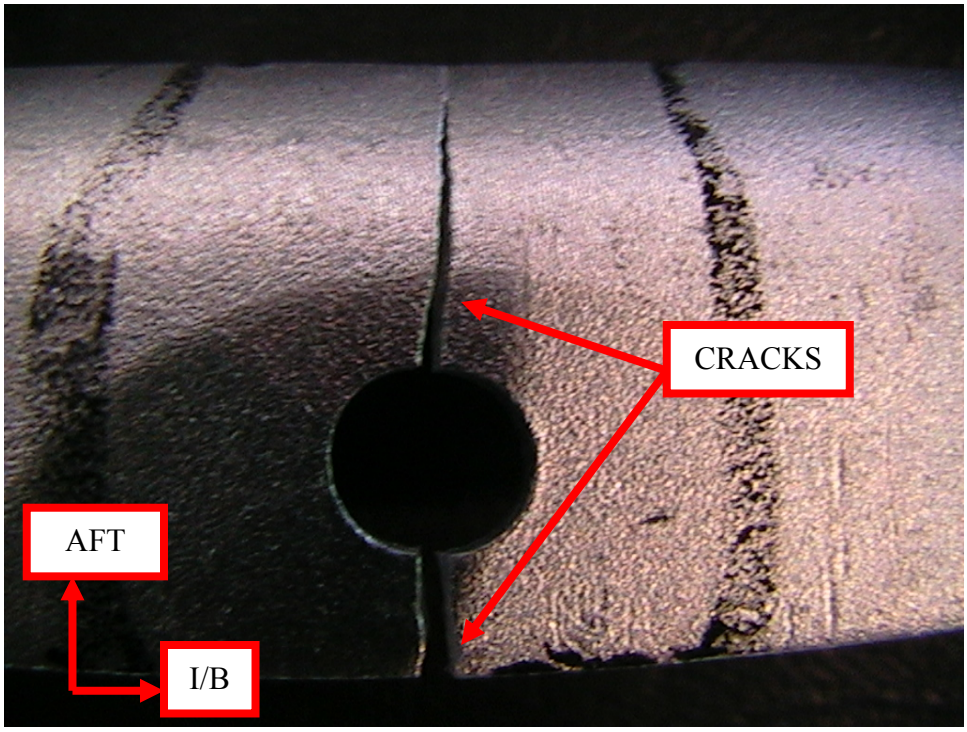

Figure 143. Crack in the Left Wing Rear Spar Forward Lower Spar Cap WS 64

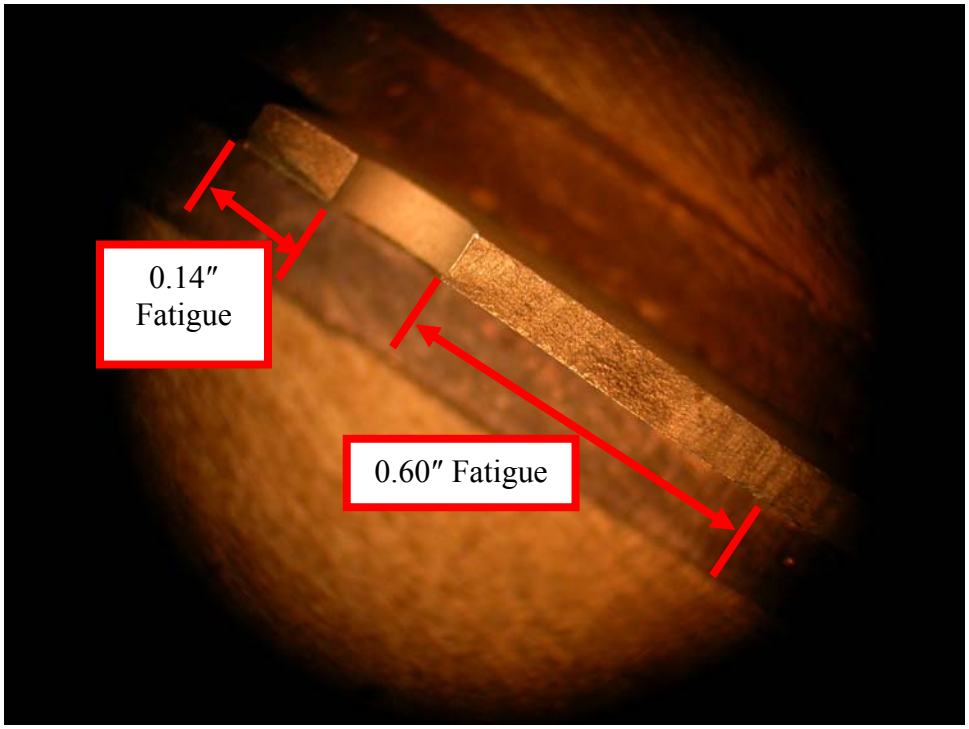

Figure 144. Crack Face of Crack in the Left Wing Rear Spar Lower Doubler WS 64

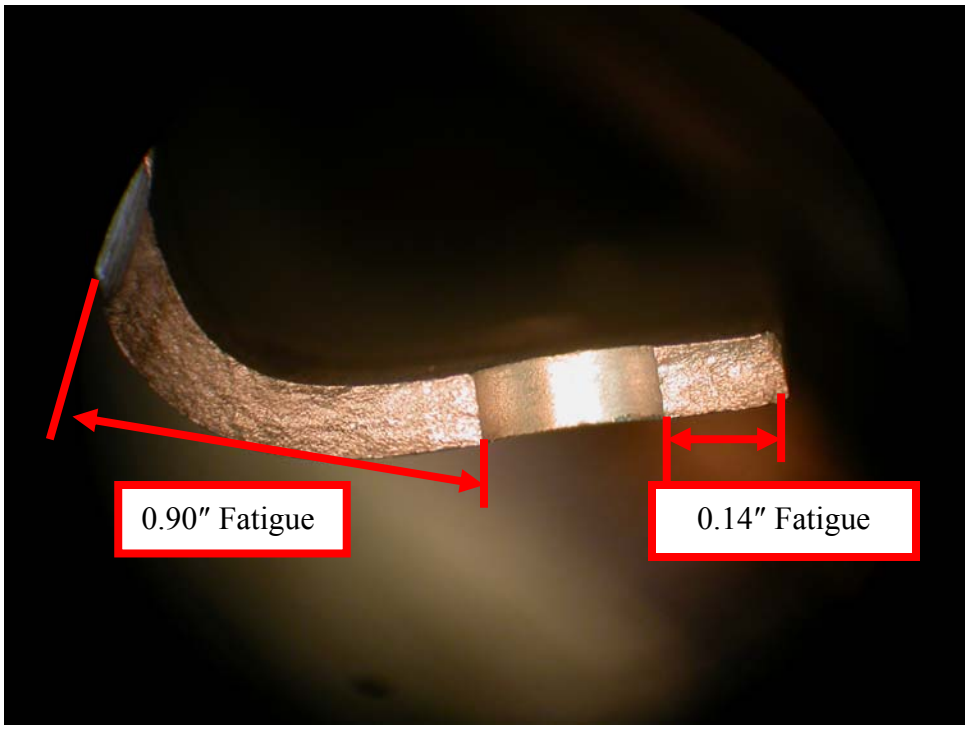

Figure 145. Crack Face of Crack in the Left Wing Rear Spar Forward Lower Spar Cap WS 64

3.4.1.4 Left Wing Attachment Fittings.

Two areas of corrosion were observed on the bathtub attachment fittings. The rear spar upper bathtub fitting had a 0.04-square-inch area of corrosion with a maximum thickness loss of 4.2%, which is classified as light-moderate and is shown in figure 146. Another area of pitting corrosion was observed on the front spar lower bathtub fitting, shown in figure 147, at WS 24. This light corrosion, pictured in figure 148, covered a surface area of 0.09 square inch with a maximum pit depth of 0.002 inch, resulting in a thickness loss of 1.2%.

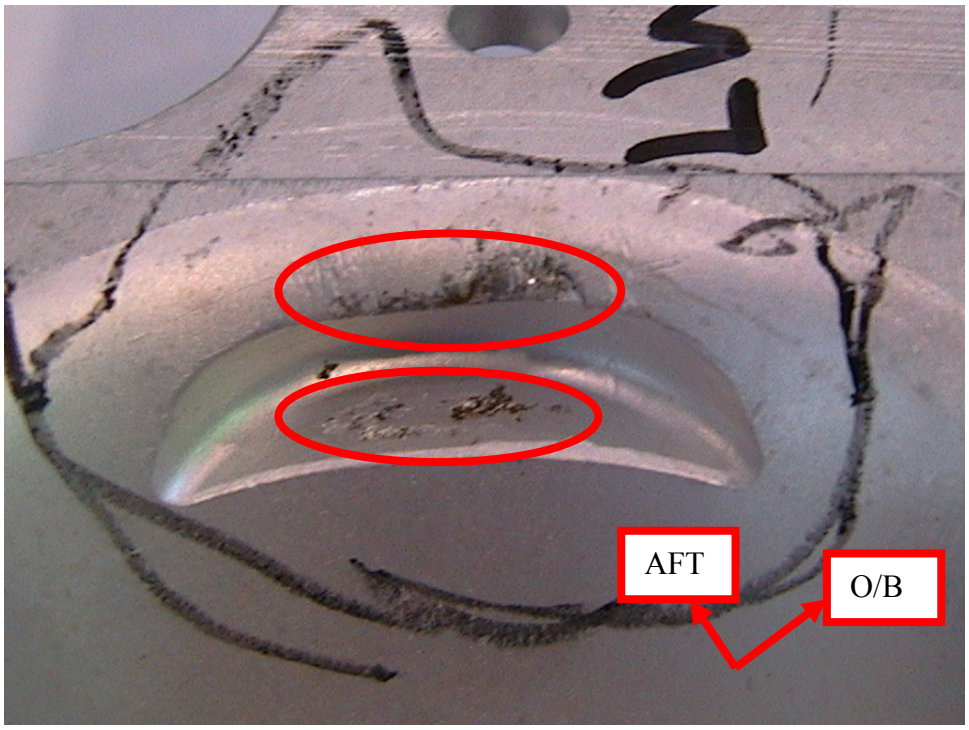

Figure 146. Pitting Corrosion on the Left Wing Rear Spar Upper Bathtub Fitting WS 27

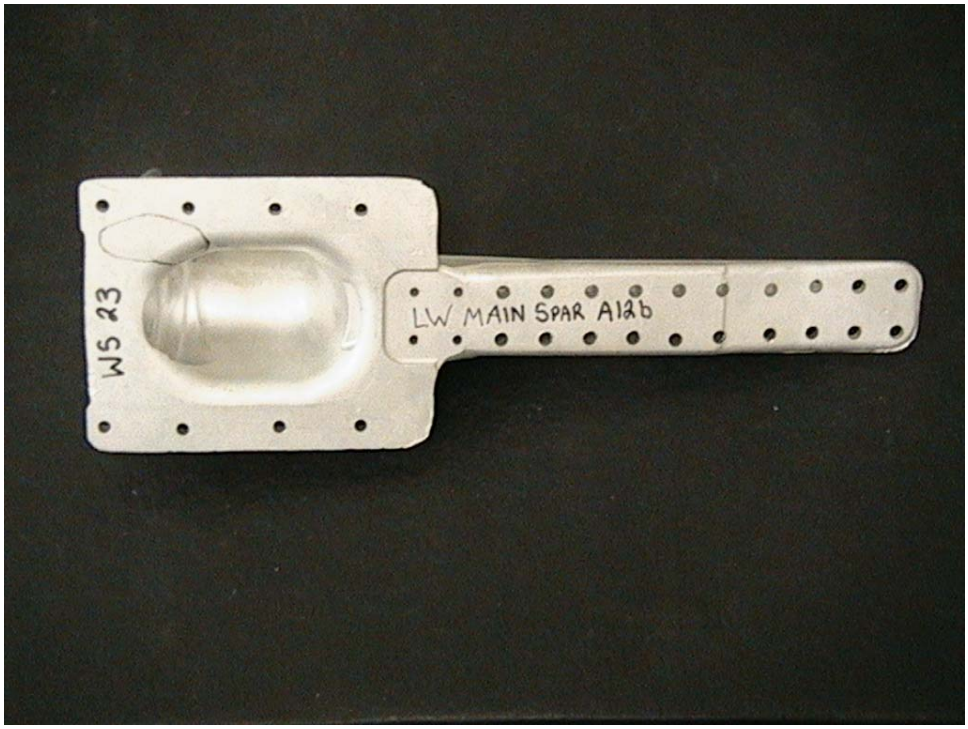

Figure 147. Left Wing Front Spar Lower Bathtub Fitting WS 23-35

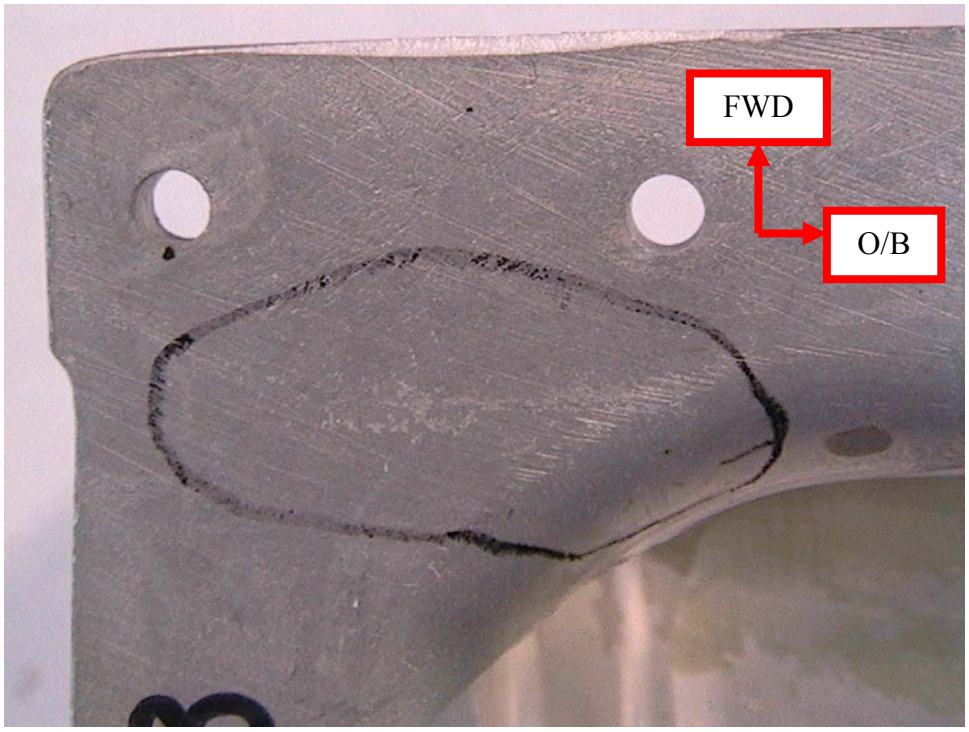

Figure 148. Pitting Corrosion on the Left Wing Front Spar Lower Bathtub Fitting WS 24

3.4.2 Right Wing.

Five cracks and ten areas of corrosion were found on the right wing. Five instances of pitting, four occurrences of intergranular corrosion, and one location of exfoliation corrosion were found on the right wing. The cracks occurred on the leading-edge forward and aft lower spar caps, while corrosion was observed on the front spar web, front spar upper cap, and the rear spar upper bathtub fitting. This corrosion ranged in extent from light to severe.

3.4.2.1 Right Wing Front Spar.

Severe pitting corrosion was scattered across the surface of the front spar web, as shown in figure 149. This corrosion covered 0.13 square inch with a maximum pit depth of 0.009 inch, resulting in a maximum localized thickness loss of 18%. Intergranular corrosion, pictured in figures 150 and 151, was observed from WS 89.5 to 90. This area of corrosion measured 0.626 inch in length and resulted in a 100% localized thickness loss. A similar area of intergranular corrosion, occurring at WS 110, is pictured in figures 152 and 153. This area of corrosion also measured 0.626 inch in length and resulted in a 100% thickness loss.

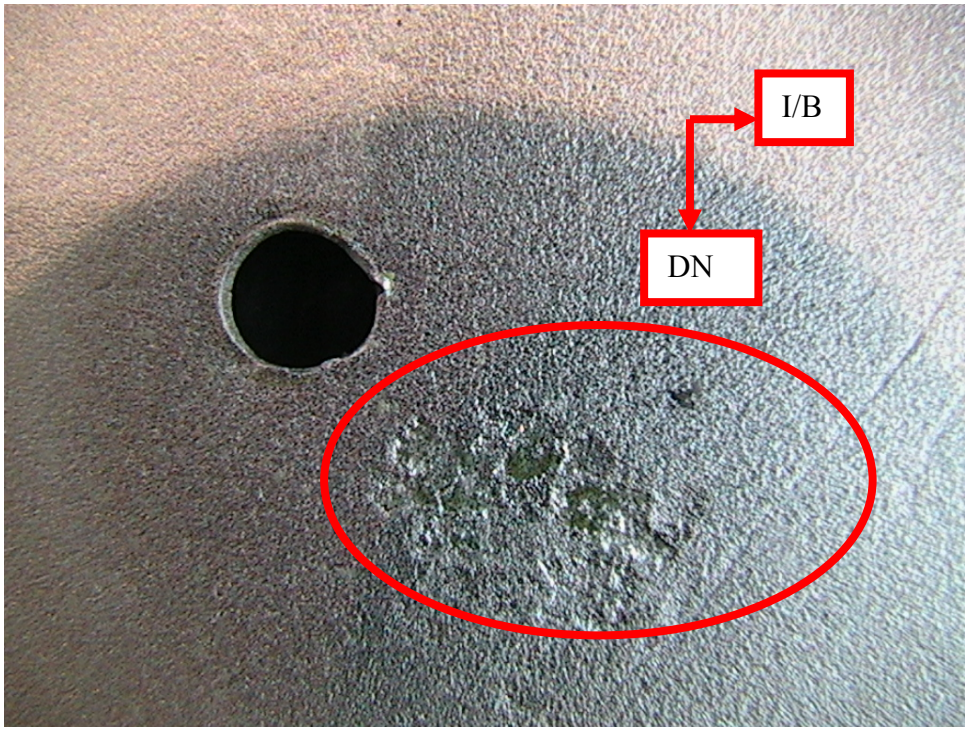

Figure 149. Scattered Pitting Corrosion on the Right Wing Front Spar Web WS 33-56

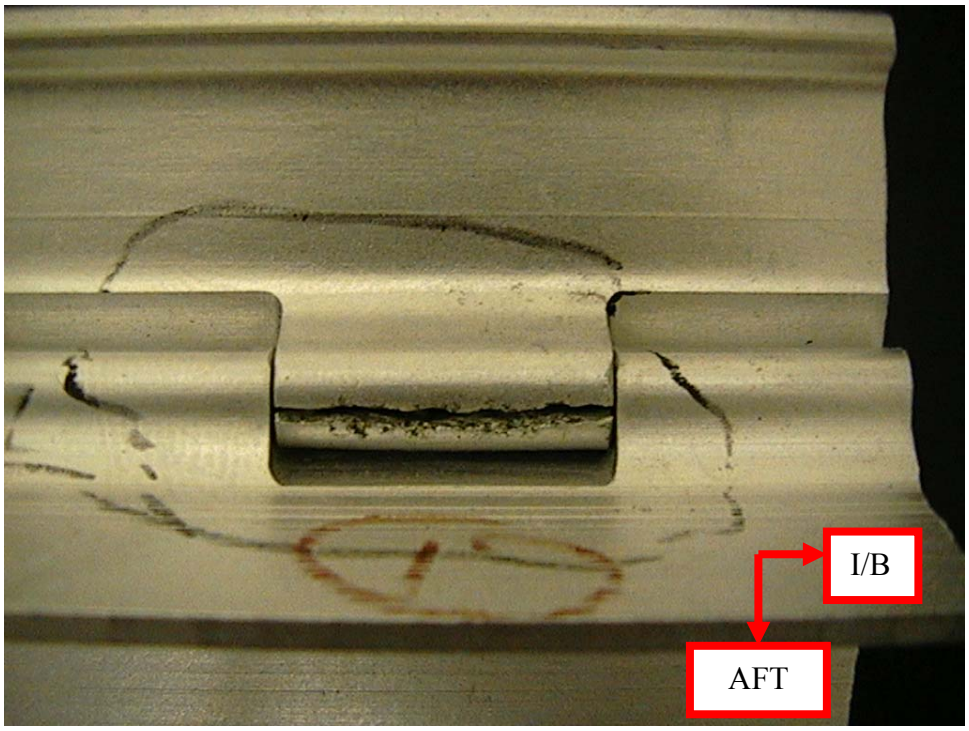

Figure 150. Intergranular Corrosion on the Right Wing Front Spar Upper Cap
WS 89.5-90 Bottom View

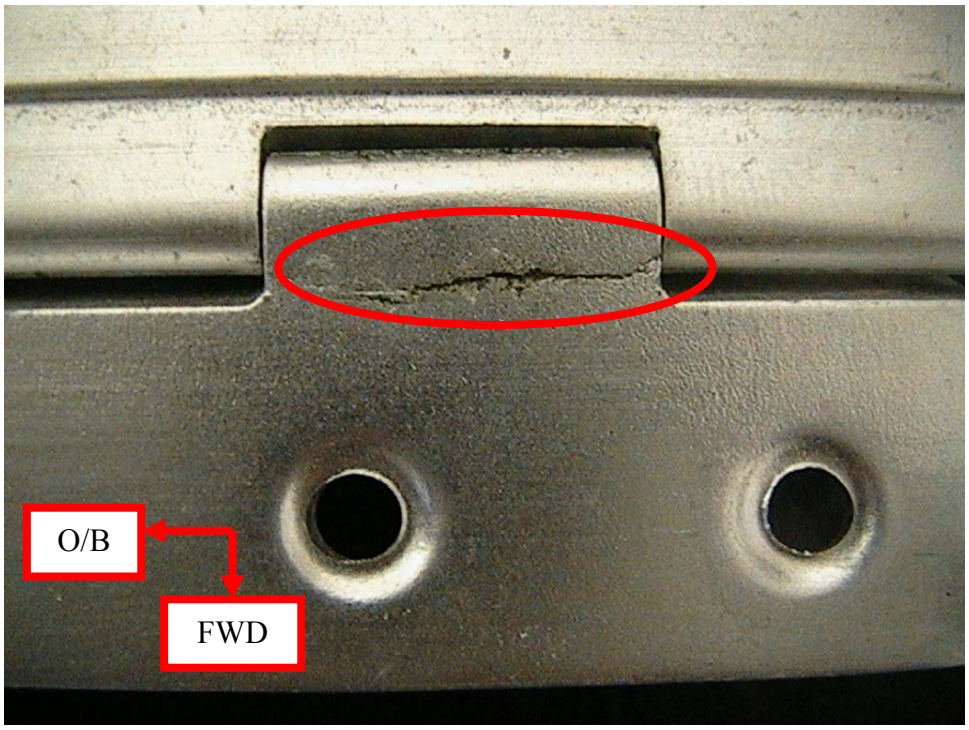

Figure 151. Intergranular Corrosion on the Right Wing Front Spar Upper Cap WS 89.5-90 Top View

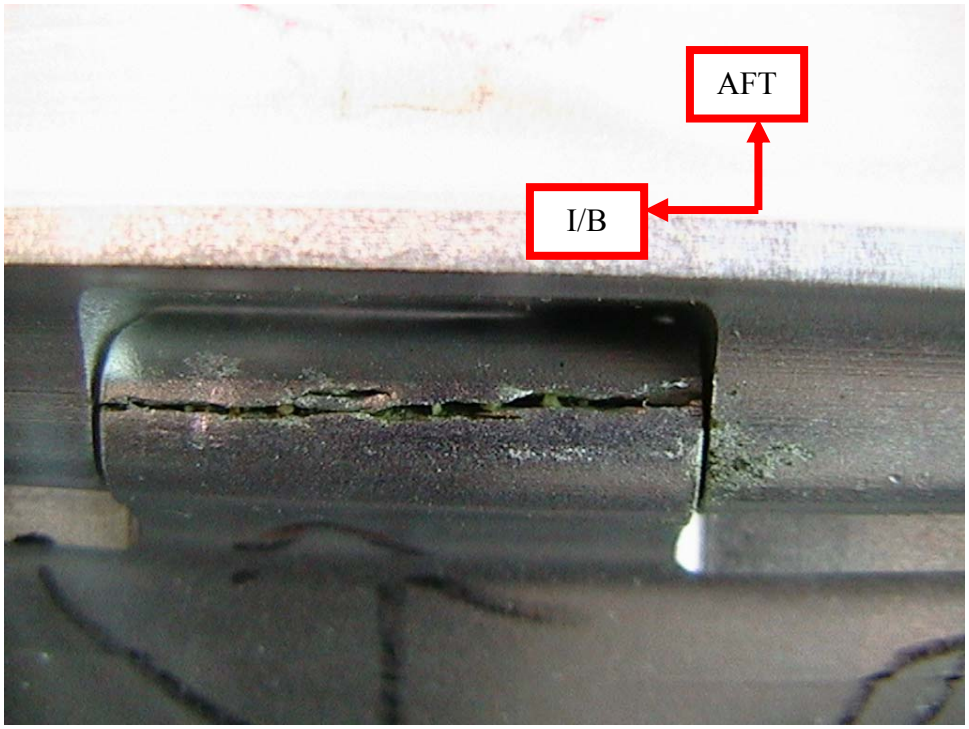

Figure 152. Intergranular Corrosion on the Right Wing Front Spar Upper Cap WS 110 Bottom View

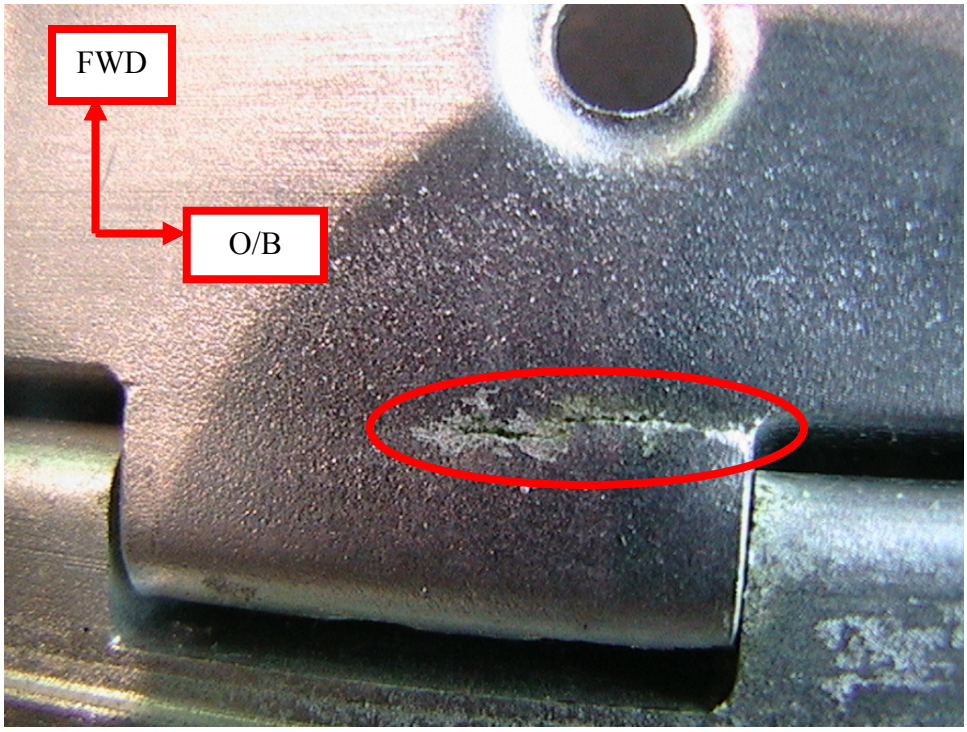

Figure 153. Intergranular Corrosion on the Right Wing Front Spar Upper Cap
WS 110 Top View

Pitting corrosion, pictured in figure 154, occurred from WS 122 to 126 on the front spar upper cap. This corrosion encompassed 0.53 square inch and resulted in a 3.4% thickness loss, which is classified as light-moderate corrosion. Figure 155 shows an area of intergranular corrosion and an area of exfoliation corrosion located at WS 184. This through-thickness corrosion measures 0.626 inch in length. Intergranular corrosion, located at WS 185.5, measured 0.841 inch and resulted in a 100% localized thickness loss. This corrosion is shown in figure 156. Another area of intergranular corrosion, measuring 0.432 inch in length and resulting in a 100% localized thickness loss, was located at WS 187, and this area is pictured in figures 157 and 158. Pitting corrosion, scattered across the surface of the upper cap, covered a surface area of 8.75 square inches and resulted in a 1.1% thickness loss, which is classified as light.

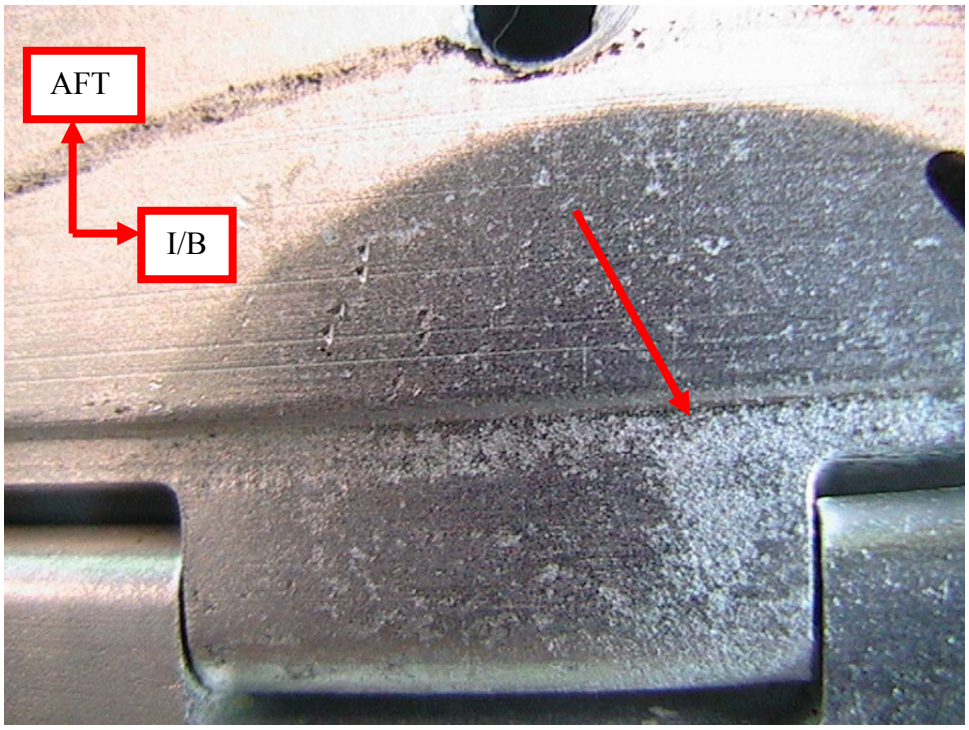

Figure 154. Corrosion on the Right Wing Front Spar Upper Cap WS 122-126

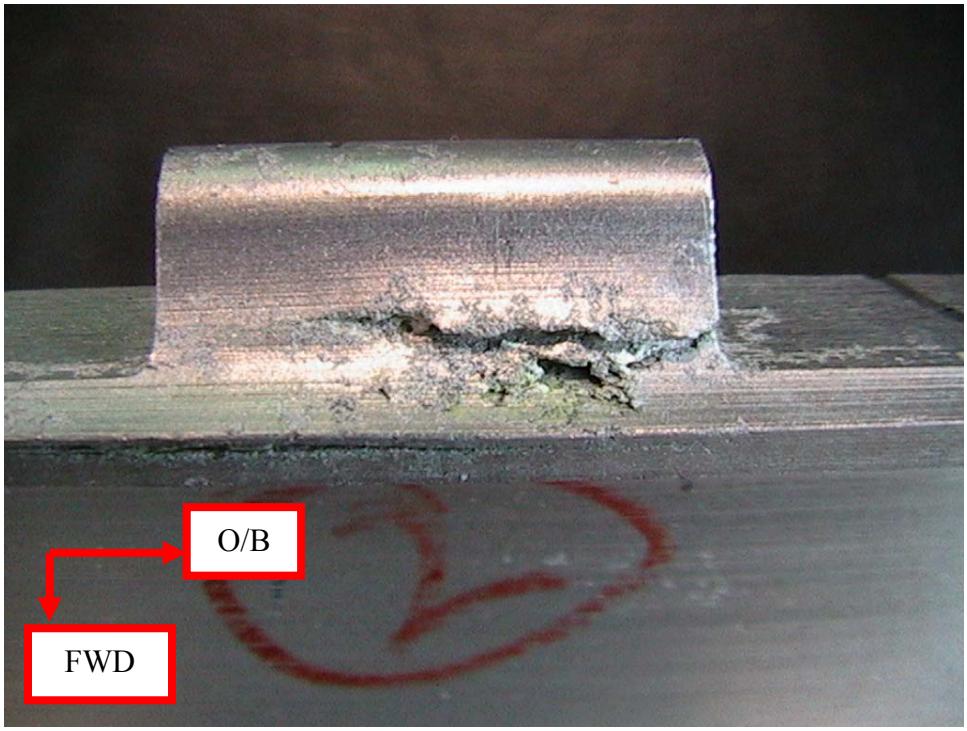

Figure 155. Intergranular Corrosion on the Right Wing Front Spar Upper Cap WS 184

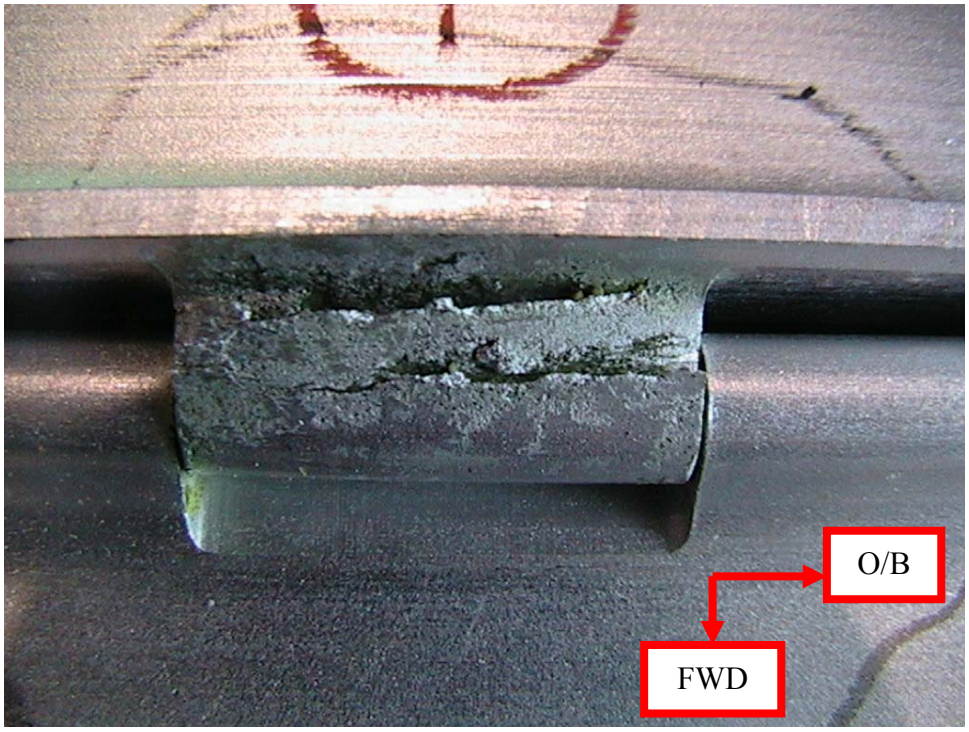

Figure 156. Intergranular Corrosion on the Right Wing Front Spar Upper Cap WS 185.5

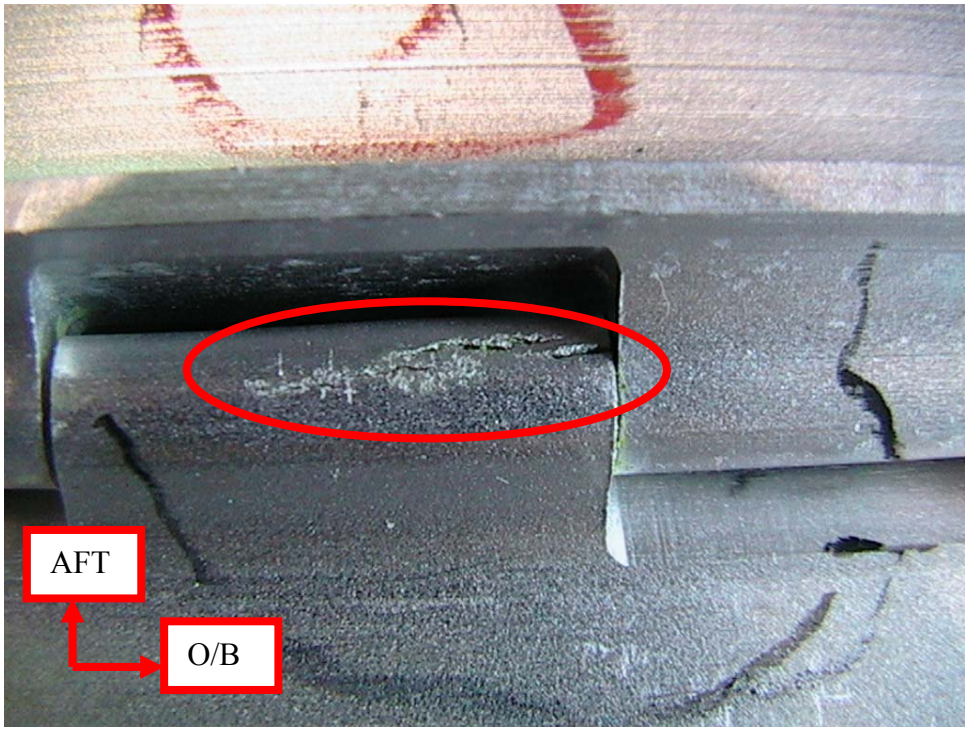

Figure 157. Intergranular Corrosion on the Right Wing Front Spar Upper Cap WS 187 Bottom View

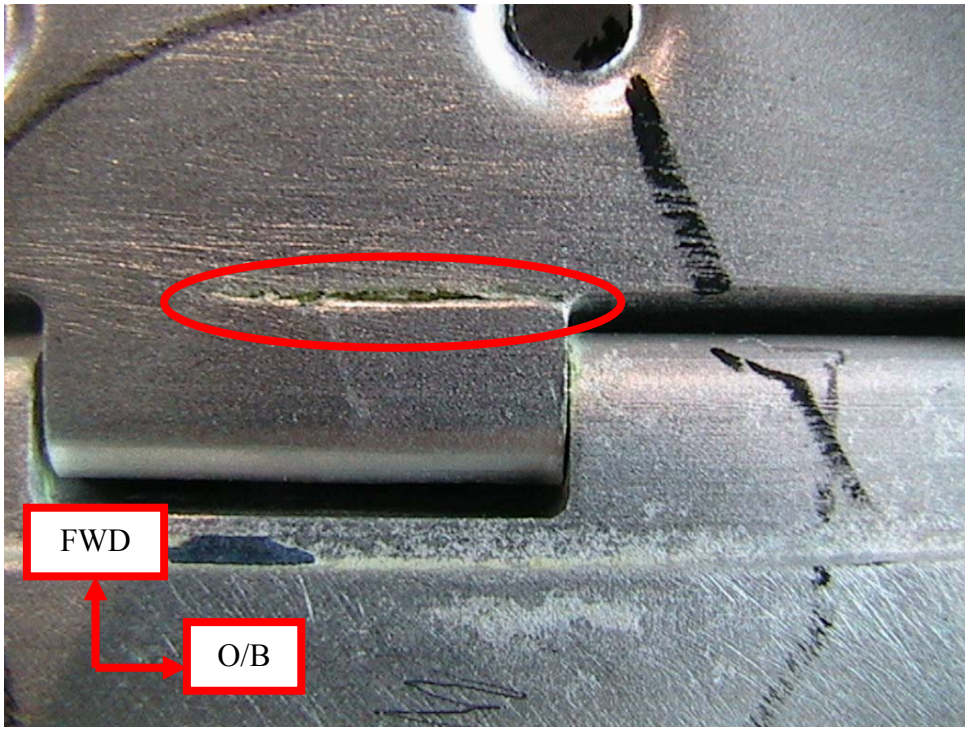

Figure 158. Intergranular Corrosion on the Right Wing Front Spar Upper Cap WS 187 Top View

3.4.2.2 Right Wing Leading-Edge Spar.

A 1.05-inch crack, pictured in figure 159, was found on the forward lower spar cap at WS 47.5. The crack face picture, showing that the failure was due solely to fatigue, is provided in figure 160. Another crack, measuring 1.3 inches, was observed on the aft lower spar cap at WS 64.5, and it is pictured in figures 161 and 162. Figure 163 shows the crack face with extensive metal smearing, which prevented the determination of a failure mode for this crack. Figure 164 shows two cracks located at WS 65.25 and 65.5 in the forward lower spar cap. These cracks measured 0.55 and 0.44 inch, respectively. The crack face picture for the crack located at WS 65.25 is shown in figure 165, and the crack face picture of the crack at WS 65.5 is provided in figure 166. The failure mode of both cracks was determined to be fatigue. Another crack was observed in the forward lower spar cap at WS 68.25. This crack, shown in figure 167, measured 0.495 inch in length. This crack was caused by fatigue, as shown in the crack face picture provided in figure 168.

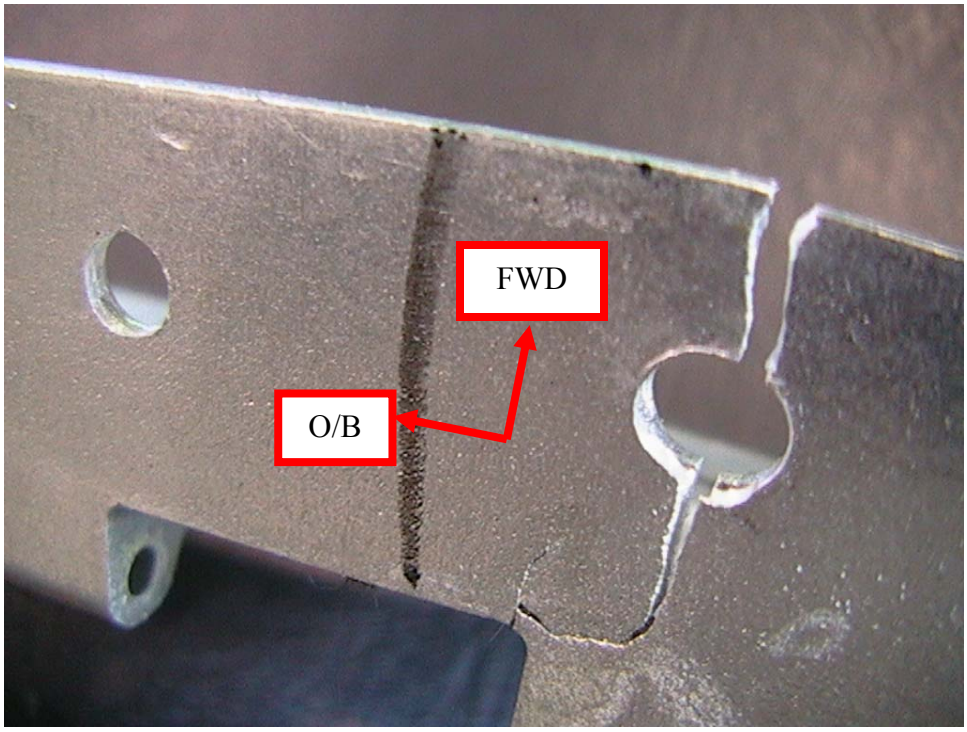

Figure 159. Crack in the Right Wing Leading-Edge Forward Lower Spar Cap WS 47.5

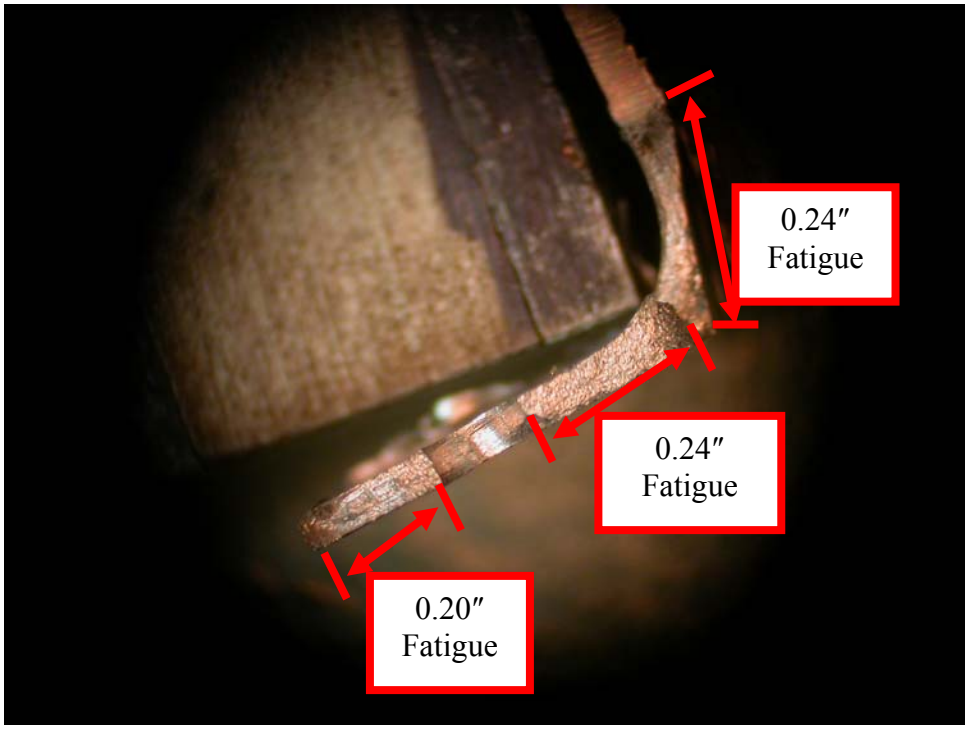

Figure 160. Crack Face of the Crack in the Right Wing Leading-Edge Forward Lower Spar Cap WS 47.5

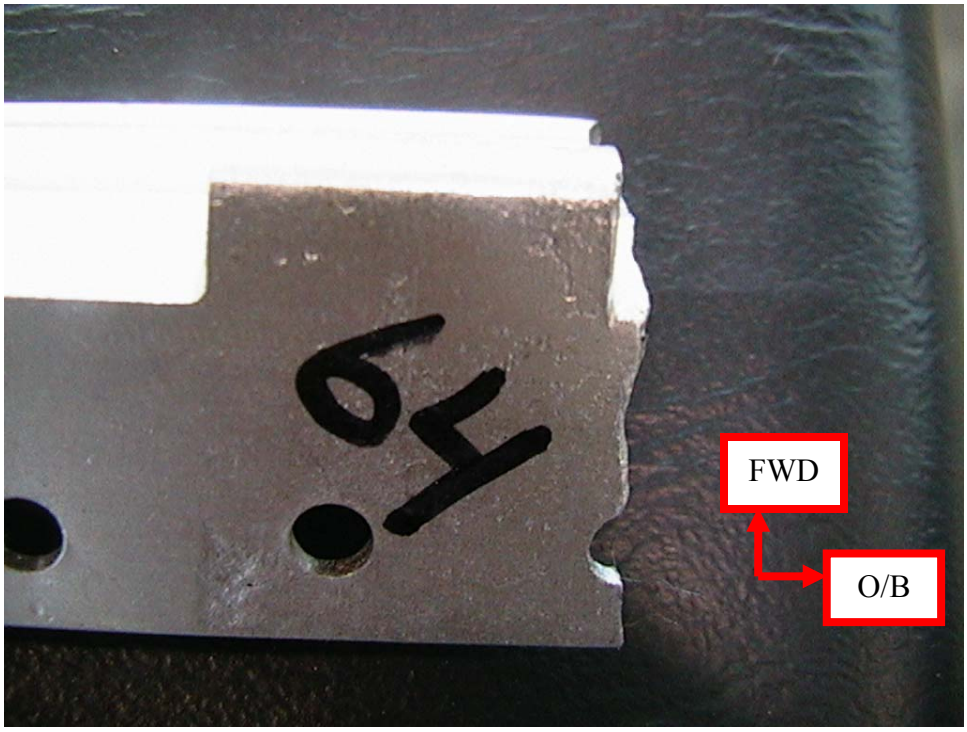

Figure 161. Crack in the Right Wing Leading-Edge Aft Lower Spar Cap WS 64.5 Top View

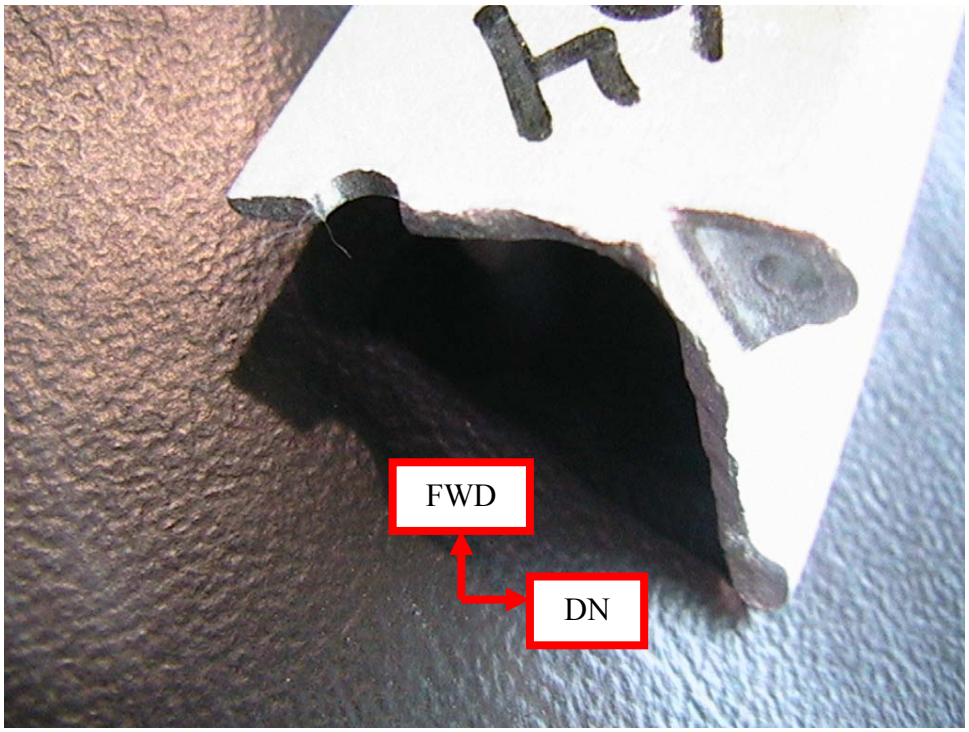

Figure 162. Crack in the Right Wing Leading-Edge Aft Lower Spar Cap WS 64.5

Figure 163. Crack Face of the Crack in the Right Wing Leading-Edge Aft Lower Spar Cap WS 64.5

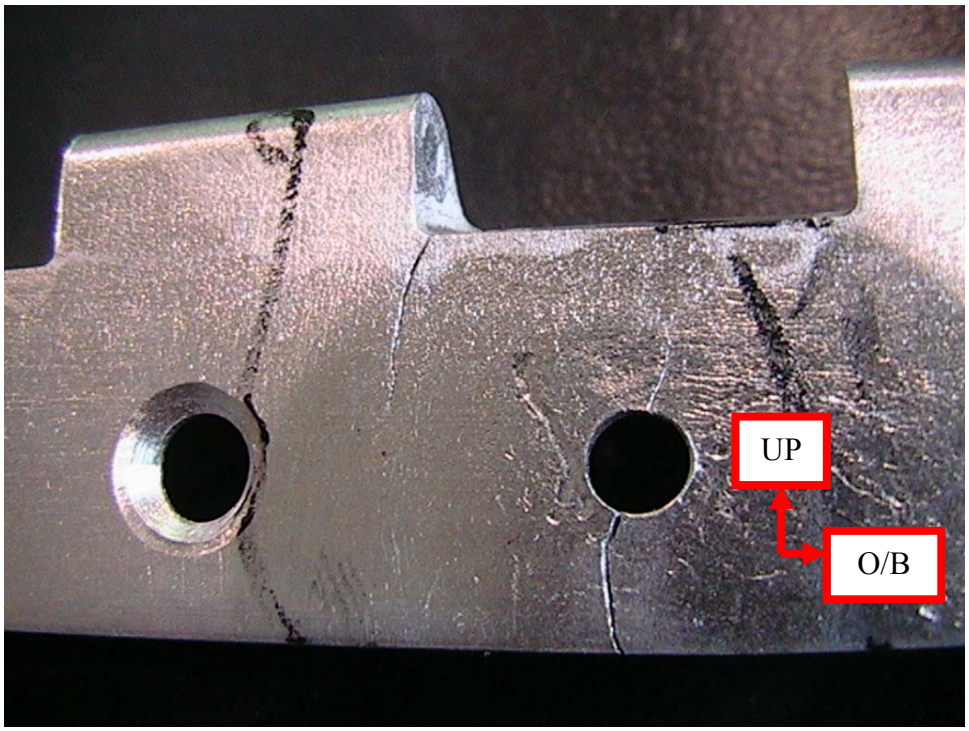

Figure 164. Cracks in the Right Wing Leading-Edge Forward Lower Spar Cap WS 65.25 and 65.5

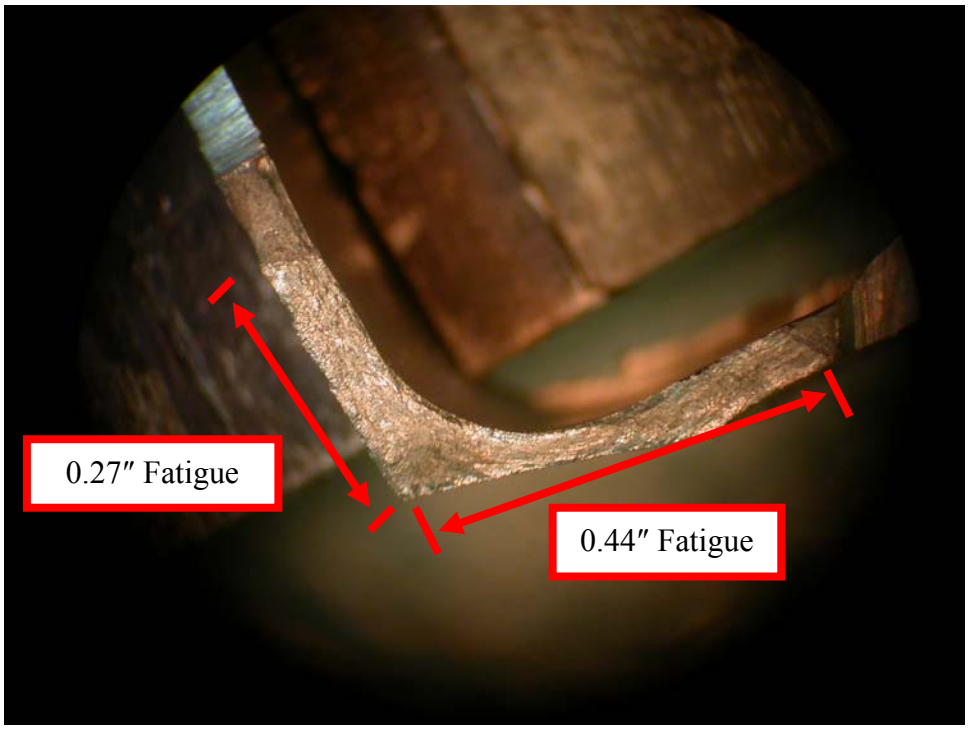

Figure 165. Crack Face of the Crack in the Right Wing Leading-Edge Forward Lower Spar Cap WS 65.25

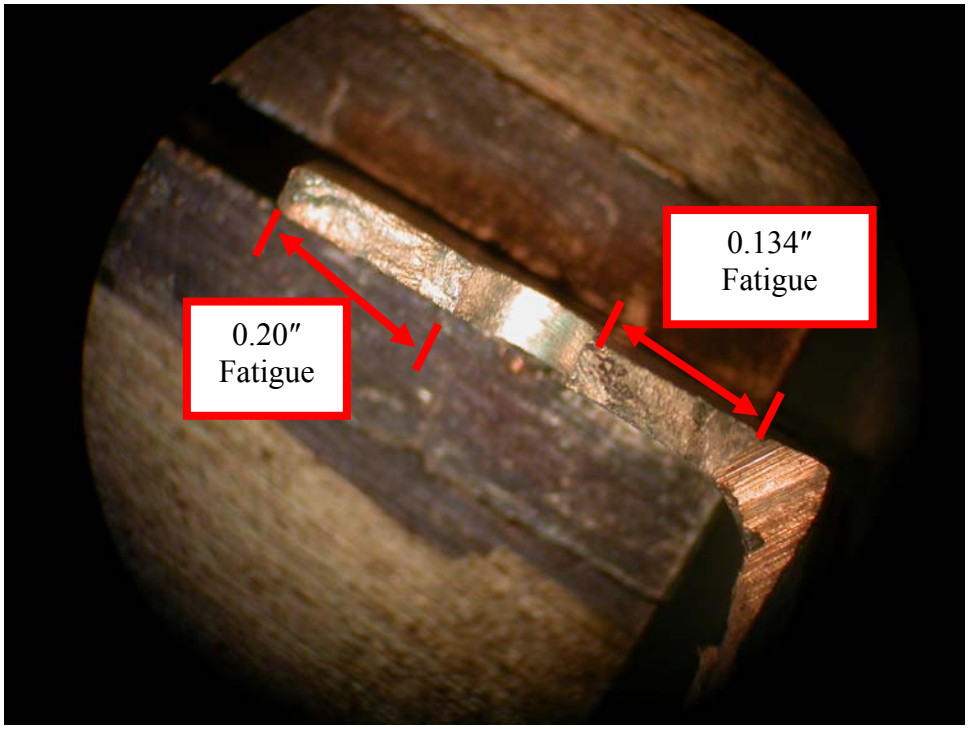

Figure 166. Crack Face of the Crack in the Right Wing Leading-Edge Forward Lower Spar Cap WS 65.5

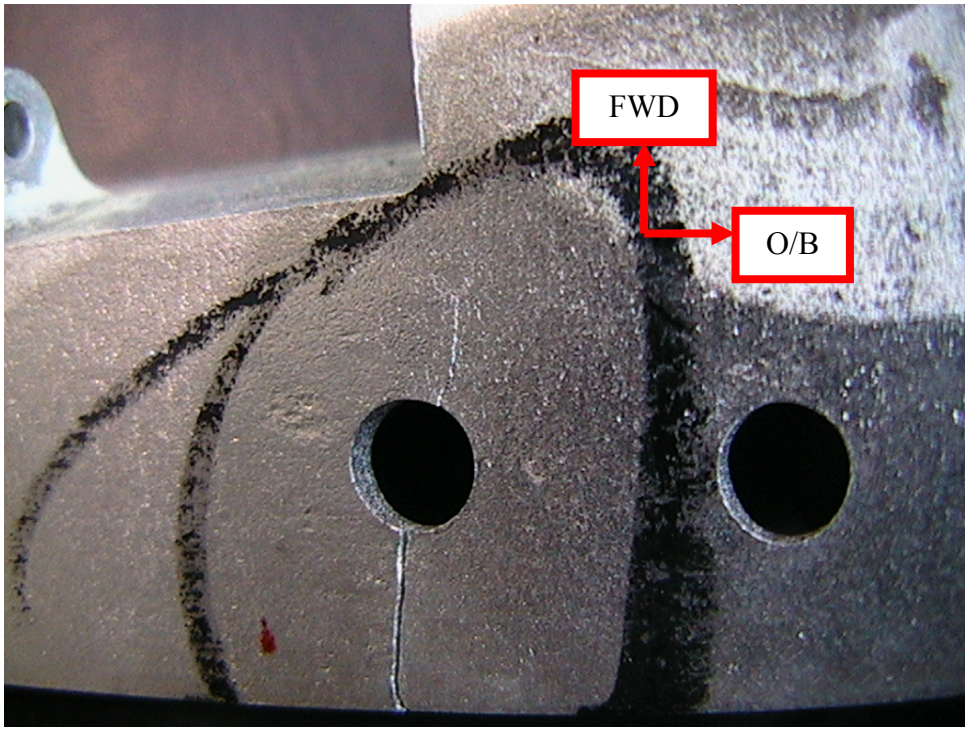

Figure 167. Crack in the Right Wing Leading-Edge Forward Lower Spar Cap WS 68.25

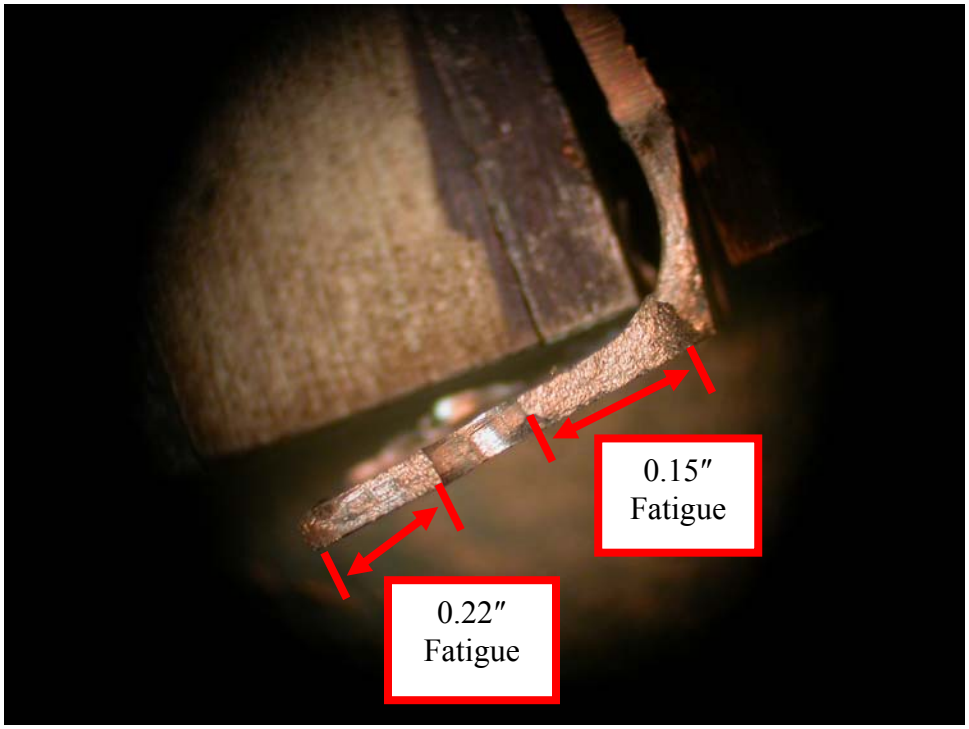

Figure 168. Crack Face of the Crack in the Right Wing Leading-Edge Forward Lower Spar Cap WS 68.25

3.4.2.3 Right Wing Rear Spar.

No defects were observed on the right wing rear spar during the microscopic examinations.

3.4.2.4 Right Wing Attachment Fittings.

Two small areas of corrosion were found on the right wing rear spar upper bathtub fitting The light corrosion area at WS 27, shown in figure 169, had a total surface area of 0.02 square inch, with a maximum pit depth of 0.004 inch. This depth resulted in a maximum thickness loss of 2.4%. Another light corrosion area, located at WS 25, covered a total surface area of 0.09 square inch, and this area is shown in figure 170. This area had a maximum pit depth of 0.002 inch, which resulted in a maximum thickness loss of 1.2%.

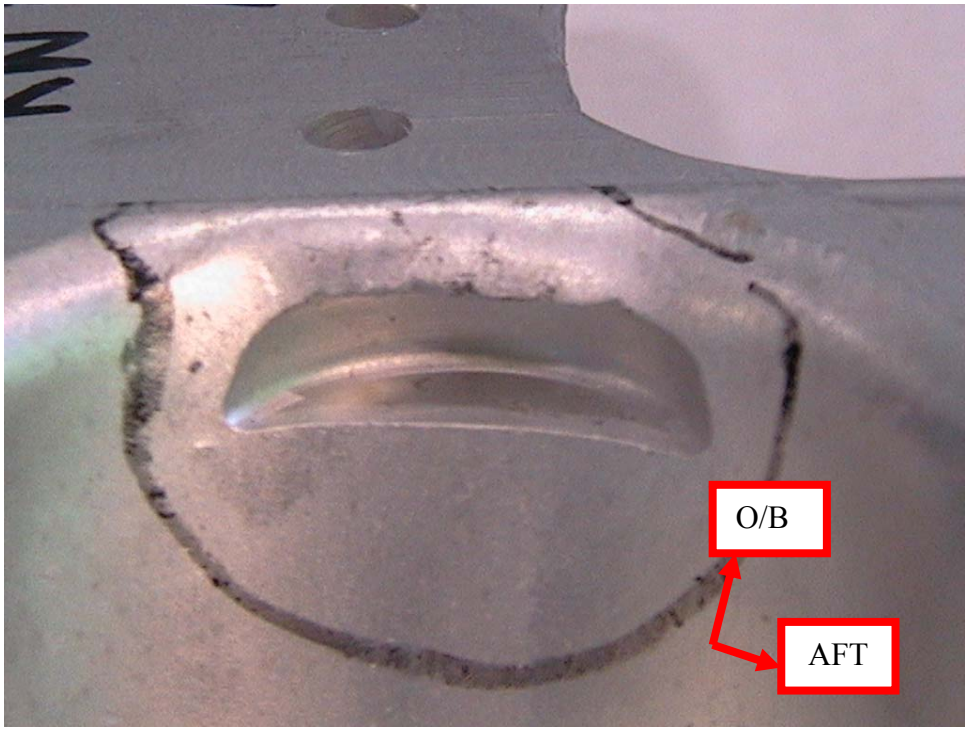

Figure 169. Pitting Corrosion on the Right Wing Rear Spar Upper Bathtub Fitting WS 27

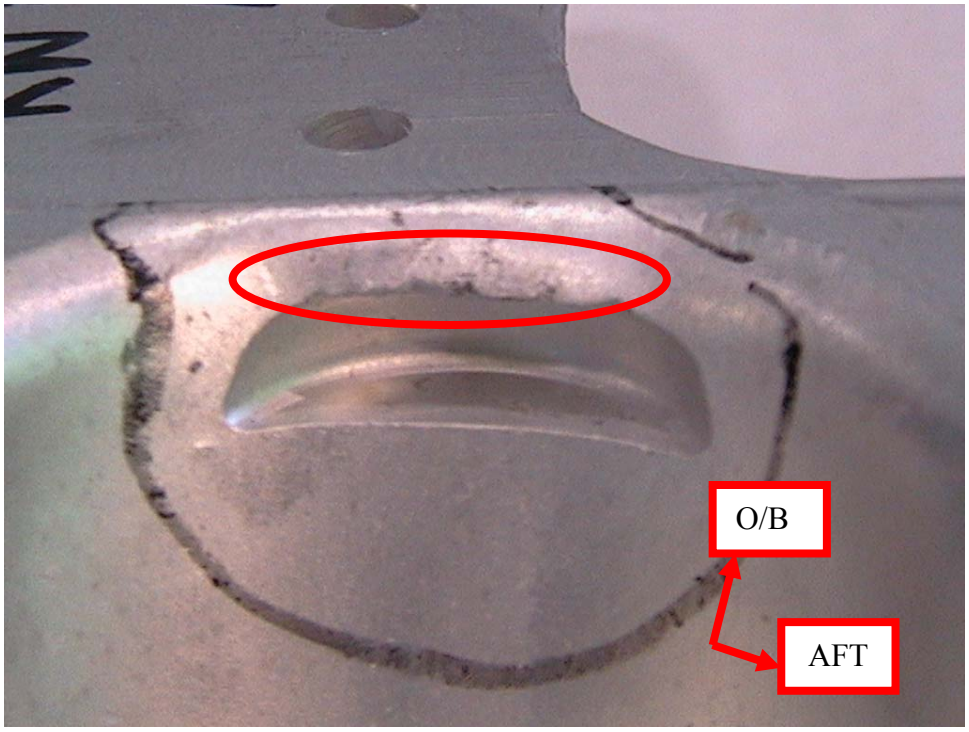

Figure 170. Pitting Corrosion on the Right Wing Rear Spar Upper Bathtub Fitting WS 25

3.5 SUMMARY OF SECOND WS FINDINGS.

Table 2 provides a summary of all findings on the second set of T-34A wings.

Table 2. Summary of Findings for T-34A WS 2

Part Description	Defect Location NDI	Defect Location Microscopic Examination	Flaw Type	Flaw Extent NDI	Flaw Extent Microscopic Examination
Left Wing Front Spar Web	WS 37-42	None	Pitting corrosion	0.8 square inch	None
Left Wing Front Spar Web	None	WS 23-56	Pitting corrosion	None	0.08 square inch 30% thickness loss
Left Wing Front Spar Web	None	WS 30.5	Pitting corrosion	None	0.04 square inch 13.3% thickness loss
Left Wing Front Spar Upper Cap	WS 39.5	None	Mechanical damage	0.2 inch	None

Table 2. Summary of Findings for T-34A WS 2 (Continued)

Part Description	Defect Location NDI	Defect Location Microscopic Examination	Flaw Type	Flaw Extent NDI	Flaw Extent Microscopic Examination
Left Wing Front Spar Upper Cap	WS 118-122.5	WS 120	Exfoliation corrosion	3.5 inches	2.07 square inches 100% thickness loss
Left Wing Front Spar Upper Cap	WS 136-142.75	WS 136-142.75	Exfoliation/intergranular corrosion	6.3 inches	1.16 square inches 100% thickness loss
Left Wing Front Spar Upper Cap	WS 139	None	Intergranular corrosion	0.6 inch	None
Left Wing Front Spar Upper Cap	WS 156.25-157.25	WS 156.25-157.25	Exfoliation corrosion	0.75 inch	0.95 inch 100% thickness loss
Left Wing Front Spar Upper Cap	WS 156.75	None	Mechanical damage	0.6 inch	None
Left Wing Front Spar Upper Cap	WS 157.25	None	Intergranular corrosion	0.31 inch	None
Left Wing Front Spar Upper Cap	WS 157.25	WS 158.25	Intergranular corrosion	0.35 inch	0.613 inch 100% thickness loss
Left Wing Front Spar Upper Cap	WS 163.75	None	Intergranular corrosion	0.25 inch	None
Left Wing Front Spar Upper Cap	WS 164	WS 164	Exfoliation corrosion	0.8 inch	0.95 inch 100% thickness loss
Left Wing Front Spar Upper Cap	WS 164	None	Mechanical damage	0.6 inch	None
Left Wing Front Spar Upper Cap	WS 166.5	None	Exfoliation corrosion	0.25 inch	None
Left Wing Front Spar Upper Cap	WS 166.75	None	Intergranular corrosion	0.6 inch	None

Table 2. Summary of Findings for T-34A WS 2 (Continued)

Part Description	Defect Location NDI	Defect Location Microscopic Examination	Flaw Type	Flaw Extent NDI	Flaw Extent Microscopic Examination
Left Wing Front Spar Upper Cap	WS 170.25	WS 170.25	Exfoliation/intergranular corrosion	0.7 inch	0.76 inch 100% thickness loss
Left Wing Front Spar Upper Cap	WS 170.25	None	Intergranular corrosion	0.07 inch	None
Left Wing Front Spar Upper Cap	WS 171.25	None	Exfoliation corrosion	1 inch	None
Left Wing Front Spar Upper Cap	WS 171.5	WS 170.5	Intergranular corrosion	0.6 inch	0.96 inch 100% thickness loss
Left Wing Front Spar Upper Cap	WS 174	None	Pitting corrosion	0.008 square inch	None
Left Wing Front Spar Upper Cap	WS 174.25	WS 174.5	Pitting corrosion	0.013 square inch	0.013 square inch 80% thickness loss
Left Wing Leading-Edge Aft Lower Spar Cap	WS 64	WS 64.5	Crack	1.3 inches	1.325 inches
Left Wing Leading-Edge Aft Lower Spar Cap	WS 57-69	WS 59-64	Pitting corrosion	1.6 square inches	1.62 square inches 7.2% thickness loss
Left Wing Leading-Edge Aft Upper Cap	WS 100.5-102.5	WS 100.5-101	Pitting corrosion	0.8 square inch	0.08 square inch 10.3% thickness loss
Left Wing Rear Spar Lower Doubler	WS 64	WS 64	Crack	0.8 inch	0.8 inch
Left Wing Rear Spar Lower Cap	WS 64	WS 64	Crack	0.6 inch	0.722 inch

Table 2. Summary of Findings for T-34A WS 2 (Continued)

Part Description	Defect Location NDI	Defect Location Microscopic Examination	Flaw Type	Flaw Extent NDI	Flaw Extent Microscopic Examination
Left Wing Rear Spar Upper Bathtub Fitting	WS 27	WS 27	Intergranular/ pitting corrosion	0.1 square inch	0.04 square inch 4.2% thickness loss
Left Wing Rear Spar Upper Bathtub Fitting	None	WS 24	Pitting corrosion	None	0.09 square inch 1.2% thickness loss
Right Wing Front Spar Web	WS 36-48	WS 33-56	Pitting corrosion	0.13 square inch	0.13 square inch 18% thickness loss
Right Wing Front Spar Upper Cap	WS 89.5-90	WS 89.5-90	Intergranular corrosion	0.65 inch	0.626 inch 100% thickness loss
Right Wing Front Spar Upper Cap	WS 109.5	WS 110	Intergranular corrosion	0.65 inch	0.626 inch 100% thickness loss
Right Wing Front Spar Upper Cap	None	WS 122-126	Pitting corrosion	None	0.53 square inch 3.4% thickness loss
Right Wing Front Spar Upper Cap	WS 183.5	WS 184	Exfoliation corrosion	1 inch	0.626 inch 100% thickness loss
Right Wing Front Spar Upper Cap	WS 184	None	Intergranular corrosion	0.4 inch	None
Right Wing Front Spar Upper Cap	WS 185.25	WS 185.5	Intergranular corrosion	0.6 inch	0.841 inch 100% thickness loss
Right Wing Front Spar Upper Cap	WS 185.25	None	Intergranular corrosion	0.4 inch	None
Right Wing Front Spar Upper Cap	WS 187	WS 187	Intergranular corrosion	0.4 inch	0.432 inch 100% thickness loss

Table 2. Summary of Findings for T-34A WS 2 (Continued)

Part Description	Defect Location NDI	Defect Location Microscopic Examination	Flaw Type	Flaw Extent NDI	Flaw Extent Microscopic Examination
Right Wing Front Spar Upper Cap	WS 187	None	Intergranular corrosion	0.4 inch	None
Right Wing Front Spar Upper Cap	None	Scattered on Surface	Pitting corrosion	None	8.75 square inches 1.1% thickness loss
Right Wing Leading-Edge Forward Lower Spar Cap	WS 47.5	WS 47.5	Crack	1.05 inches	1.05 inches
Right Wing Leading-Edge Aft Lower Spar Cap	WS 64	WS 64.5	Crack	1.3 inches	1.3 inches
Right Wing Leading-Edge Forward Lower Spar Cap	WS 65.25	WS 65.25	Crack	0.6 inch	0.55 inch
Right Wing Leading-Edge Forward Lower Spar Cap	WS 65.5	WS 65.5	Crack	0.4 inch	0.44 inch
Right Wing Leading-Edge Forward Lower Spar Cap	WS 68.25	WS 68.25	Crack	0.5 inch	0.495 inch

Table 2. Summary of Findings for T-34A WS 2 (Continued)

Part Description	Defect Location NDI	Defect Location Microscopic Examination	Flaw Type	Flaw Extent NDI	Flaw Extent Microscopic Examination
Right Wing Rear Spar Upper Bathtub Fitting	WS 25	WS 25	Pitting corrosion	0.02 square inch	0.09 square inch 1.2% thickness loss
Right Wing Rear Spar Upper Bathtub Fitting	WS 27	WS 27	Pitting corrosion	0.08 square inch	0.02 square inch 2.4% thickness loss

4. SUMMARY.

To aid with the assessment of aging acrobatic aircraft, the FAA contracted with the Aging Aircraft Research Laboratory at the NIAR to teardown and inspect two sets of wings from a high-time T-34A aircraft. Due to the recent history of fatigue cracking and failure, a destructive evaluation of the T-34A would be useful to the FAA for specifically addressing T-34A concerns, and in a general sense, assessing the condition of a high-time acrobatic category aircraft. The teardown evaluation involved performing the inspections prescribed in AD 2001-13-18; disassembly to gain access to the underlying primary structure; paint removal and etching of the wing primary structure to enhance damage detection; post-disassembly nondestructive inspections, and a detailed microscopic examination of all primary structure. Selected cracks were also analyzed to determine failure modes.

On the first set of T-34A wings, 4 cracks and 11 areas of pitting corrosion were observed on the left wing, and only 5 areas of corrosion were found on the right wing. The four cracks on the left wing were located on the rear spar web, rear spar lower cap, and rear spar lower doubler. These cracks ranged in length from 0.078 to 0.172 inch. The cracks on the rear spar lower doubler and cap were determined to be caused by fatigue. Of the 11 areas of corrosion documented on the left wing, 6 were categorized as severe, causing a maximum localized thickness loss of 15% to 23.5%. The severe corrosion was located on the left wing front spar forward and aft upper caps and the rear spar web. Two areas of light corrosion were identified on the left wing front and rear spar inboard landing gear attachment fittings. These areas of corrosion caused localized thickness losses of 0.5% and 1.1%. Corrosion was also found on the left wing front spar upper and lower bathtub fittings and the left wing rear spar lower bathtub fitting. Accurate classifications of the corrosion severity on bathtub fittings were not possible due to the location of the corrosion in the fitting. Two areas of light corrosion were observed on the right wing front and rear spar inboard landing gear attachment fittings, resulting in maximum localized thickness losses of 2.2% and 1.1%. Three areas of corrosion were identified on the right wing front spar upper and lower bathtub fittings and the right wing rear spar upper bathtub fitting. As with the

fittings on the left wings, accurate pit depth measurements were not possible on the bathtub fittings due to the location of the corrosion in the fittings.

On the second set of T-34A wings, three cracks, nine areas of pitting corrosion, ten areas of intergranular corrosion, seven areas of exfoliation corrosion, and three instances of mechanical damage were noted on the left wing. The cracks were located on the left wing leading-edge aft lower spar cap, rear spar lower doubler, and rear spar lower cap. These cracks ranged in length from 0.722 to 1.325 inches. Of the nine areas of pitting corrosion, four were classified as severe, resulting in localized thickness losses of 10.3% to 80%. This severe corrosion was observed on the left wing front spar web, front spar upper cap, and the leading-edge aft upper cap. Other areas of pitting corrosion were documented on the front spar web, front spar upper cap, leading-edge aft lower spar cap, and the rear spar upper bathtub fitting. Four of the ten areas of intergranular corrosion resulted in areas of complete localized thickness loss. Most of the intergranular corrosion was identified on the left wing front spar upper cap. The only additional location was one area of light-moderate intergranular corrosion on the left wing rear spar upper bathtub fitting. Five areas of exfoliation corrosion also resulted in complete localized thickness loss on the left wing front spar upper cap. The three areas of mechanical damage, observed on the left wing front spar upper cap, ranged in length from 0.2 to 0.6 inch.

On the right wing of the second set of T-34A wings, five cracks, five areas of pitting corrosion, seven areas of intergranular corrosion, and one area of exfoliation corrosion were reported. The five cracks ranged in size from 0.44 to 1.3 inches, and they were located on the right wing leading-edge forward and aft lower spar caps. One area of severe pitting corrosion was observed on the right wing front spar web, which resulted in 18% localized thickness loss. The four remaining areas of pitting corrosion were classified as either light-moderate or light corrosion. These areas were located on the front spar upper cap and the rear spar upper bathtub fitting. Four areas of intergranular corrosion resulted in complete thickness loss, and they were located on the right wing front spar upper cap. The remaining areas of intergranular corrosion were also located on the front spar upper cap. One area of exfoliation corrosion, which caused complete thickness localized thickness loss, was found on the right wing front spar upper cap.